

JCU ePrints

This file is part of the following reference:

McLellan, John George (2004) *Numerical modelling of deformation and fluid flow in hydrothermal systems.* PhD thesis, James Cook University.

Access to this file is available from:

<http://eprints.jcu.edu.au/2131>



Chapter 5

Discrete element modelling of stress partitioning and fluid flow in the Eastern Succession of the Mount Isa Block

Abstract

Numerical modelling using the discrete element technique is employed here to examine the response of a fracture system (Eastern Succession) to an applied stress regime. Areas of low minimum principal stress and low mean stress indicate dilation and potential sites of fluid focusing, and areas of high differential stress indicate increased deformation. An initial relatively simple model is followed by more complex ones containing younger granite suites and different fault architecture. The sequence of these models corresponds to pre- and syn- to post- mineralisation for many deposits in the region. Areas that show a combination of 1) low values of mean stress (σ_m), minimum principal stress (σ_3) and fluid pressure required for failure (PF_f), in conjunction with 2) increased differential stress ($\Delta\sigma$) predicting shear failure or low values predicting tensile failure, provide the best targeting solution for mineralisation. Many areas with these features correlate well with deposits and prospects in the region. These models also predict areas that at present have no known deposits.

5.1 General Introduction

The ability to numerically simulate and ‘map’ the effects of deformation can provide important data in understanding the spatial and temporal consequences of such processes. ‘Stress Mapping’ is a technique that has been used in determining the magnitude and distribution of stress in many mineralised terranes (e.g. Oliver *et al.*, 1990, 2001a; Holyland *et al.*, 1993; Holyland & Ojala, 1997; Jiang *et al.*, 1997; Mair *et al.*, 2000; Stephens, 2003). Areas of low minimum principal stress (σ_3) and low mean stress (σ_m) may indicate dilation and potential sites of fluid focusing, and are of great interest in mineralised hydrothermal systems. The ability to predict areas that are more susceptible to failure, and hence focus fluids, can be advantageous in defining sites of increased prospectivity within any region. The close relationship between deformation and fluid flow has been considered as the main process involved in genesis of many hydrothermal ore deposits, and the role of faulting in this process has been explored by many previous authors (e.g. Philips, 1972; Sibson *et al.*, 1988; Cox, 1995).

There are two main modelling techniques employed to simulate the response of rocks to deformation and subsequent fluid flow, and these can be broadly categorised as continuous and discontinuous modelling. Continuous modelling treats rock masses as an elasto-plastic continuum and focuses on pervasive fluid flow through this medium (Chapters 3, 4 and 6), whereas discontinuum modelling treats rock masses as elastic fractured discrete systems or blocks and focuses on the fluid flow along boundaries between such blocks. The distinct element program UDEC (Universal Distinct Element Code, Itasca

2000b) is used here to examine the effects of deformation and fluid flow along faults and rock boundaries in the Eastern Succession of the Mt. Isa Block, during several stages of its protracted deformation history. Discrete Element Modelling was considered the technique most suited to this study as economic grade mineralisation and the majority of the deposits in the Eastern Succession have a close spatial relationship with faults. The results are then used for comparisons and integration with prospectivity analysis of the district.

5.2 Background Geology

This section presents a synthesis of the general tectonostratigraphic and intrusive history of the Mt. Isa Block, particularly the Eastern Succession. It will then examine the fault architecture of the area and give a current synthesis of a prospectivity analysis undertaken by Mustard *et al.* (2004) in relation to fault orientations. A synthesis of the tectonostratigraphic history of the Mt. Isa Block has been presented in Chapter 4, and some repetition of information may occur in this chapter.

5.2.1 Mount Isa Block

The Mount Isa Block of Northwest Queensland is essentially comprised of three major tectonic units; from west to east, The Western Fold Belt (Western Succession), the Kalkadoon-Leichhardt Belt and the Eastern Fold Belt (Eastern Succession)(Fig 5.1), which are predominantly north-south trending sedimentological and structural domains (O'Dea *et al.* 1997; Blake & Stewart, 1992). The general geology of the area is characterised by lower to middle

Proterozoic meta-sedimentary rocks, rhyolitic and basaltic meta-volcanic rocks, gabbro, dolerite and widespread I-type granites.

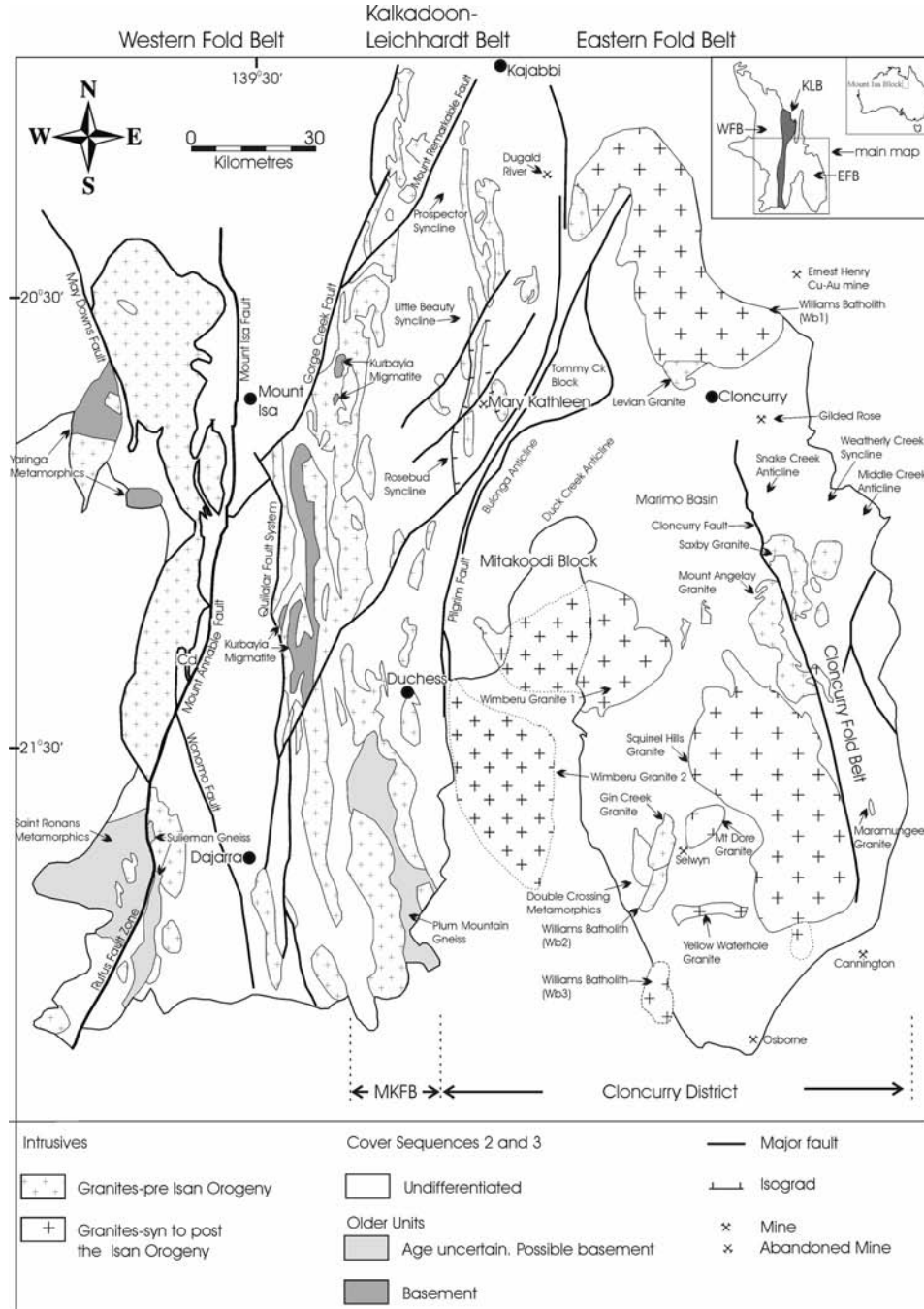


Figure 5.1. Location (inset) and general geology of the Western, Kalkadoon-Leichhardt and Eastern Fold Belts showing the further division of the Eastern Fold Belt into the Mary Kathleen Fold Belt (MKFB) and Cloncurry District. The spatial distribution of Cover Sequences 1-3 and intrusive features pre- and syn- to post- Isan Orogeny are shown, (modified from Williams, 1998), as well as some of the major mineral deposits in the Eastern Succession.

Two major stratigraphic cycles have been recognised within the Mt. Isa Block, both of which are proposed to have been deposited in intraplate sedimentary basins (Blake & Stewart, 1992). The first cycle is represented by a spatially restricted basement sequence (see Fig. 4.2 Chapter 4), comprising the Yaringa Metamorphics, Kurbayia Migmatites, Plumb Mountain Gneiss and Double Crossing Metamorphics, which were deformed and metamorphosed during the Barramundi Orogeny (1870 Ma) (Etheridge *et al.* 1987). The second cycle took place during at least four episodes of intracratonic rifting, and these rift cycles deposited three cover sequences (Page & Sun, 1998; Blake & Stewart, 1992), prior to the Isan Orogeny (ca. 1600-1500 Ma; Blake & Stewart, 1992).

Cover sequence 1 (1870 – 1840 Ma) is restricted to a narrow strip, mainly represented by the Leichhardt Volcanics and intrusions of I-type Kalkadoon granites, and known as the Kalkadoon-Leichhardt Belt. This belt then acted as a 'high', and Cover sequences 2 and 3, related to separate basin forming events, were consequently formed on the eastern and western sides (Eastern & Western Successions). Cover sequence 2 (ca. 1790-1720 Ma), is dominated by bimodal volcanic rocks, clastic and carbonate metasediments, and deposited on both east and west sides of the Pilgrim Fault. The development of Cover Sequence 2 also involved widespread intrusive igneous activity (e.g. Wonga Batholith, 1750-1740 Ma; Page, 1983) (Fig. 4.2). Cover sequence 3 (ca. 1680 - 1595 Ma), best represented in the Western Fold Belt, unconformably overlies Cover Sequence 2, and consists mainly of metamorphosed volcanoclastic rocks, conglomerates, sandstones, shales and carbonate rocks. During Cover sequence 3 bimodal volcanism accompanied sedimentation (Hill *et al.* 1992),

and several large intrusions including the Sybella Batholith (~1670 Ma) were emplaced (Page & Bell, 1986)(Fig. 4.2).

5.2.2 Eastern Succession Tectonostratigraphy

The Eastern Fold Belt (or Eastern Succession) can be further divided into the Mary Kathleen Fold Belt (MKFB) and the Cloncurry District, which are separated by the Pilgrim fault zone (Fig. 5.1). The Eastern Succession is host to metamorphosed sediments and mafic volcanic rocks (Soldiers Cap Group), calcareous meta-sedimentary rocks (Corella and Doherty Formations) minor pre-Isan intrusions and widespread post Isan Orogeny intrusive rocks (Williams and Naraku Batholiths). Geochronological ages are given in Fig. 4.2. Stratigraphic links with the rest of the Mt. Isa Block and Australian Proterozoic sequences have been tenuous mainly due to structural complexity, but hold great economic interest as a result of the Cloncurry District discoveries of the 1990's (e.g. Osborne, Ernest Henry, Cannington). Page & Sun (1998) demonstrated that the Soldiers Cap Group (ca. 1655 Ma), which was previously dated at 1880-1810 Ma (Beardsmore *et al.* 1988), and 1800-1780 Ma (Blake, 1987), is now younger and considered part of Cover Sequence 3. This has an interesting consequence, as the Soldiers Cap Group, which is host to mineralisation in the Eastern Succession, is now thought to be similar in age to the Mt. Isa and McNamara Groups of the Western Fold Belt, which host giant shale-hosted Pb-Zn-Ag ± Cu deposits.

The lowest stratigraphic units of Cover Sequence 2 to outcrop in the Eastern Succession are the Magna Lynn metabasalt, and clastic sediments and felsic

metavolcanic rocks of the Argylia Formation (ca. 1762 ± 3 Ma to 1781 ± 3 Ma). Overlying this formation is the Marraba Volcanics (flood basalts) and the Mitakoodi Quartzite (clastic sediments) of the Malbon Group (ca. 1755 ± 3 Ma) which has a corresponding stratigraphic equivalent (Ballara Quartzite) in the Mary Kathleen Fold Belt. The Mary Kathleen Group comprised of calcsilicate rocks and the marble dominated Corella Formation (ca. 1750 ± 7 Ma) conformably overlies the Mitakoodi and Ballara Quartzites. The Mt. Fort Constantine Volcanics (ca. 1742 ± 6 Ma), which is spatially restricted to the northern Cloncurry district, are temporally associated with several 1750 – 1740 Ma intrusions in the area (e.g. Gin Creek and Levian Granites). The uppermost unit of Cover Sequence 2 is represented by the calcsilicate and marble dominated Doherty Formation (ca. 1725 ± 3 Ma), but as this Formation is also intruded by 1740 Ma granites, it is probably equivalent to the Corella Formation.

The lowest stratigraphic unit of Cover Sequence 3 in the Eastern Succession is represented by the Fullarton River Group, which comprises the Gandry Dam Gneiss (ca. 1676 ± 5 Ma) and the New Hope Arkose, which corresponds to the Kuridala Formation (< 1670 Ma) on the western side of the Cloncurry Fault. The stratigraphy on the west of the Cloncurry fault e.g. Kuridala Formation, Answer Slate (< 1670 Ma), Marimo Slate (ca. 1655 ± 4 Ma) and the Staveley Formation, formerly known as the Mary Kathleen Group (Blake, 1983), now appears laterally continuous with the Soldiers Cap Group. The Llewellyn Creek Formation, which conformably overlies the Fullarton River Group, is comprised of thick bedded turbidites, and this forms the basal unit of the Soldiers Cap Group. Conformably overlying the Llewellyn Creek Formation are the Mount

Norna Quartzite (ca. 1654 ± 4 Ma) mainly composed of metamorphosed sandstones, siltstones and mudstones, and the Toole Creek Volcanics (ca. 1658 ± 8 Ma) comprised of metadolerites, metabasites and minor meta-sediments. Rubenach (pers. comm.) has identified parts of Cover Sequence 3 which are intruded by 1686 ± 8 Ma tonalites, placing further uncertainty on the stratigraphy of the Eastern Succession.

5.2.3 Intrusive history

The earliest intrusive phases in the Eastern Succession, prior to Cover Sequence 3, are coincident with the 'Wonga' extensional event (Holcombe *et al.*, 1992; Pearson *et al.*, 1992; Davis *et al.*, 2001) and include the Wonga Batholith (ca. 1750 – 1730 Ma), Dipvale Granite (ca. 1746 ± 7 Ma), Levian Granite (ca. 1746 ± 8 Ma) and the Gin Creek Granite (ca. 1741 ± 7 Ma). This intrusive period was accompanied with Na-Ca-K metasomatism, NaCl-rich scapolitization and skarn development (Oliver, 1995), and corresponds to the 'Big' event in the Western Succession (Southgate *et al.*, 2000). The Ernest Henry Diorite (1660 ± 13 Ma to 1657 ± 7 Ma) was contemporaneous with the 'Sybella' event and emplacement of the Sybella Granite in the Western Fold Belt, and coincides with the 'Gun' event in the Western Succession (Southgate *et al.*, 2000). The 'Williams and Naraku' event comprise multiple K-rich intrusive phases which have been spatially and temporally associated with at least some of the Proterozoic Fe oxide Cu-Au-Co mineralisation in the Cloncurry district (Pollard *et al.* 1998; Williams, 1998), and represent the most voluminous distribution of intrusive rocks in the Eastern Fold Belt. The oldest intrusions related to the Williams and Naraku Batholith, and informally known as the

Saxby or Mt. Angelay Igneous Complex, are; the Marramungee Granite (ca. 1545 ± 11 Ma), Mt. Margaret Granite (ca. 1530 ± 8 Ma) and the Mt. Angelay Granite (ca. 1523 ± 4 Ma). A younger suite of the Williams and Naraku Batholith is comprised of the Mount Dore Granite (ca. 1516 ± 10 Ma), Squirrel Hills Granite, Wimberu Granite (ca. 1508 ± 4 Ma), and the Yellow Waterhole Granite (ca. 1493 ± 8 Ma). There are no clear links to major intrusive activity in the Western Fold Belt at this time, however, minor pegmatitic intrusions are coincident e.g. Mica Creek Pegmatites (ca. 1532 ± 7 Ma).

5.2.4 Deformation, Metamorphism and Metallogensis

A complex and protracted deformational and metamorphic history is evident within the Mt. Isa Block, related to tectonic disturbance and ensialic rifting between 1900 and 1500 Ma. Following the 'Wonga' extensional event (ca. 1750 – 1730 Ma) there are three main deformational events during the Isan Orogeny (D_1 , D_2 and D_3) as initially proposed by Bell (1983)(see Table 4.1. Chpt. 4). Several authors have attempted to correlate the deformational events across both the Eastern and Western Fold Belts (Page & Bell, 1986; Etheridge *et al.* 1987; Holcombe *et al.* 1991; O'Dea *et al.* 1997; Adshead-Bell, 1998; Bell & Hickey, 1998; Laing, 1998; Mares, 1998), however, within fold and thrust belts structural history can be complicated and Betts *et al.* (2000) warns of relying on a holistic regional correlation. Although these deformational events are not well correlated throughout the Mt Isa Block, it remains a useful classification for the Eastern Fold Belt.

Sub-horizontal extensional shearing during the 'Wonga' event is evident by early tectonic features recognised so far only in the Mary Kathleen Fold Belt (Holcombe *et al.*, 1991; Pearson *et al.*, 1992). Following the 'Wonga' event several faulting and folding events have been recognised throughout the Eastern Fold Belt (O'Dea *et al.*, 1997). The (ca. 1600 Ma) Diamantina Orogeny (e.g. Laing, 1998) was originally thought to predate the 1550 – 1500 Ma Isan Orogeny, but abundant recent ages for the Isan Orogeny stretching back to 1590 Ma place the separation of these orogenies in doubt, and here the term Isan Orogeny covers the 1590 – 1500 Ma period.

Within the Eastern Fold Belt, D_1 is thought to have taken place as a result of north-south compression (Page & Sun, 1998; Rubenach & Lewthwaite, 2002; Sayab, 2003a; 2003b) and may have been responsible for the juxtaposition of Cover Sequence 3 against Cover Sequence 2 (Laing, 1998). A major east-west compressional event (D_2) (ca. 1590 – 1550 Ma), resulting in N/S trending tight to isoclinal upright folds and pervasive steep axial plane foliations, is commonly coincident with the peak of metamorphism in the Eastern Fold Belt. Several major shear zones have also been attributed to this D_2 event e.g. The Mount Dore and Eloise shear zones (Laing, 1998). Overprinting of many D_2 structures is attributed to one or more (ca. 1540 -1500 Ma) compressional events (D_3), resulting in NW and NE trending open folds, faults and shear zones, broadly coincident with emplacement of the Williams & Naraku Batholiths and Cu-Au mineralisation.

The peak of metamorphism in the Mt. Isa Block (upper amphibolite facies) was reached during D_2 , and this displays a complex low-pressure, high-temperature anticlockwise P-T-t path, (e.g. Rubenach, 1992; Rubenach & Barker, 1998; Rubenach & Lewthwaite, 2002). In particular, the metamorphic peak in the southeast region, is thought to have taken place around 1590 Ma (Perkins & Wyborn, 1998; Giles & Nutman, 2003), although earlier work suggested somewhat younger ages around 1550 Ma (Page, 1983; Page & Bell, 1986). The Western Fold Belt displays a growth of peak metamorphic assemblages that statically overprint S_2 fabrics (O'Dea *et al.*, 1997) which implies there may have been a hiatus between D_2 and D_3 . D_3 folding, shear zones and related faults were retrograde relative to D_2 (e.g. Oliver, 1995), but the absolute timing is poorly constrained. Relationships with granites of the Williams Batholith suggest D_3 occurred between 1540 and 1500 Ma.

The Mt. Isa Block shows extraordinary extensive regional sodic-calcic metasomatism, such as in the Mary Kathleen Fold Belt (Oliver, 1995) and the Cloncurry District (Williams, 1998; De Jong & Williams, 1995). Two major metasomatic events are distinguishable a) pre – syn metamorphism (1600 – 1590 Ma) which has been noted around the Osborne deposit (Rubenach *et al.*, 2001) and b) post-peak metamorphism (1540-1480 Ma), during granite emplacement e.g. Williams and Naraku Batholiths, in the Cloncurry District (Mark, 2001; Pollard, 2001; Pollard *et al.*, 1998; De Jong & Williams, 1995). Metasomatic fluids utilised major structural conduits (e.g. Cloncurry Fault, Pilgrim Fault) for infiltration into the surrounding country rocks, but is also very widespread. Na-Ca alteration commonly predates mineralisation in many of the

Fe oxide Cu-Au deposits (Perkins & Wyborn, 1998; Williams, 1998; French, 1997; Adshead, 1995).

The Mt. Isa Block is host to many economic deposits, some world class, such as Mt. Isa Cu, Mt. Isa Pb-Zn-Ag, Cannington Ag-Pb-Zn, Century Zn-Pb and Ernest Henry Cu-Au. Many of the deposits remain controversial in both ore genesis mechanisms and timing of mineralisation. Epigenetic processes are predominantly responsible for the majority of the Cu-Au deposits in the eastern Mt. Isa Block, with most models (e.g. Williams, 1998; Mark *et al.*, 2001; Wang & Williams, 2001) favouring a role for igneous-related hypersaline fluids. Fluid inclusion characteristics, stable isotope data and the close temporal relationships of mineralisation to felsic intrusions suggest that granitic fluids were responsible, at least in part, for many Cu-Au iron oxide deposits of the eastern succession (Pollard *et al.*, 1998; Williams, 1998; Oliver *et al.*, 2001b; Wang & Williams, 2001). Most deposits within the region are characterised by strong structural controls (Bell *et al.*, 1988; Laing, 1993; Valenta, 1994; Oliver, 1995) and major faults in the area have been suggested as fluid conduits responsible for mineralisation. Many of the deposits e.g. Osborne, Starra-Selwyn, Mt. Elliot, Monakoff, Eloise and Ernest Henry Cu-Au deposits, share several similar characteristics, all of which define the Cloncurry association of mesothermal ironstone-hosted Cu-Au deposits (Williams, 1998). At least one of these deposits (Osborne), however, may have formed during regional metamorphism prior to emplacement of the Williams Batholith (Rubenach *et al.*, 2001). The numerical modelling in the main part of this chapter focuses attention on the structural scenarios pertinent to the latter part of the Isan

Orogeny in which fluid flow and mineralisation was hosted mostly in D_3 structures.

5.2.5 Prospectivity

Recent work within the pmd*CRC has evaluated the prospectivity of the Eastern Fold Belt (Mustard *et al.*, 2004). One of the primary aims of the analysis was to determine the relationship of faults and fault architecture to mineralised terrains. Prospectivity analysis indicates that the main fault orientations favourable for mineralisation are N/S, S/SE or E/NE trending structures, particularly where jogs or bends are indicated. Fault intersections also appear to be important, in particular intersections of E/NE and S/SE faults with all other fault orientations. The faults developed synchronously with D_3 , or represent earlier faults reactivated during D_3 .

Partitioning of stress during deformation is important, as this may have a considerable effect on 1) strain rates within rock packages, 2) distribution of failure within and around faults e.g. fault reactivation, and 3) effects on fluid flow within faults and porous media (Oliver *et al.*, 1990). The presence of igneous intrusions within the area will have affected how the fault architecture and rock packages responded to an applied stress, particularly when the solidified intrusions acted as competent bodies.

5.3 Conceptual Models

Prior to any numerical study a conceptual model needs to be derived. This allows the user to define many 'what if' scenarios and allows major questions to

be addressed. This section describes the methodology used, questions to be addressed and the conceptual models derived to enhance the present work of the Pmd*CRC prospectivity analysis of the Eastern Fold belt.

5.3.1 Methodology and conceptual models

Examination of geological maps of the Eastern Fold Belt (Fig. 5.2) provided information required in setting up two conceptual models (Fig. 5.3, 5.4). These models were based on two distinct temporal periods 1) Model 1 (1540-1530 Ma), post regional metamorphism and older plutons but pre-Williams Batholiths, and 2) Model 2 (1530-1480 Ma), with additional younger fault architecture and post-tectonic plutons including the Williams-Naraku Batholiths (1530-1480 Ma). These time periods were selected to bracket and overlap with the main mineralisation period for many deposits in the district, coinciding with and following granite emplacement around 1530 Ma. Mapping information and a

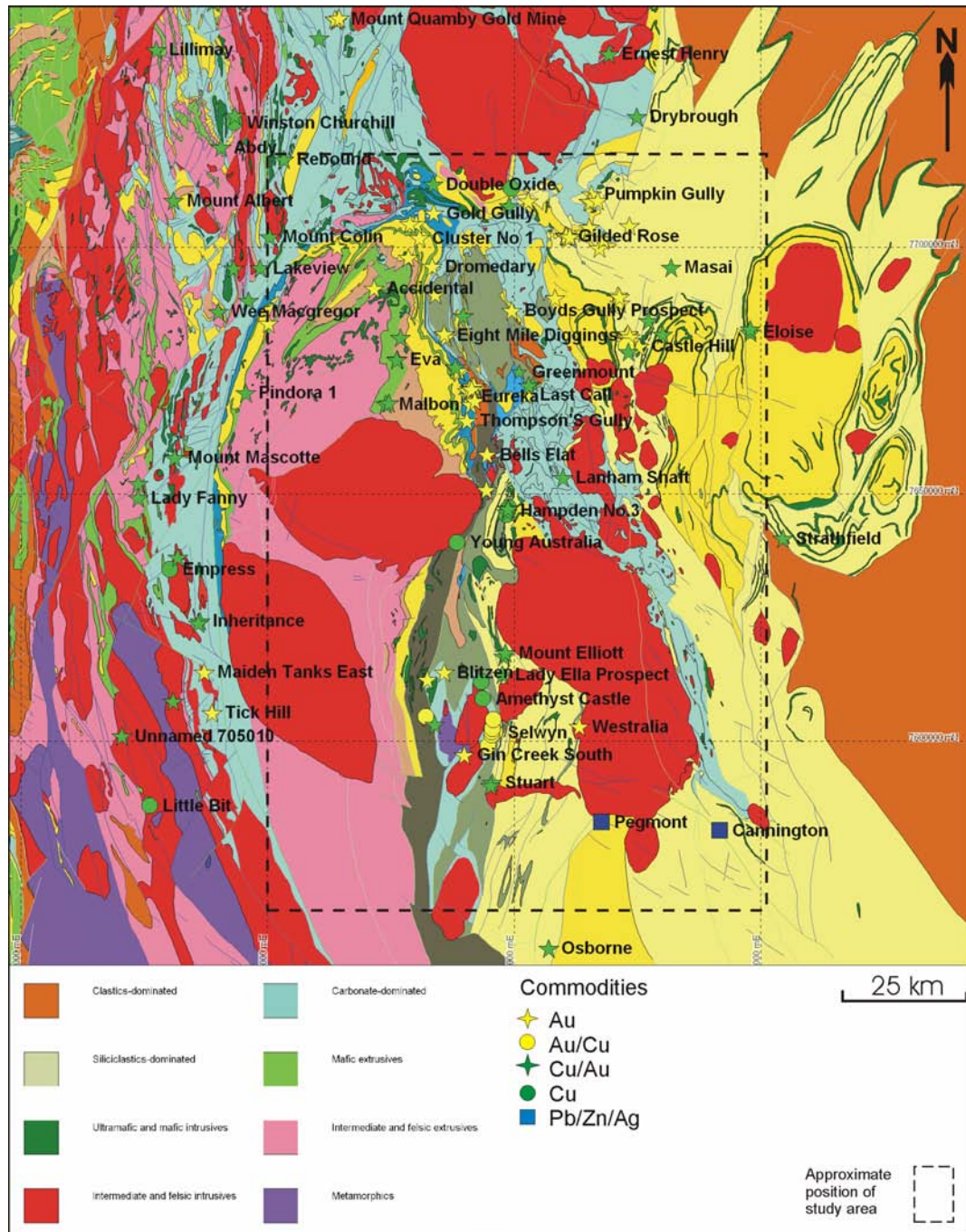


Figure 5.2. A detailed geological map of the Eastern Fold Belt highlighting the major deposits and study area undertaken (modified from NWQMP report, 2000).

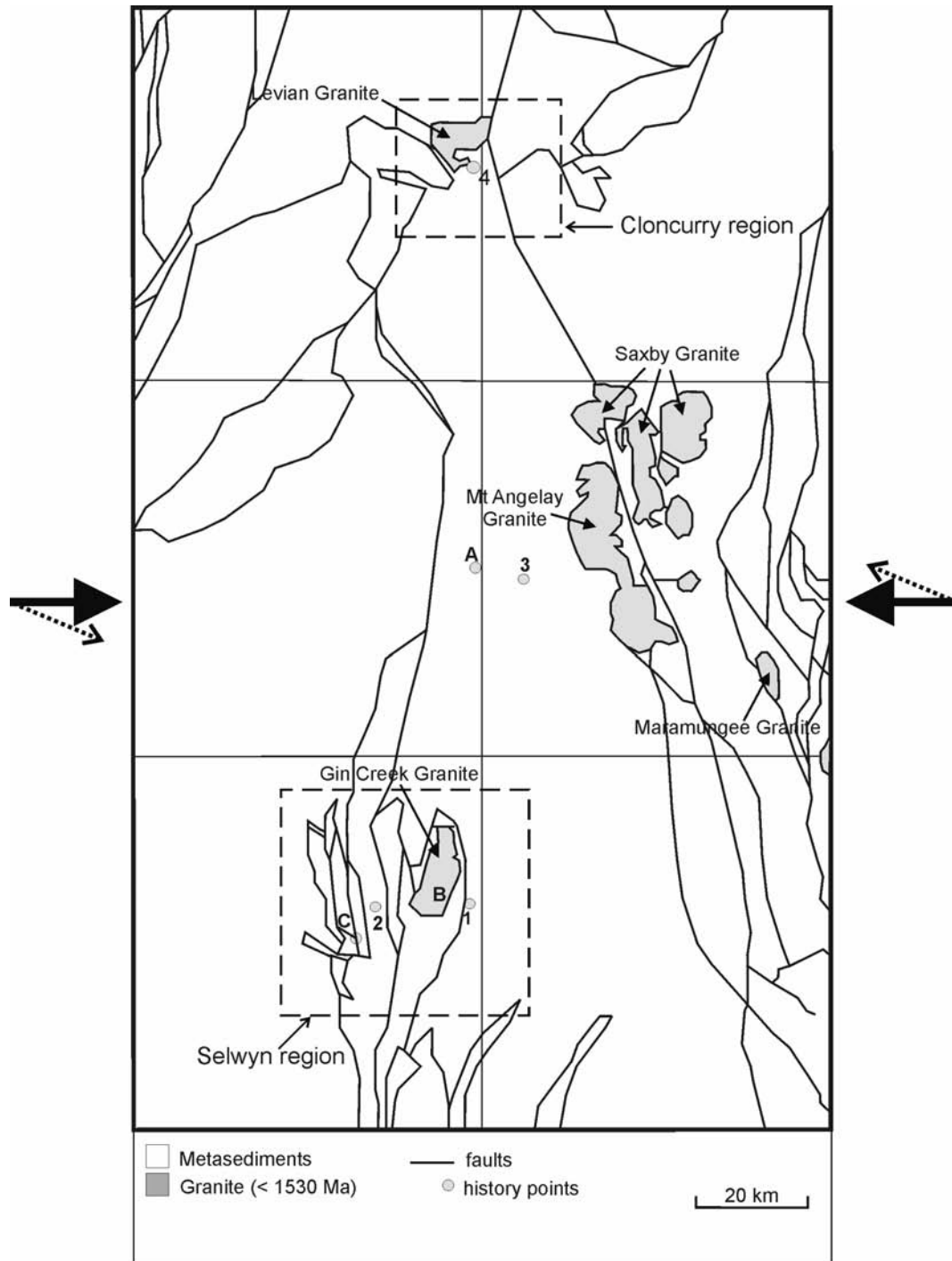


Figure 5.3. Conceptual Model 1 showing basic geological features and structures. Boundary conditions are appropriate to an east-west compression ($\sigma_1 = 90^\circ$) and a rotation of σ_1 to 112.5° . Note: history point locations and inset locations of the Selwyn and Cloncurry regions are shown.

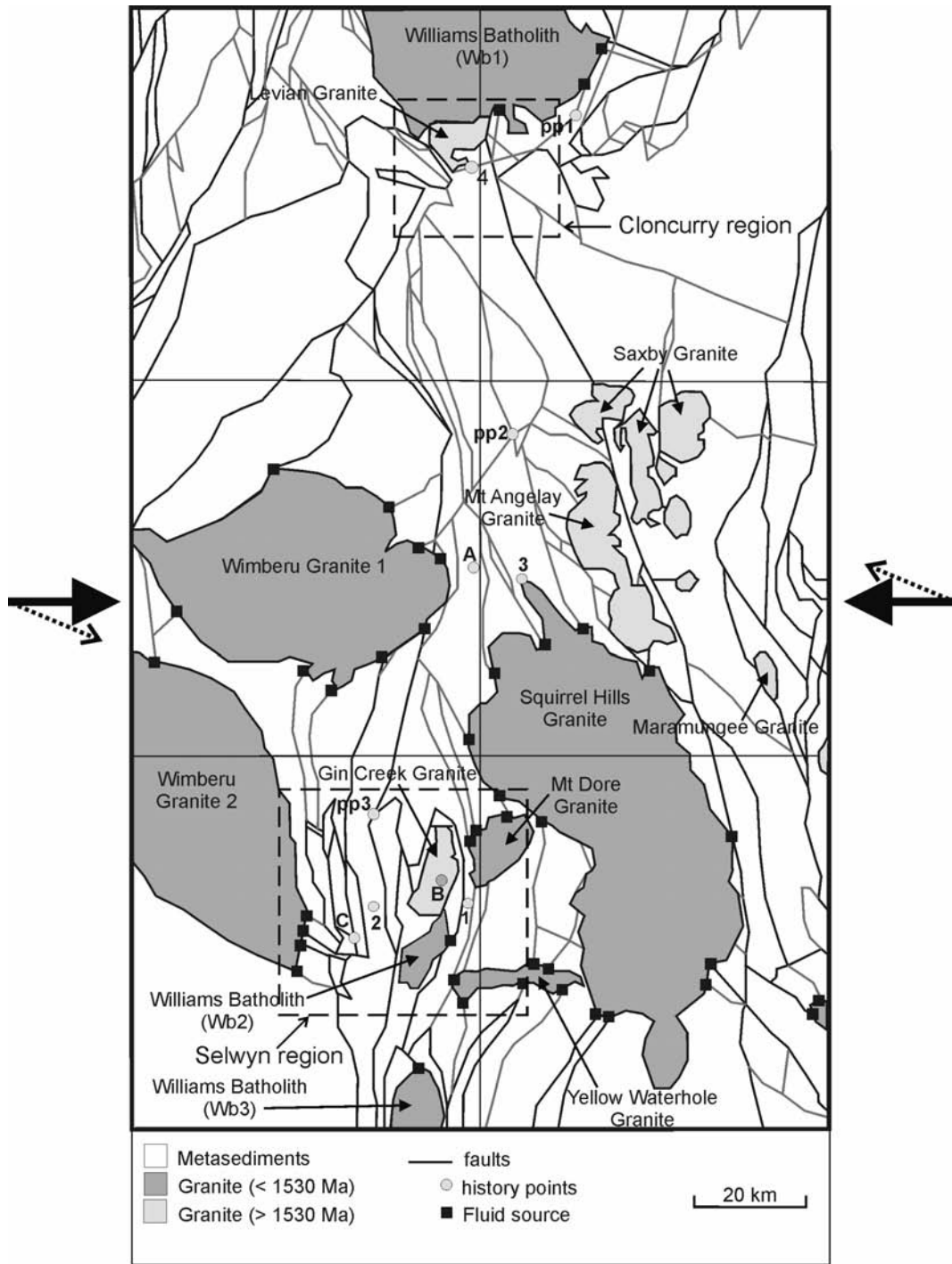


Figure 5.4. Conceptual Model 2 showing more complex geological features and structures. Boundary conditions are appropriate to an east-west compression ($\sigma_1 = 90^\circ$) and a rotation of σ_1 to 112.5° . Note: history point locations and inset locations of the Selwyn and Cloncurry regions are shown.

literature review (including the Qld. Dept. of Natural Resources, Mines and Energy (QDNRME) NW Qld. Minerals Province Study) provided the approximate timing of intrusive features and faults. Model 1 was set up to simulate the effect of an applied far field stress on the area. The models consist of early intrusive features such as the Wonga Granite and Gin Creek Granite (~1740 Ma), and examines their spatial and temporal association with major faults. Model 2 consists of younger intrusions and a more detailed fault architecture, which allows examination of the response of the intrusive bodies and younger faults to the imposed stress regime. As these models are based on 2-dimensional data they have limitations and a lower confidence level than a 3-dimensional study, however, a 2-dimensional study can be validated by certain assumptions prior to the modelling process. Several deposits within the area are structurally controlled and have a close association with faults; therefore it is assumed that these faults have acted as the main fluid pathways for mineralising processes. Many fault geometries within the area also display a strike-slip displacement; hence the main modelling interest is based on lateral fluid flow rather than vertical flow or a dip-slip fault environment. Finally, the ability to determine the influence of granites on stress partitioning in 2-dimensions may be useful in understanding their effect on structural controls on a broader scale. This conceptual approach allowed the following questions to be addressed;

1. What influence have intrusions in the Eastern Succession had on the partitioning of stress during deformation?

2. What influence has deformation had on the fault architecture and potential opening and closing of fluid pathways?
3. What faults, or orientation of faults, have a greater influence on failure and fluid flow?
4. What influence has fluid had on the failure of faults?
5. Does discrete numerical modelling predict areas of known mineralisation and any potentially unknown prospective locations?

5.4 Numerical Modelling

Following the conceptual model setup, several conditions must be set. These conditions include the numerical approach, boundary conditions and model parameters. This section introduces the modelling approach and gives an overview of the software used and its capabilities. The 'hard model' boundary conditions and input parameters used in this study are also described.

5.4.1 Modelling approach

The localisation of most deposits in the Eastern Succession, on or very close to faults, suggests that discrete element modelling of faults and contacts may be a suitable approach. The discontinuous approach to modelling the interfaces or contacts between discrete bodies must take into account two types of mechanical behaviour; 1) behaviour of the discontinuities, and 2) behaviour of the solid material involved. Blocks of material within these models may be assigned rigidity or a deformable property, and the contacts between blocks may also be given a deformable property.

5.4.2 UDEC (Universal Distinct Element Code) overview

UDEC is a two dimensional numerical program based on the distinct element method for discontinuum modelling (Itasca, 2000b). The code enables a numerical simulation of the response of discontinuous media e.g. jointed or fractured rock mass, subjected to either static or dynamic loading. The models are represented by discrete blocks, and the discontinuities represented as boundary conditions between blocks. UDEC allows large displacements and rotation of blocks and discrete blocks. The discrete blocks are subdivided into a finite difference mesh and each zone or element within the mesh behaves according to a prescribed linear or non-linear stress/strain law. UDEC uses a time-marching scheme to solve equations of motion (Zhang and Sanderson, 2002), and the relative motion of the discontinuities is governed by a linear or non-linear force displacement relationship for movement, in both the normal and shear directions.

UDEC calculates force and displacement according to Newton's law's of motion. As the force depends on displacement, the force/displacement calculation is done over one time instant. The central difference scheme is 'second order accurate' which is an important characteristic that prevents long-term drift in a distinct element model (Zhang & Sanderson, 2002). Fracture deformability or the response of fractures, in the normal direction, is based on the stress-displacement relationship which is assumed to be linear, and is governed by the stiffness properties applied to the fractures. The fractures have a limiting tensile strength and when exceeded, failure occurs. Similarly in shear, the response is controlled by the shear stiffness, and shear stress is limited by a

combination of cohesive and frictional strength of the fracture. Dilation of fractures may occur at the onset of slip, and this dilation is governed by a specified dilation angle. Fluid flow is allowed through the fractures and calculated by a fully coupled mechanical-hydraulic analysis. Fracture conductivity is dependent on mechanical deformation and, conversely, fluid pressure affects the mechanical behaviour of the fractures. Fluid flow in joints is modelled as flow between domains, and flow rates can be calculated in two different ways depending on the contact present. In the case of a point-to-edge contact, flow is primarily derived by a pressure gradient ($p_1 - p_2$), however, when an edge-to-edge contact is present flow is calculated by the 'cubic law' (see Chpt. 2 section 2.2.5) for flow in a planar fracture, which accounts for contact edge lengths. UDEC has been proven as a useful numerical tool in simulating geological processes (e.g. Oliver *et al.*, 2001a, 1990; Mair *et al.*, 2000; Holyland & Ojala, 1997), and in particular for fault arrays and fluid flow (e.g. Oliver, 1995; Jiang *et al.*, 1997; Zhang and Sanderson, 2002). The main and obvious disadvantage of UDEC is the inability to model porous media flow through deformable blocks in conjunction with discrete fracture flow. Also, there are geometric restrictions on fault geometries (see 5.4.4).

5.4.3 Sensitivity Analysis

Several sensitivity analyses were carried out to examine the effect of geometry, boundary conditions, rock properties and joint properties. This allowed a more comprehensive insight into what parameters were most likely to affect the modelling procedure.

As the geometry was based on map inferences many of the faults at the scale of operation consisted of sharp bends and corners. It was therefore important to examine the effect of sharp vs. smooth bends and what influence this would have on the modelling results (Fig. 5.5ab). There is a notable partitioning of stress around the smooth bends compared to the sharp bends (Fig. 5.6a-d); however, there is no major influence on the stress patterns at the broader modelling scale. It was therefore considered feasible to model the geometry inferred from the available mapping, even if the input fault bends were sharper than actual field patterns.

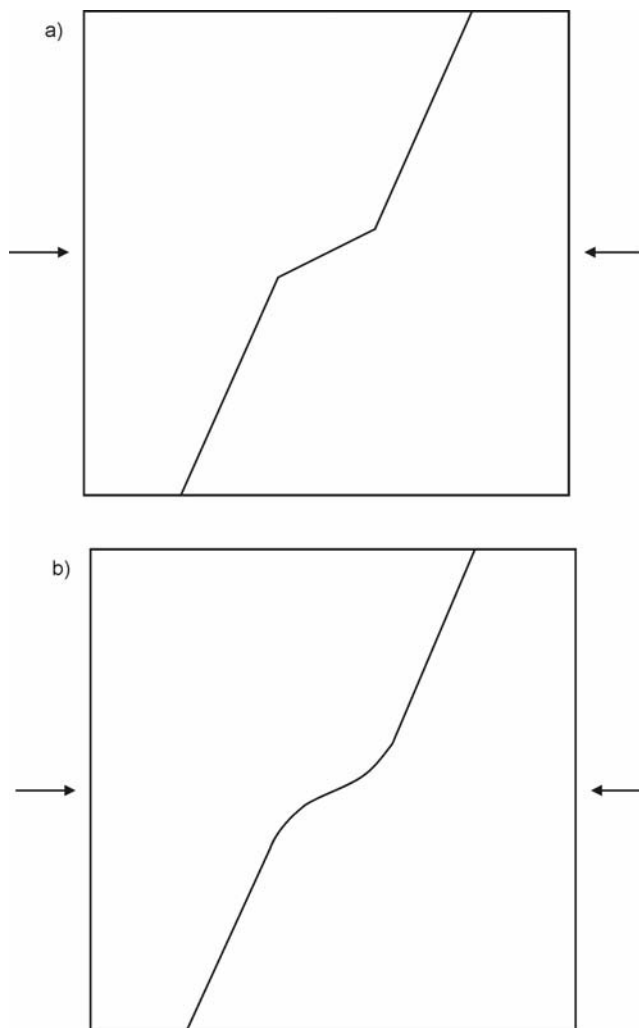


Figure 5.5. Conceptual models for sensitivity testing of **a)** sharp versus **b)** smooth geometrical bends. Boundary conditions are appropriate to east-west compression.

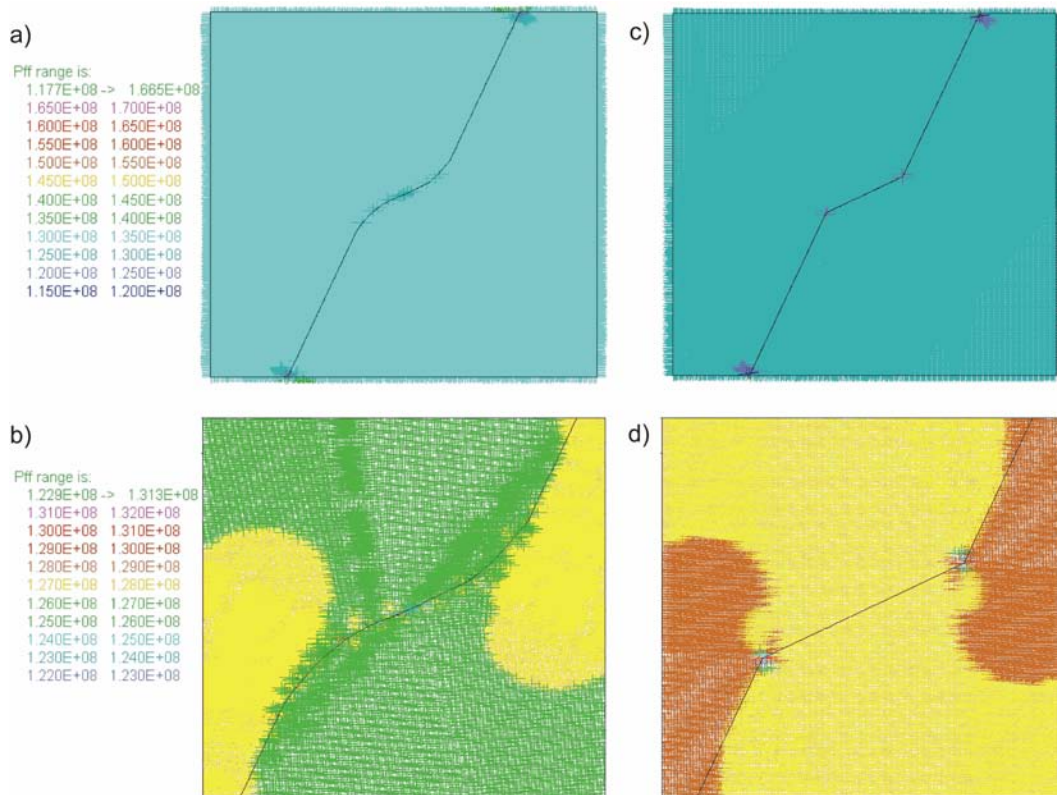


Figure 5.6. UDEC results of sensitivity testing of geometrical features **a)** fluid pressure required for failure (PF_f) for a smooth geometrical bend **b)** magnified plot of same **c)** PF_f for a sharp geometrical bend, and **d)** magnified plot of same. Note: similar overall result in values, with a more gradual spread of values noticeable in the smooth models.

Joint friction angle appears to be one of the most sensitive parameters in relation to the potential failure of faults. Friction angles were modified from 5° to 35° to examine the change in deformation patterns and to compare any differences in areas of failure. A reduction in joint friction angle increased the incidence of fractures reaching their shear stress limit and also lowered fluid pressure required for failure, especially for friction angles less than 10° (Fig. 5.7a-d). A moderate to high friction angle was used in the main models of this study, similar to faults and geological contacts of previous authors (e.g. Oliver *et al.*, 1990; Jiang *et al.*, 1997; Stephens, 2003). Cohesion values were also

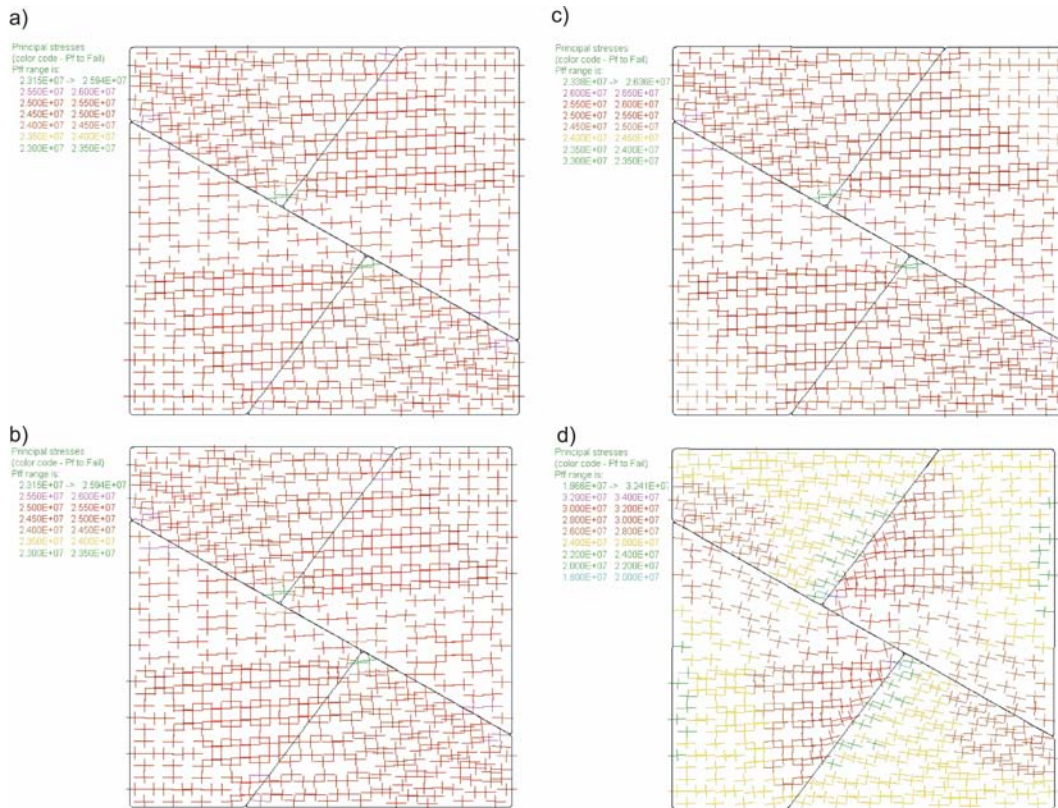


Figure 5.7. UDEC results of sensitivity testing of four variations in friction angle values. All values given are for PF_f . Friction angle values for the four models **a)** 35° **b)** 20° **c)** 10° and **d)** 5°. Note the least variation between models is seen in the higher friction angle values; lower values produce significantly different results.

investigated and fault contacts were given very low cohesion values in accordance with Sibson (1985) and Zhang & Sanderson (2002). Joint normal and shear stiffness also has a major effect on the deformation of fractures. The normal displacement of fractures is controlled by the normal stress and normal stiffness of the fracture according to the relationship of stress displacement and stiffness, such that;

$$\Delta\sigma_n = -k_n \Delta\mu_n \quad (7.1)$$

where $\Delta\sigma_n$ is the effective normal stress increment, k_n the normal stiffness and $\Delta\mu_n$ the normal displacement increment. Sensitivity testing showed that lowering the stiffness of the fracture results in more closure during deformation which in turn decreases the aperture of the fracture and hence reduces volumetric fluid flow and increases fluid velocities (Fig. 5.8a-f). Results from the sensitivity testing were incorporated into the setup of the main Eastern Succession models.

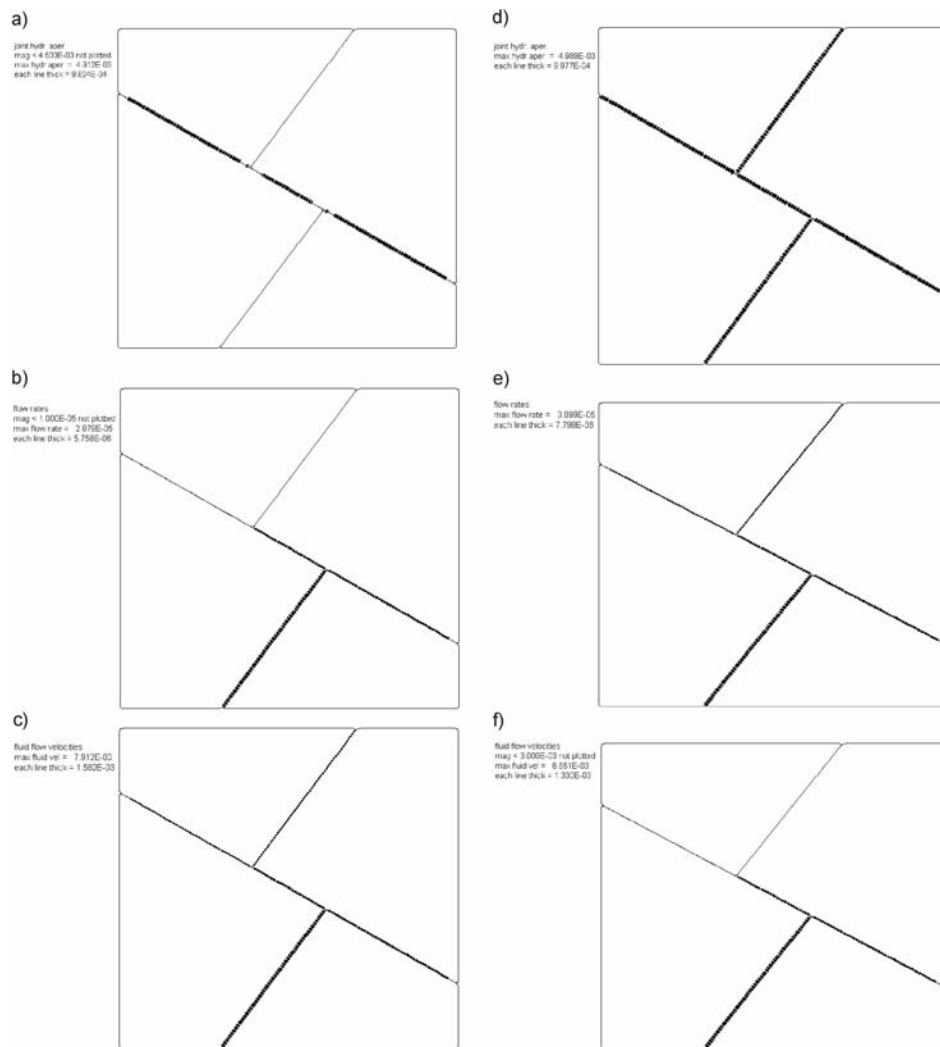


Figure 5.8. UDEC results of sensitivity testing of stiffness parameters of fractures. Results display the effects on aperture width, volumetric fluid flow rates and fluid flow velocities. Diagrams **a to c** represent joints with lower fracture stiffness values and **d to f** representing higher fracture stiffness values. Lower fracture stiffness result in greater closure of apertures, lower volumetric flow rates and higher flow velocities (**a to c**). Higher fracture stiffness results in less closure of apertures, higher volumetric flow rates and lower flow velocities (**d to f**).

5.4.4 Boundary conditions and model parameters

Models 1 and 2 both cover an area 200km x 124km within the Eastern Succession. The geometry of the models was constructed by drawing fractures from the 1:100 000 maps of the area. Due to limitations of the UDEC program, no fractures can be inserted that are not directly or indirectly connected to the model edges, hence all fractures are joined. A rounding parameter is assigned to each block, which applies to the contact mechanics, to prevent unrealistic locking of the corners during the modelling process. All blocks are divided into smaller zones of a maximum of 1 km edge length. The constitutive model behaviours are elastic-plastic Mohr-Coulomb for the deformable blocks, and Coulomb slip failure for the fault and granite contacts.

In all models a compressive tectonic setting is applied with boundary conditions representing an overall east-west shortening with σ_1 orientated at 90° (some models have a rotation of σ_1 to 112.5°) and the in-situ and boundary stress conditions correspond to around 7 km depth. These stress conditions are set at a ratio of $\sigma_1 / \sigma_2 = 1.2$ and $\sigma_3 / \sigma_2 = 0.8$, which are similar ratios to values used by Mair *et al.* (2000), Zhang & Sanderson (2002) and Stephens (2003). The imposed stresses ($\sigma_1 = 210$ MPa, $\sigma_2 = 175$ MPa, $\sigma_3 = 140$ MPa) are within reasonable ranges of CO₂ fluid inclusion entrapment pressures estimated for the Eastern Succession to be equivalent or greater than 200 MPa (e.g. Adshead, 1995; Rotherham *et al.*, 1998; Mark *et al.*, 2001) and general depths of ore formation for many deposits found in the district, e.g. Starra – 7.5 km (Rotherham *et al.*, 1998) and Lightning Creek – 6.25 km (Perring *et al.*, 2000),

correspond well to the estimated depth and stress applied to the models (σ_2 – 175 MPa at 7 km).

Models were run to equilibrium by examining the relationship between unbalanced forces and displacements. The unbalanced force indicates when a mechanical equilibrium state (or the onset of joint slip or plastic flow) is reached for a static analysis, and a model is in exact equilibrium if the net nodal force vector at each block centroid or grid point is zero. The maximum nodal force vector is also referred to as the “unbalanced” or “out-of-balance” force (Itasca, 2000b). The maximum unbalanced force will never exactly reach zero for a numerical analysis and the model is considered to be in equilibrium when the maximum unbalanced force is small compared to the representative forces in the problem. If the unbalanced force approaches a constant non-zero value, it is indicative of joint slip or block failure and plastic flow within the model. The unbalanced force for these models was monitored and a settling or constant non-zero value was seen by approximately 1500 steps (Fig. 5.9). Mohr circle diagrams were constructed to calculate changes in stress and failure criteria as a means of validating the numerical simulations (Fig. 5.10). History points were placed (see Fig. 5.3, 5.4) to monitor changes in physical parameters at particular locations throughout the procedure.

Physical properties chosen for both the rocks and joints materials (Table. 5.1) are similar to those of previous authors (e.g. Oliver *et al.*, 1990; Holyland & Ojala, 1997; Jiang *et al.*, 1997; Zhang & Sanderson, 2002; Stephens, 2003) and represent metasediments, granite, lithological contacts and faults. Granite

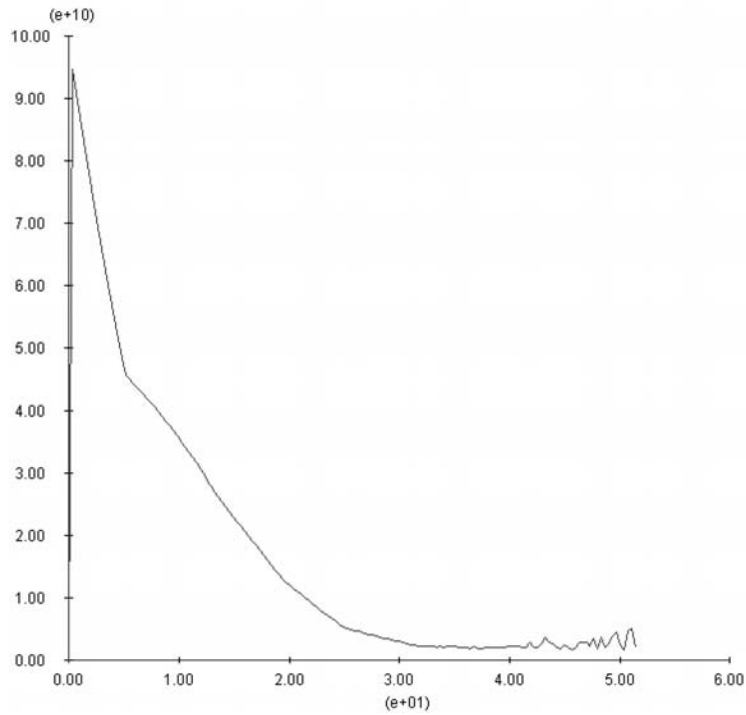


Figure 5.9. UDEDEC plot of unbalanced history at approx 1500 cycles for Model 1.

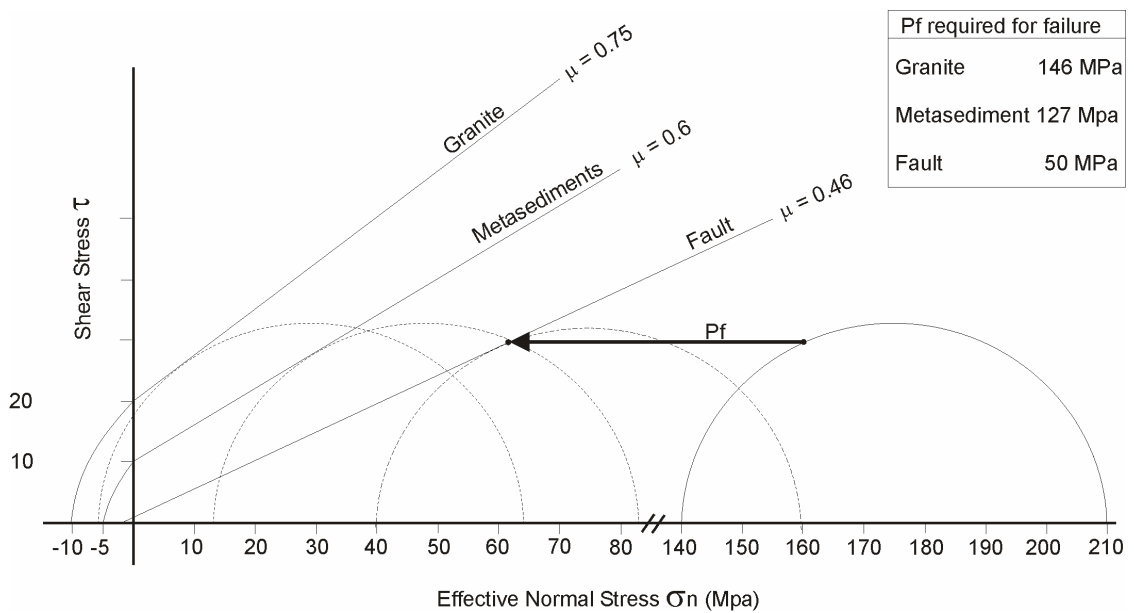


Figure 5.10. Mohr diagram with failure envelopes representing granite, metasediments and faults. Fluid pressure required for contact with the failure envelopes was calculated using a fixed differential stress value, as a baseline for comparison with model results.

intrusions were chosen to be the most competent rock type, and the lithological contacts were assigned a higher stiffness than the faults (Table. 5.1).

Table. 5.1. Physical properties of rocks, contacts and faults

Property	Granite	Metasediments	Lithological contact	Fault
Density (kg/m ³)	2650	2850	-	-
Bulk modulus (Pa)	49e9	25e9	-	-
Shear modulus (Pa)	27e9	25e9	-	-
Cohesion (Pa)	20e6	10e6	10e2	4e2
Tensile strength (Pa)	10e6	5e6	3e6	2e6
Friction angle (°)	37	31	35	30
Dilation angle (°)	5	4	5	5
Normal stiffness (Pa/m)	-	-	5e9	5e6
Shear stiffness (Pa/m)	-	-	1e5	1e3
Permeability factor (Pa/s)	-	-	238	300
Aperture at zero normal stress (m)	-	-	0.03	0.05
Residual hydraulic aperture (m)	-	-	0.01	0.03

5.5 Results Model 1

Four different variants of this model were run to examine the effects of rotation of σ_1 and the addition of fluid to the fractures. Certain aspects of the models have greater graphical clarity when examined in detail. The following section examines both the whole (large scale) model and smaller areas - Selwyn and Cloncurry regions (see Fig. 5.3, 5.4). Models were initially cycled in non-saturated conditions, which provided a comparison with subsequent saturated models in which high fluid pressures were established in the fractures. The variation of the orientation of σ_1 to the initial stress regime was also compared for both saturated and non-saturated conditions. Many aspects of the models were investigated, however, this contribution will focus on the criteria required for failure, mean stress (σ_m), minimum principal stress (σ_3), and differential stress ($\Delta\sigma$) values. On Mohr circle diagrams, failure may occur when effective stress conditions are such that the initial in-situ stress conditions are driven to

the failure envelope by the fluid pressure (P_f). The amount of P_f required for this to occur for a given stress state can be termed 'fluid pressure required for failure' and will be referred to from this point on as PF_f (Fig. 5.10).

5.5.1 **Model 1a:** no fluid pressure, E-W compression ($\sigma_1 = 090^\circ$)

Settling of this "dry" model was observed by ~1500 time steps (Fig. 5.9). The initial regional model displays values of mean stress (σ_m) generally ranging from ~170 MPa to 210 MPa, with the higher σ_m values being found around lithological contacts (Fig. 5.11a). On closer inspection of the Selwyn region, variations in σ_m (140 to 190 MPa) are observed with highest values on N/S trending faults, and lowest values on S/E to E/W trending faults and particularly intersections of S/E to E/W trending faults with all other orientations (Fig. 5.11b). Several areas show dilation (positive volumetric strain) which correspond well to low values of σ_3 (Fig. 5.12a), and within the Selwyn region these areas are to the west of the Gin Creek Granite (Fig. 5.12b). On the regional scale, $\Delta\sigma$ within the model varies by around 20 MPa, and several high and low areas are apparent (Fig. 5.13a). In the Selwyn region higher values of $\Delta\sigma$ are seen to the west of the Gin Creek granite and are associated with fault intersections (Fig. 5.13b). Lowest values of PF_f are primarily restricted to fault bends and intersections (Fig. 5.14a), and this is more apparent at the more detailed scale (Fig. 5.14b), which displays values of 60 to 100 MPa on most fault intersections, 20 to 60 MPa less than the surrounding metasediments and granite.

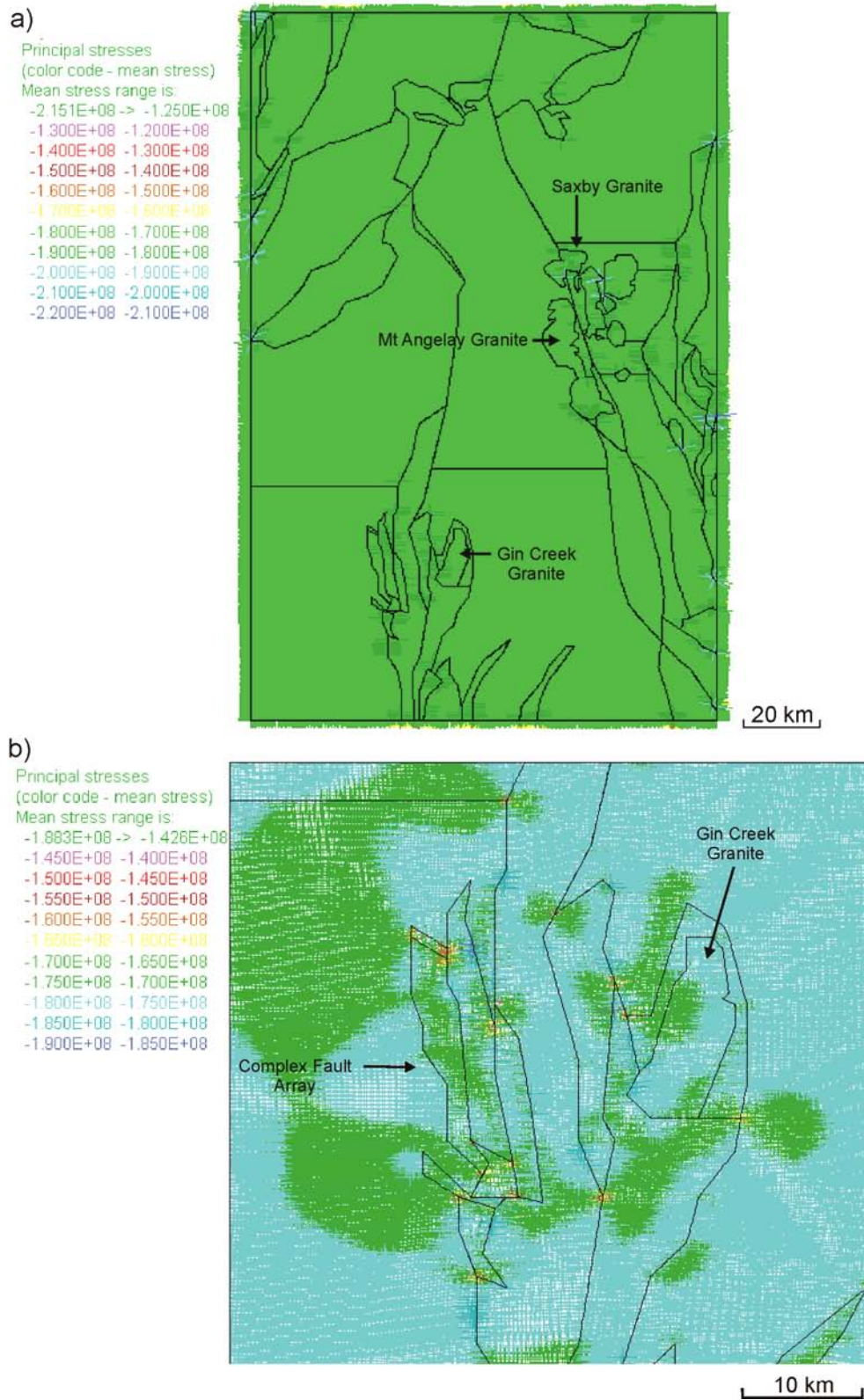


Figure 5.11. Plots of mean stress for Model 1a a) regional plot illustrating a homogenous mean stress in the majority of the model, with variations mostly noted on fault bends and granite contacts b) magnified plot of the Selwyn area showing both increased and decreased values on fault contacts.

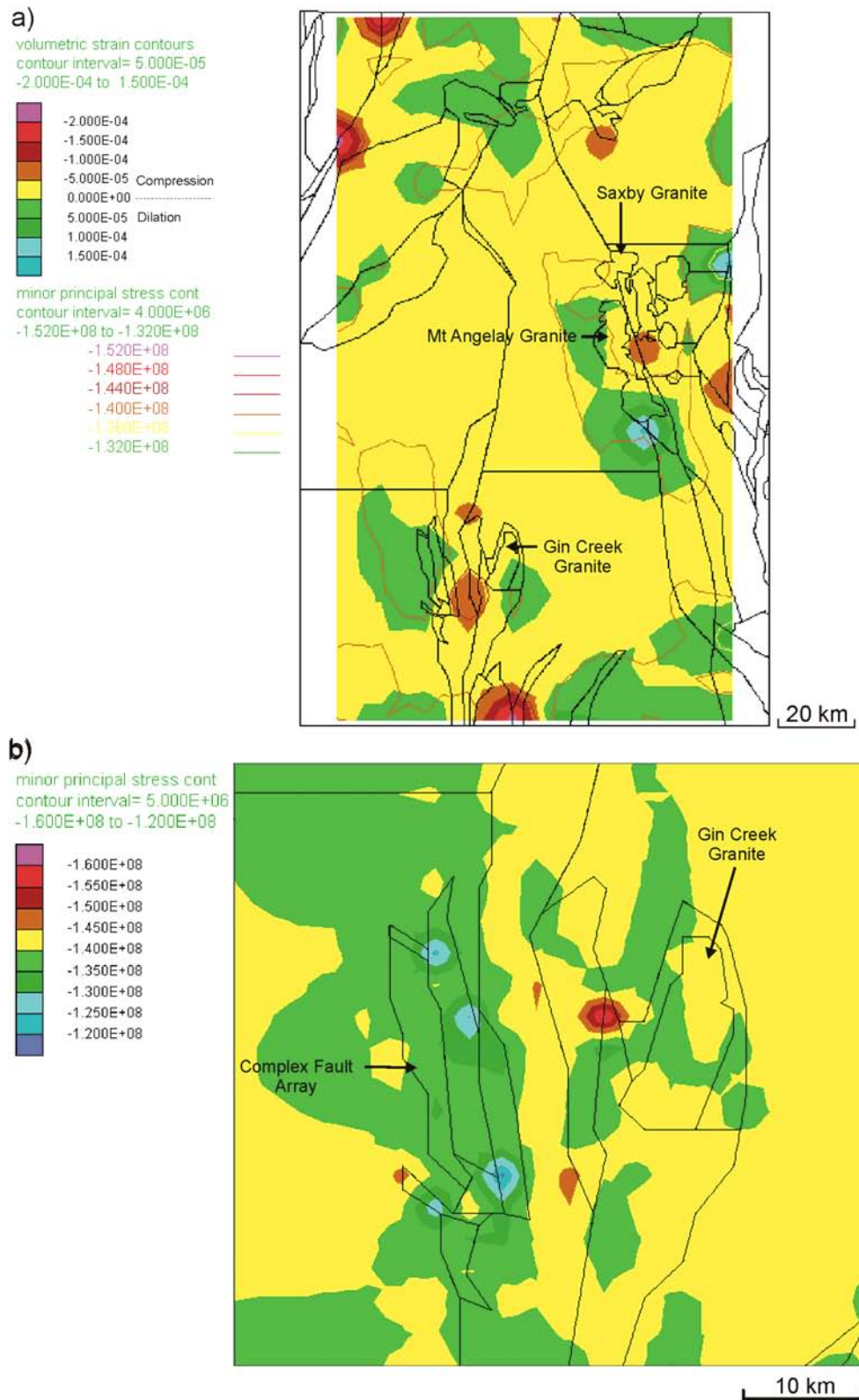


Figure 5.12. Plots of volumetric strain (dilation) and minor principal stress for Model 1a a) regional plot displaying several areas of low minimum principal stress values, which correspond to dilation or positive volumetric strain b) magnified plot of the Selwyn area showing low values at specific fault intersections west of the Gin Creek Granite.

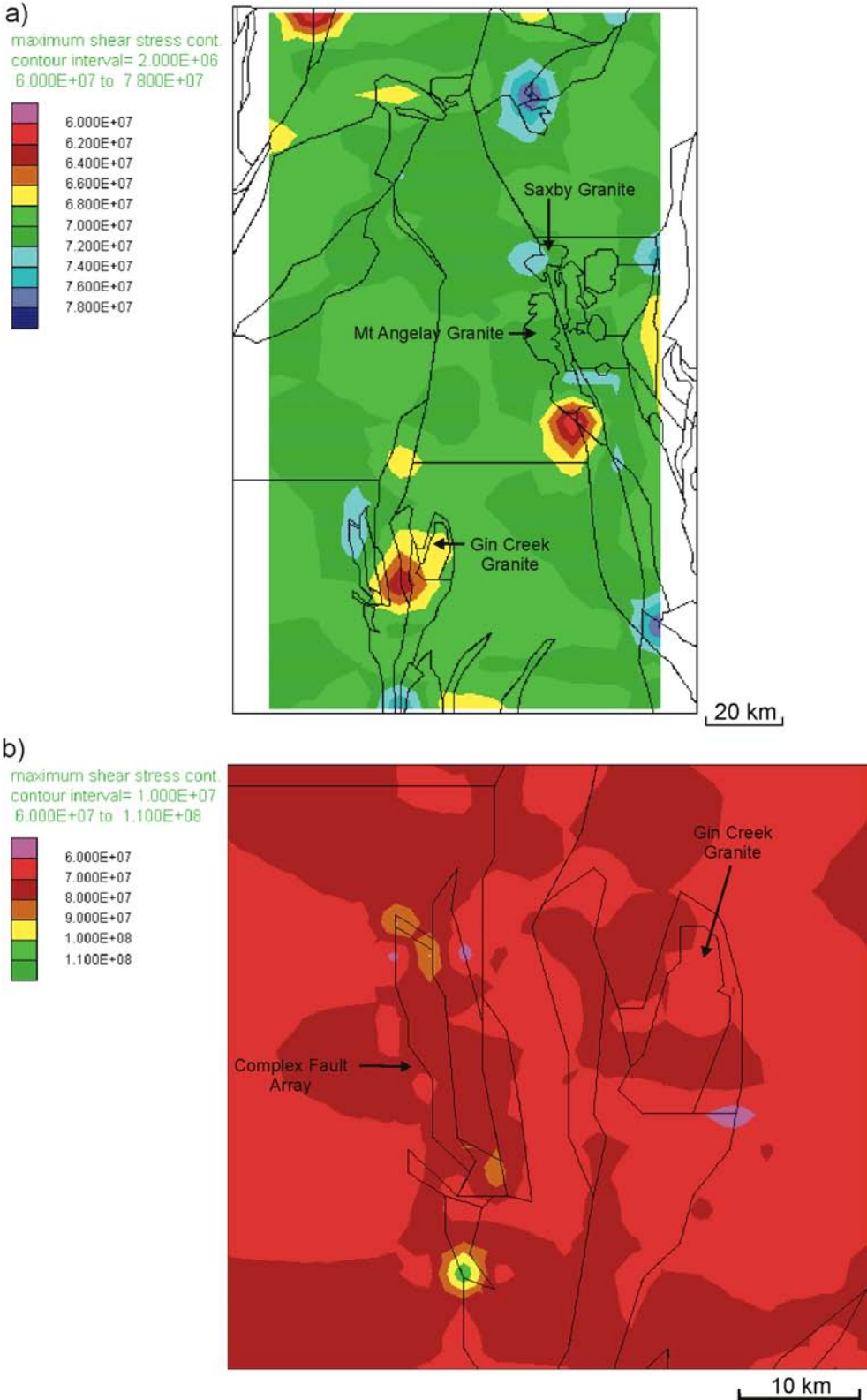


Figure 5.13. Plots of differential stress for Model 1a **a)** regional plot illustrating high values at the northern and southern ends of the Cloncurry fault and lowest values indicated at the base of the Mt Angelay granite and in the Selwyn region **b)** magnified plot of the Selwyn region.

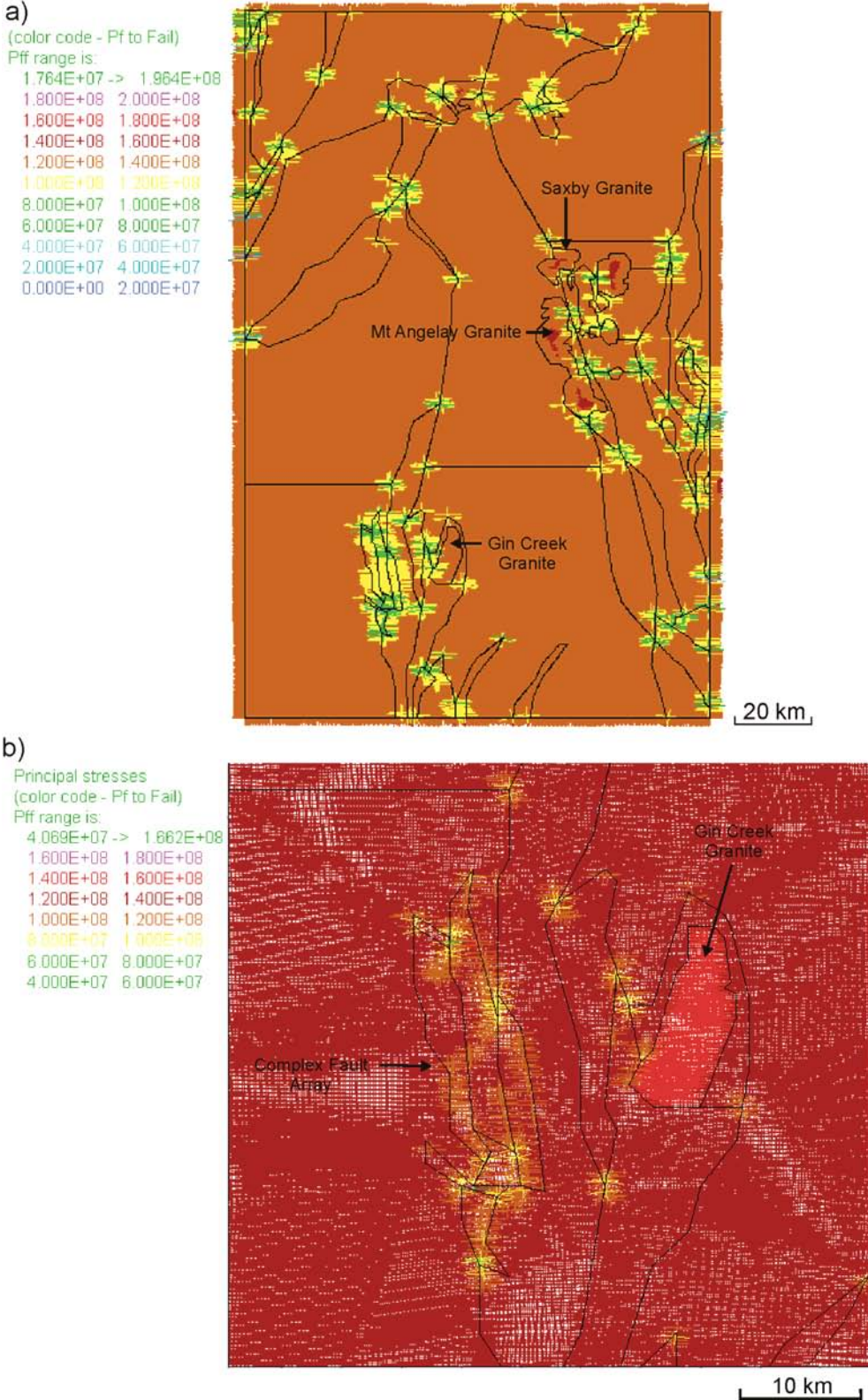


Figure 5.14. Plots of fluid pressure required for failure for Model 1a **a)** regional plot illustrating areas most likely to fail with minimum fluid pressures **b)** magnified plot of the Selwyn area showing several fault contacts and intersections most likely to fail.

In summary, this model displays preferential failure conditions around fault bends and intersections, particularly faults that are orientated at a low angle to σ_1 . Dilation and low σ_3 correspond well with areas that show lower values of σ_m and increased $\Delta\sigma$, which indicate suitable conditions for shear failure.

5.5.2 **Model 1b:** no fluid pressure, σ_1 orientated ESE-WNW (112.5°)

Rotation of σ_1 has little effect on σ_m , which displays similar values to the previous model, ranging from 170 to 200 MPa. The Selwyn region again displays lowest values on similarly orientated fault intersections (Fig. 5.15), relative to the previous model. However, values and overall distribution of σ_3 display a considerable variation from the previous model, with a decrease in some areas of up to 30 MPa (Fig. 5.16a). The distribution of low σ_3 in the Selwyn region highlights dilational areas in the southern end of the complex fault array to the west of the Gin Creek granite (Fig. 5.16b); again fault intersections appear to play an important role in this distribution. Regional distribution of $\Delta\sigma$ (Fig. 5.17a) is broadly similar to the previous model, with a low area at the southern end of the Mt Angelay granite, however, the Selwyn area does display a marked variation in values (Fig. 5.17b). Overall values of $\Delta\sigma$ are greater than in the previous model by up to 50 MPa. An overall decrease by up to 30 MPa in PF_f is seen in this model (Fig. 5.18a) and again fault intersections and bends in the Selwyn region display a higher potential for failure relative to other areas (Fig. 5.18b).

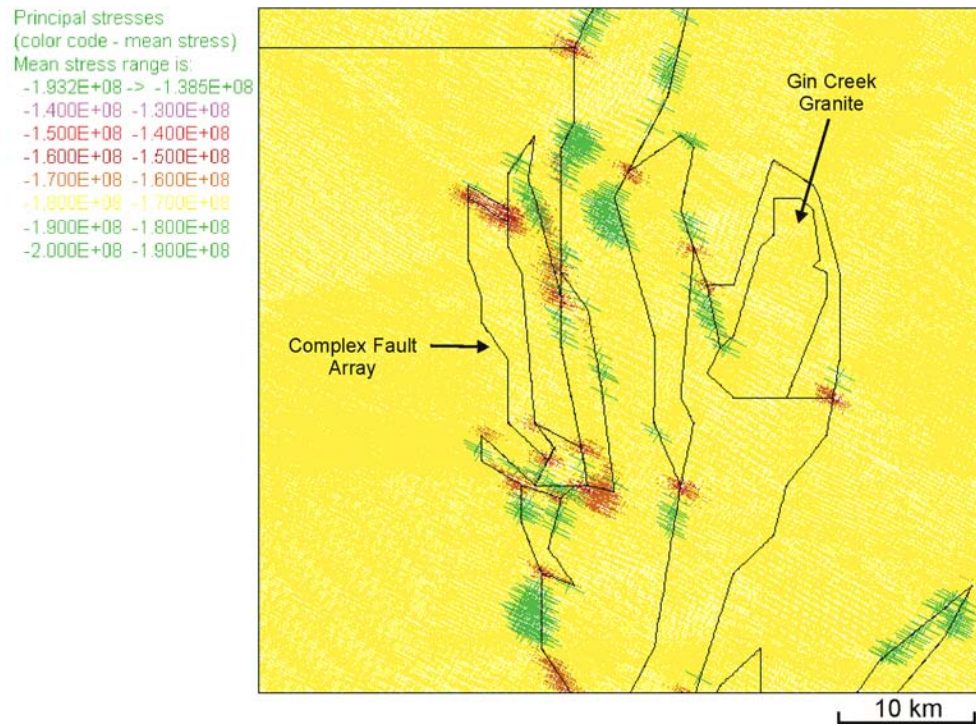


Figure 5.15. Plot of mean stress for Model 1b in the Selwyn region, illustrating homogenous values within the granite and metasediments, with large variations mostly noted on fault bends and granite contacts.

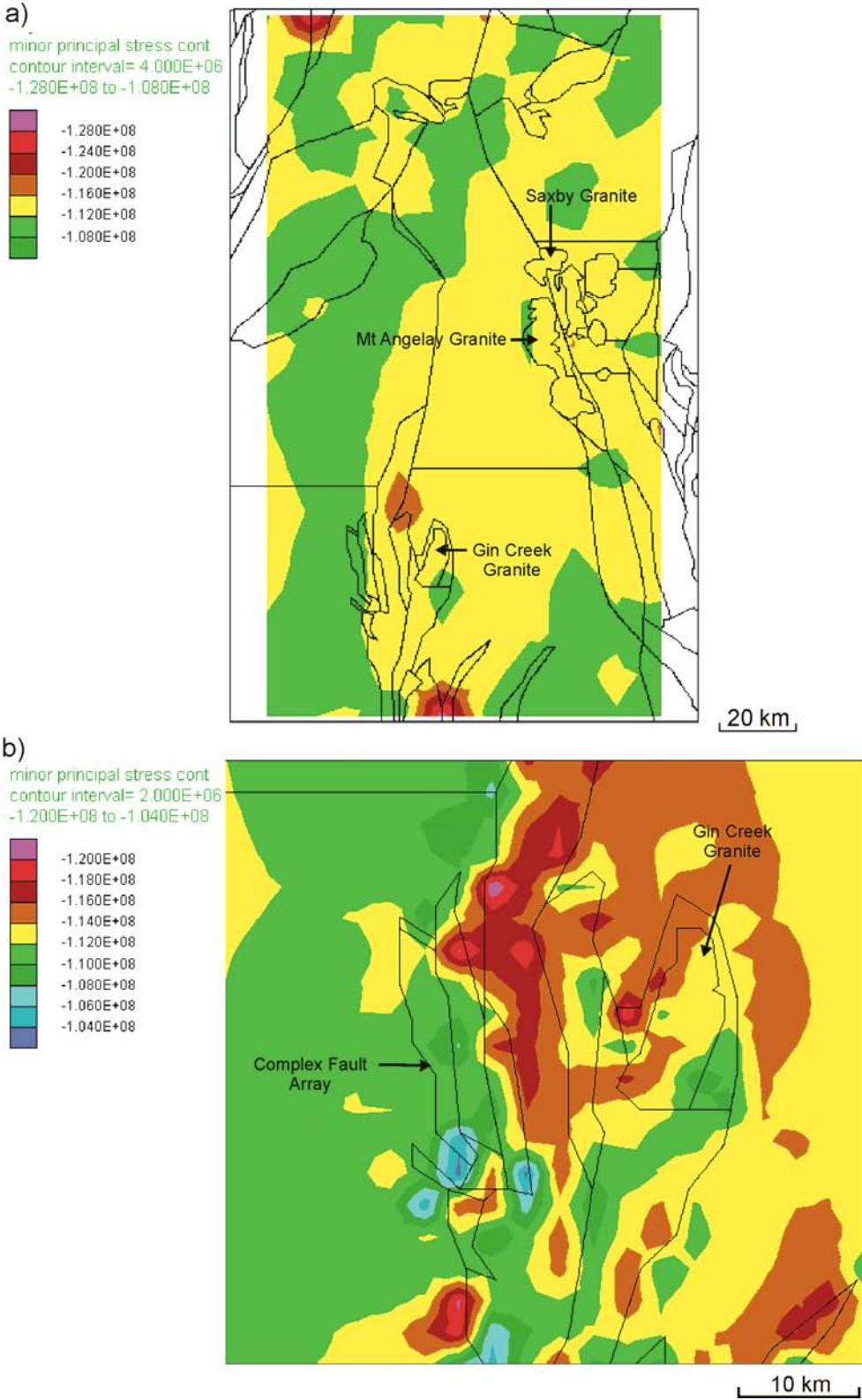


Figure 5.16. Plots of minor principal stress for Model 1b **a)** regional plot illustrating values which are lower than Model 1a **b)** magnified plot of the Selwyn area showing low values at specific fault intersections.

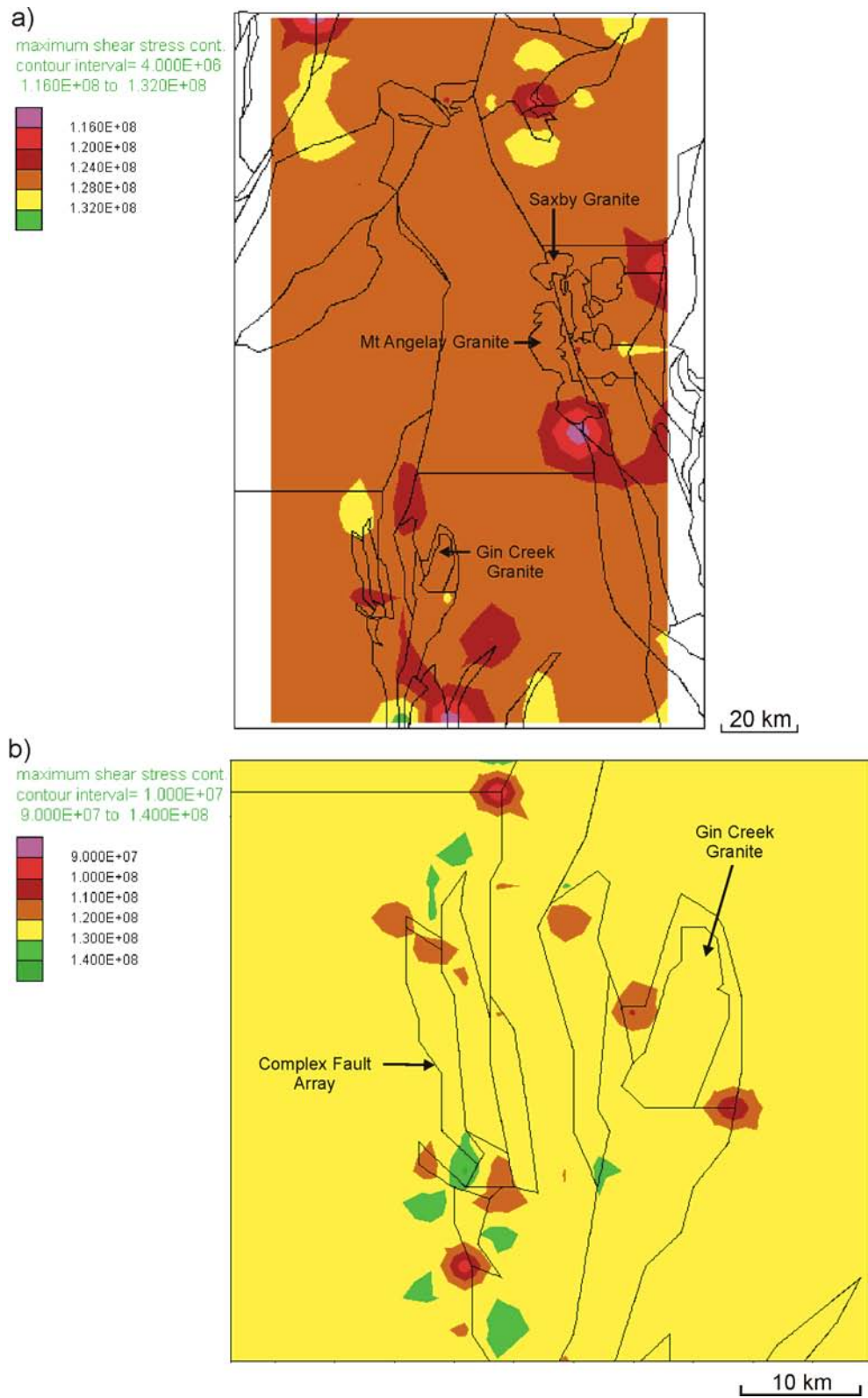


Figure 5.17. Plots of differential stress for Model 1b a) regional plot illustrating high values particularly in the Selwyn region b) magnified plot of the Selwyn region.

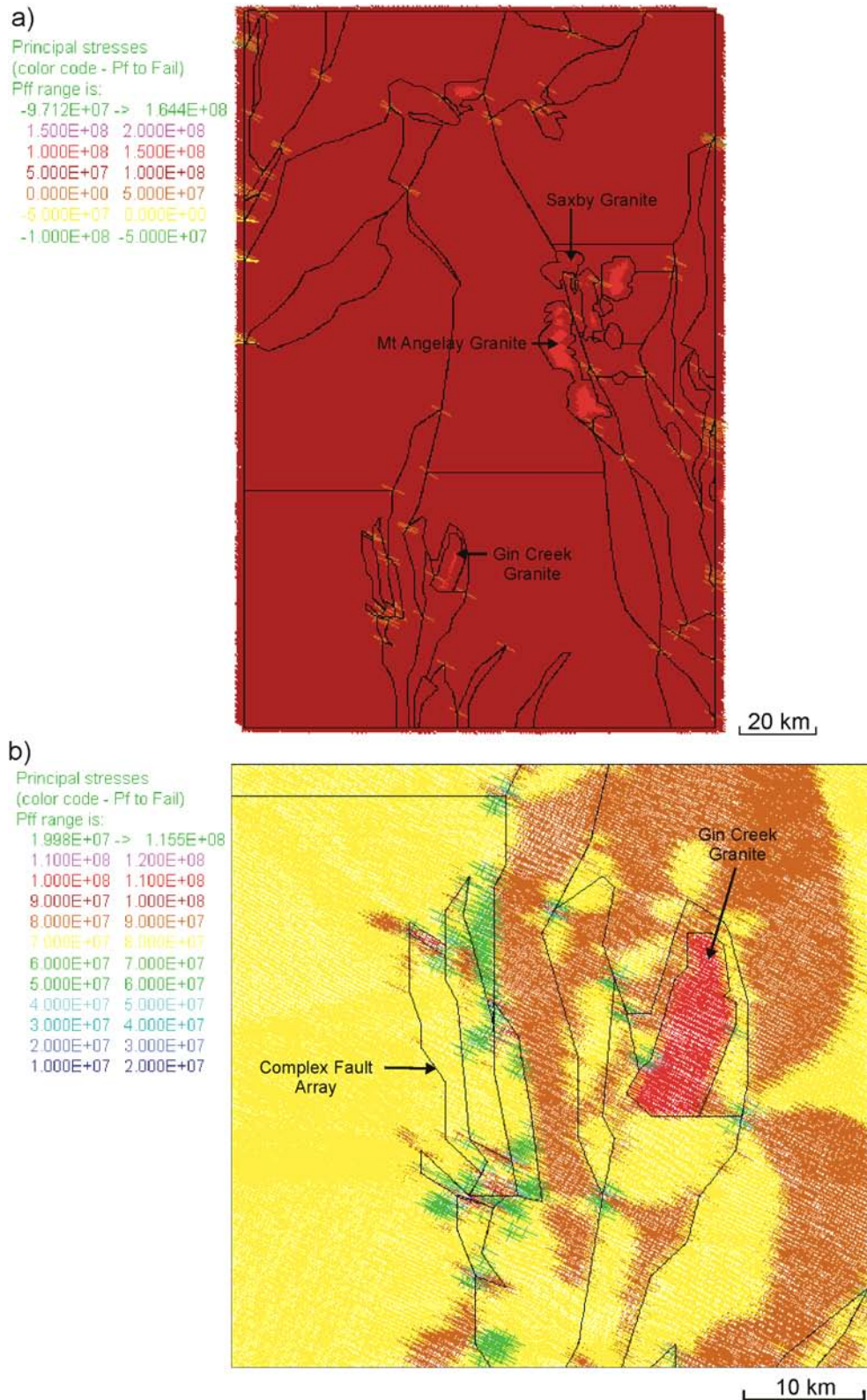


Figure 5.18. Plots of fluid pressure required for failure for Model 1b a) regional plot illustrating granites with highest values and overall values have lowered considerably from Model 1a b) magnified plot of the Selwyn area showing several fault contacts and intersections most likely to fail.

In summary, the change in orientation of σ_1 shows little effect on the values or distribution of σ_m . However, a considerable variation in the values and distribution of σ_3 relative to the previous model can be seen. The regional distribution of $\Delta\sigma$ remains broadly similar to the previous model, however higher values and a greater variation in the range of values is evident. The overall decrease in values of PF_f in this model can be linked or attributed to the increase of $\Delta\sigma$ in particular areas, which has shifted the Mohr circle towards the failure envelope.

5.5.3 **Model 1c:** fluid pressure, E-W compression ($\sigma_1 = 90^\circ$)

The introduction of fluid into model fractures results in a considerable variation in the distribution and values of σ_m from the previous models, with most faults and lithological contacts highlighted at a regional scale (Fig. 5.19a). The Selwyn region displays a clustering of higher σ_m around faults and granite contacts; with the west side of the Gin Creek granite showing the highest values (Fig. 5.19b). Regional distribution of σ_3 displays several distinctive areas that have low values, including the Selwyn and Cloncurry regions (Fig. 5.20a). The Selwyn region displays low values of σ_3 within the corridor separating the Gin Creek granite and the more complex fault array to the west, and low values are also seen around fault bends and intersections to both the east and west of the Gin Creek granite (Fig. 5.20b). These areas also correspond well to dilation and have increased values of $\Delta\sigma$ both on a regional scale (Fig. 5.21a) and at the Selwyn scale (Fig. 5.21b). The broader model scale displays two regions in the north that show increased dilation and low values of σ_3 and PF_f , otherwise the main areas of interest are in the Cloncurry region, the Mt Angelay granite and

areas in the southern half of the model (Fig. 5.22a). The Selwyn area again displays a distinct corridor with lowest values of PF_f (Fig. 5.22b).

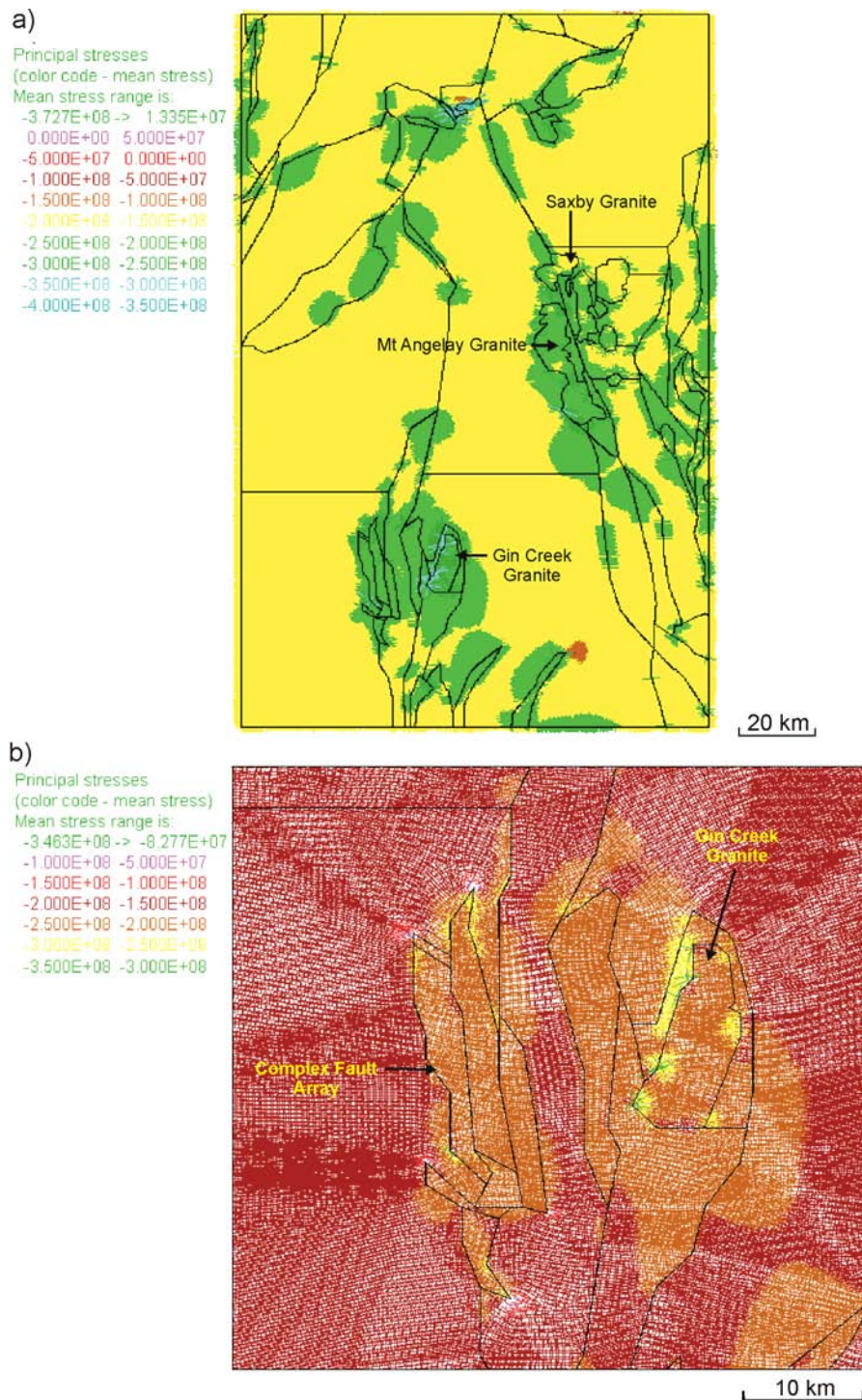


Figure 5.19. Plots of mean stress for Model 1c **a)** regional plot illustrating a considerable increase in mean stress values in comparison to earlier models, with variations mostly noted on fault bends and granite contacts **b)** magnified plot of the Selwyn area showing partitioning of stress in and around fault contacts.

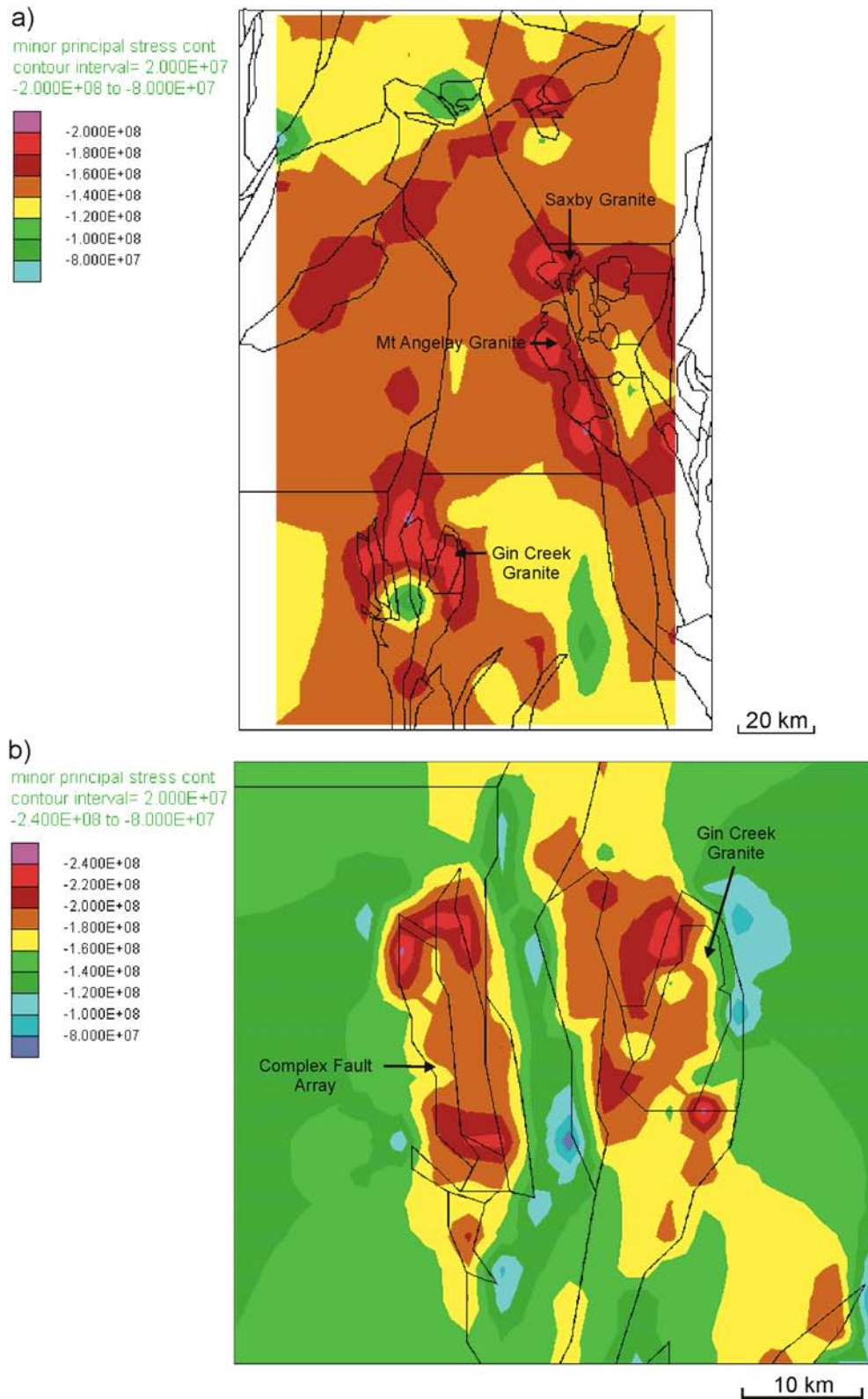


Figure 5.20. Plots of minor principal stress for Model 1c **a)** regional plot illustrating low values in the Cloncurry and Selwyn regions **b)** magnified plot of the Selwyn area showing low values at specific fault intersections and a north-south trending corridor between fault sets.

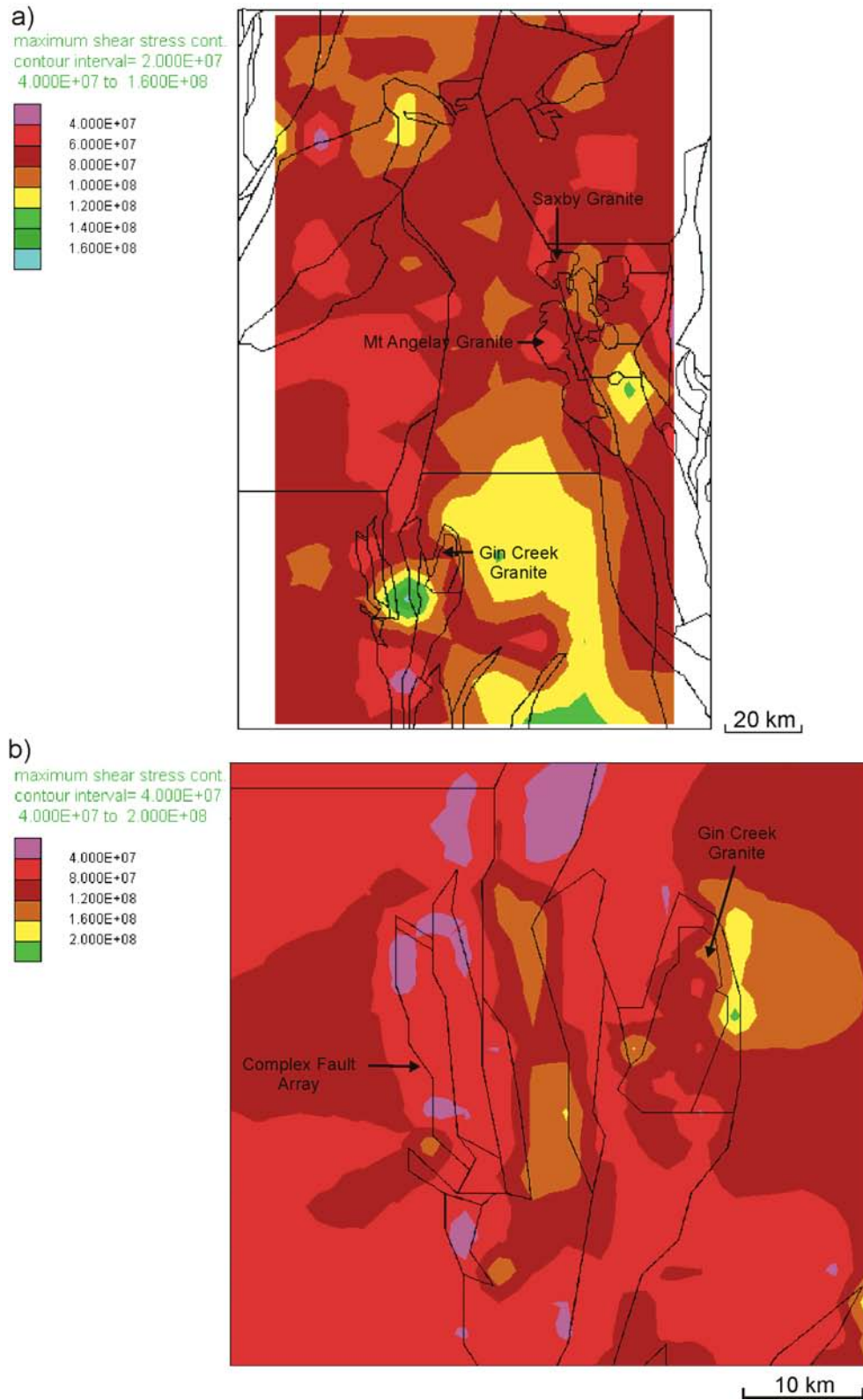


Figure 5.21. Plots of differential stress for Model 1c a) regional plot illustrating high values particularly in the Selwyn region b) magnified plot of the Selwyn region displaying a north-south trending corridor.

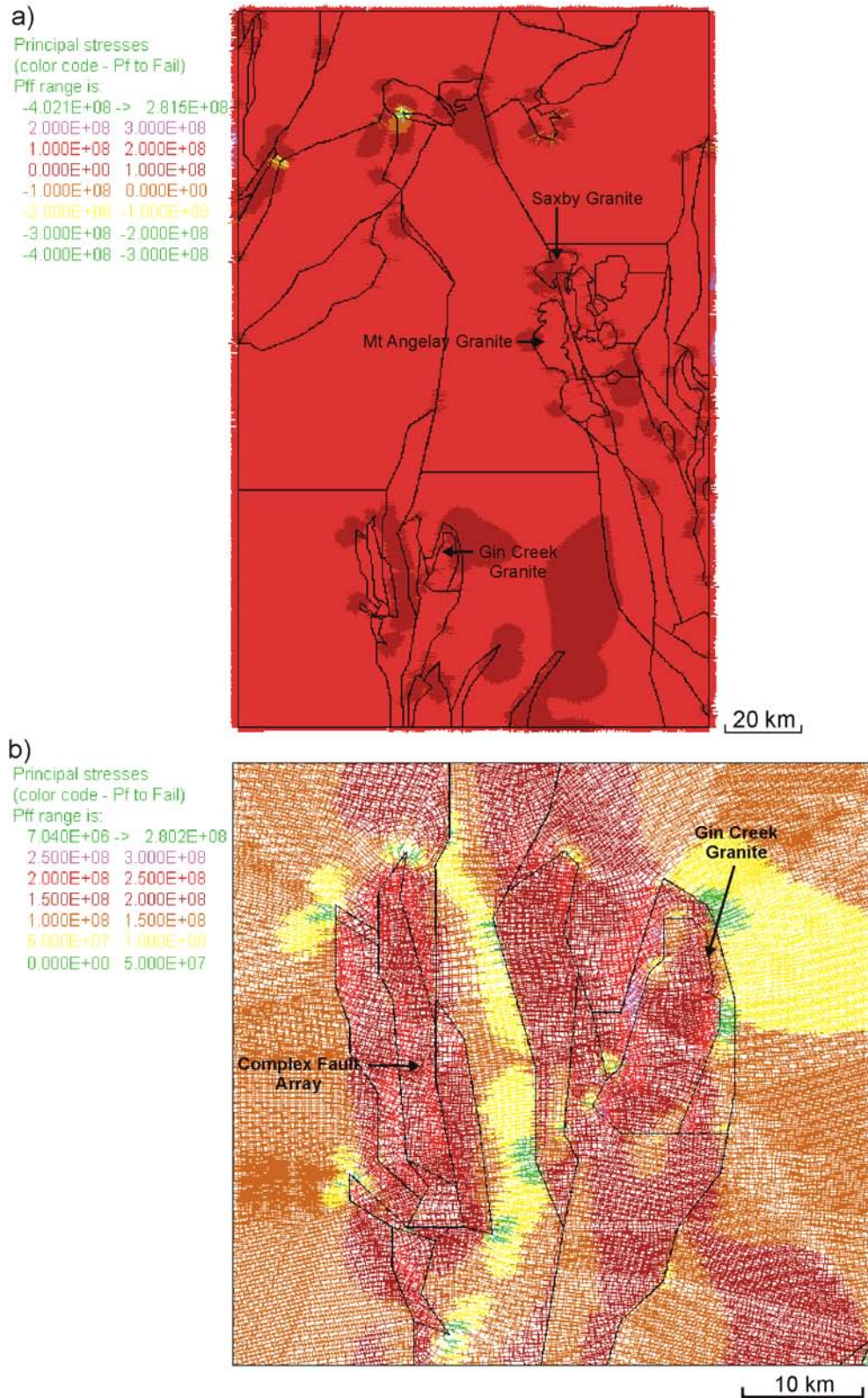


Figure 5.22. Plots of fluid pressure required for failure for Model 1c **a)** regional plot displaying main areas of interest in the Cloncurry and Selwyn regions **b)** magnified plot of the Selwyn area showing the partitioning within and around fault sets. Note: negative values indicate areas at yield.

In summary, the influence of fluid pressure within the fractures of the model results in a considerable variation in the distribution of σ_m and σ_3 from the previous models discussed. Low values of σ_3 correspond well to dilation and higher values of $\Delta\sigma$, and a distinct corridor separating the Gin Creek granite and the more complex fault array to the west is noticeable. The overall influence of fluid pressure drastically changes the distribution of all parameters, increases the overall range of values and decreases the values of σ_3 , σ_m , $\Delta\sigma$ and PF_f at several specific locations highlighted above.

5.5.4 **Model 1d:** fluid pressure, σ_1 orientated ESE-WNW (112.5°)

Rotation of σ_1 has an influence on the distribution of σ_m from the previous models, with highest values found around complex fault arrays and granites. Distinctive low values are apparent on the northern tip of the Mt Angelay granite, Cloncurry area and the southwest of the model (Fig. 5.23a). The Selwyn region displays highest values of σ_m on the northern end of the Gin Creek granite and lowest values on the west side of the complex fault array (Fig. 5.23b). On the regional scale, lowest values of σ_3 can be seen in the Cloncurry and Selwyn regions (Fig. 5.24a), with a notable decrease in values around fault arrays. In the Selwyn region there is a distinct change in distribution of σ_3 , with a noticeable area northwest of the complex fault array with lower values relative to the previous model (Fig. 5.24b). This area also corresponds to areas of high $\Delta\sigma$, as does the Saxby Granite region (Fig. 5.25a). The Selwyn region also indicates higher values of $\Delta\sigma$ (up to 80 MPa greater) than the previous model (Fig. 5.25b). Several areas in the north of the model indicate dilation and require minimum PF_f (Fig. 5.26a), and the Selwyn region

also shows areas of low PF_f , which correspond with both low σ_3 and high $\Delta\sigma$ (Fig. 5.26b). Overall, PF_f displays a larger range of values relative to the previous model, with specific areas indicating decreased values.

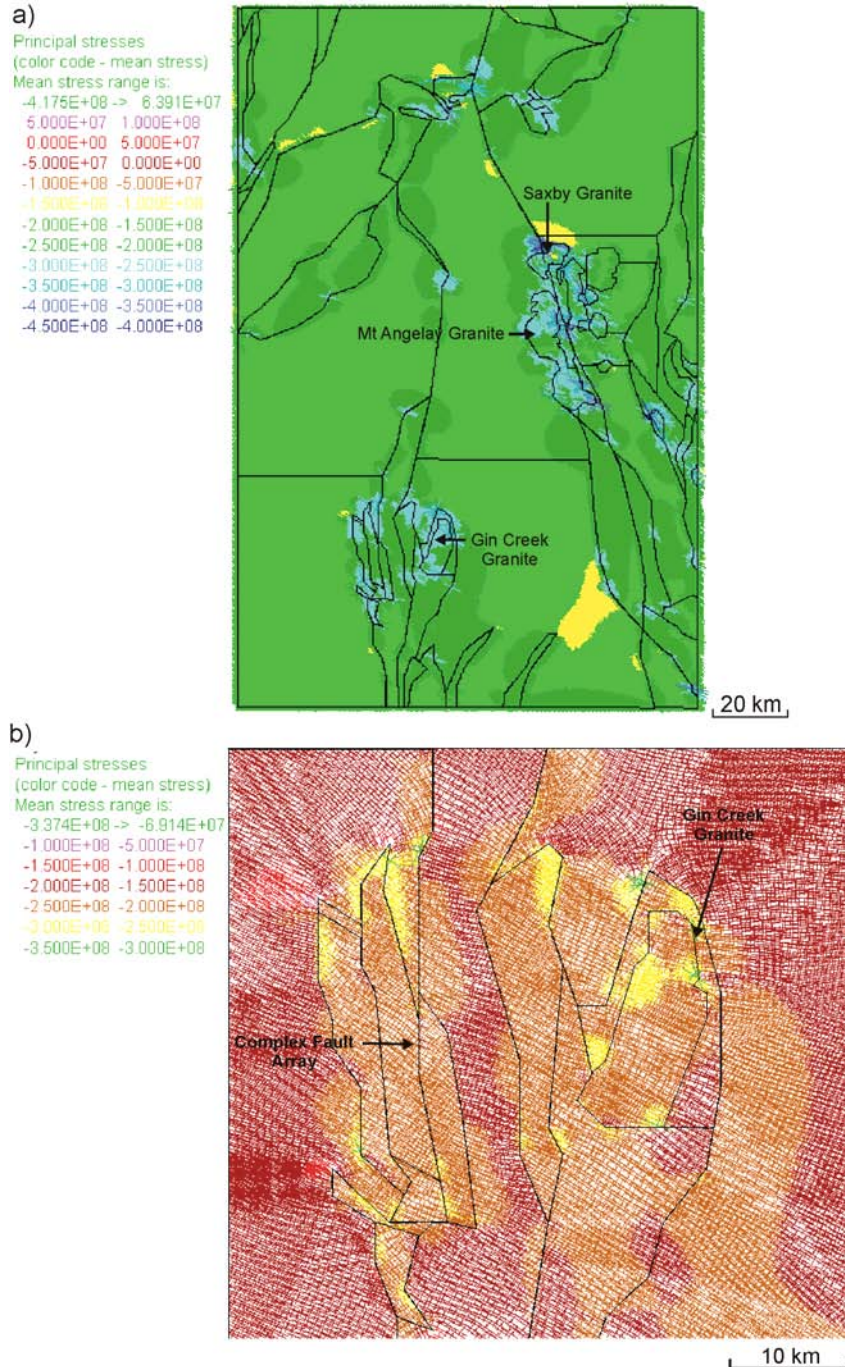


Figure 5.23. Plots of mean stress for Model 1d **a)** regional plot displaying similar mean stress values to the previous model **b)** magnified plot of the Selwyn area showing partitioning of stress in and around fault contacts. Highest mean stress values are associated with fault bends and around intersections.

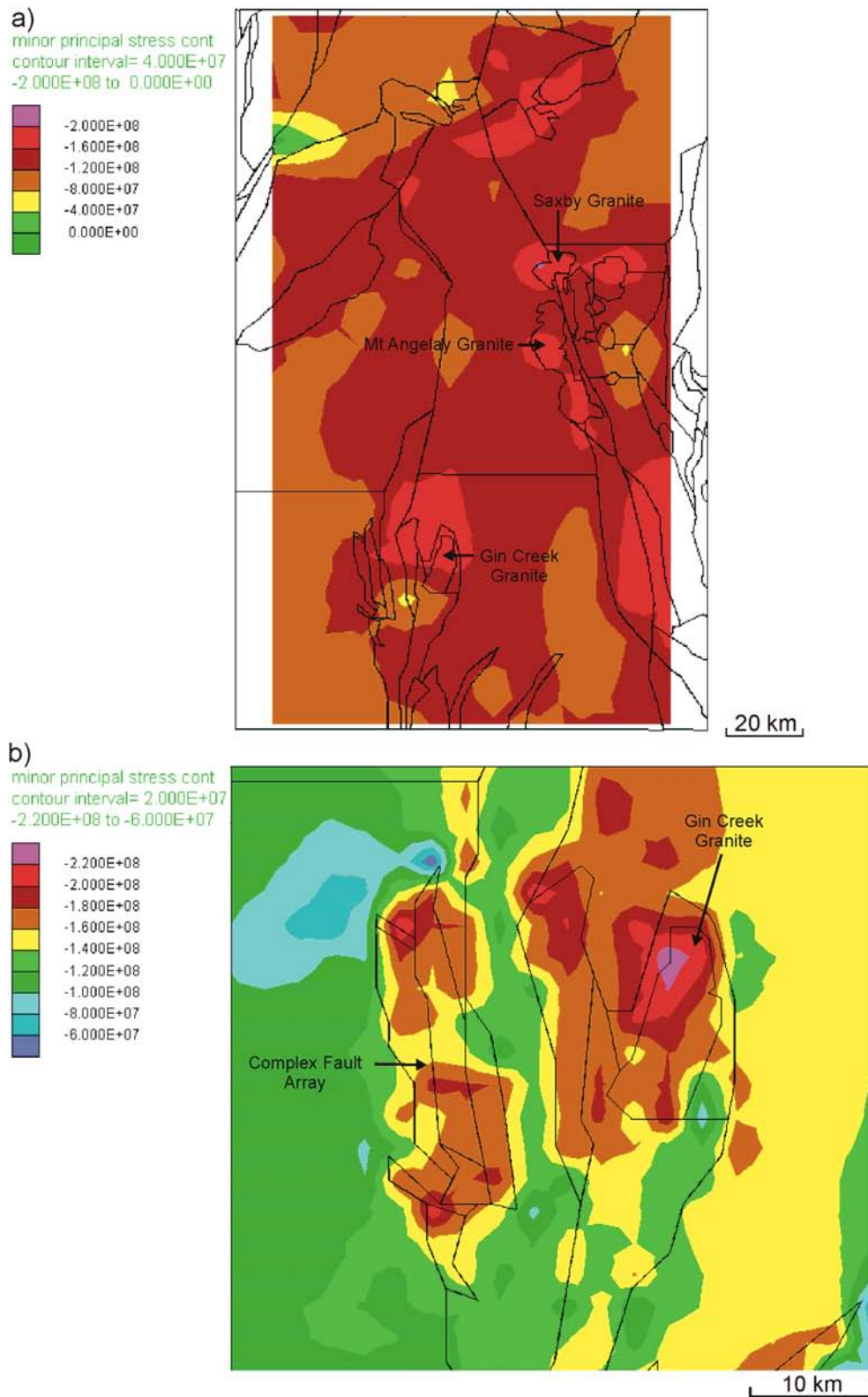


Figure 5.24. Plots of minor principal stress for Model 1d a) regional plot illustrating areas of low minimum principal stress in the Cloncurry and Selwyn regions b) magnified plot of the Selwyn area showing low values in an area northwest of the complex fault array.

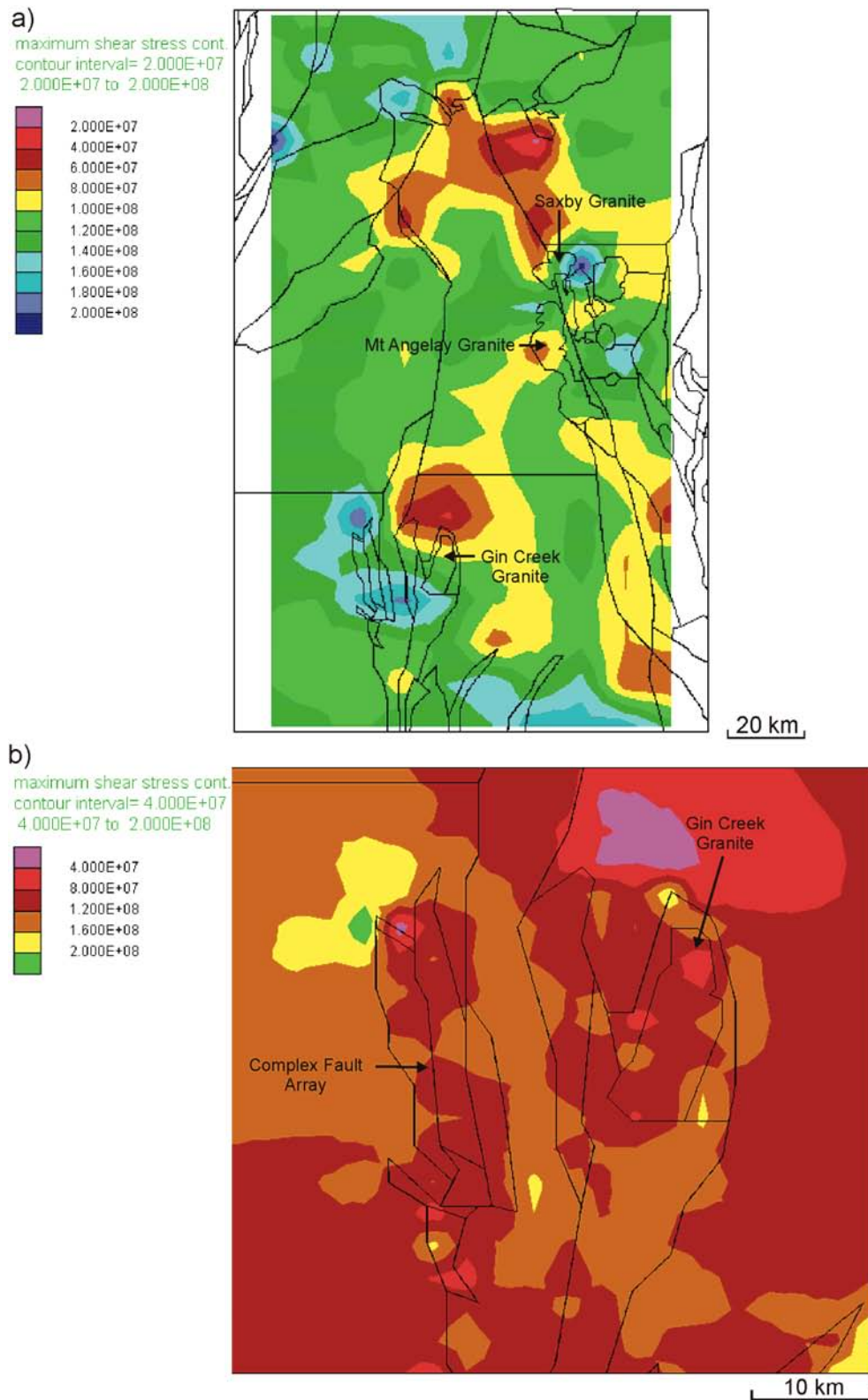


Figure 5.25. Plots of differential stress for Model 1d **a)** regional plot illustrating highest values around the Saxby granite and Selwyn region **b)** magnified plot of the Selwyn region again displaying a north-south trending corridor and an increase in values corresponding to low minimum principal stress from the previous plot.

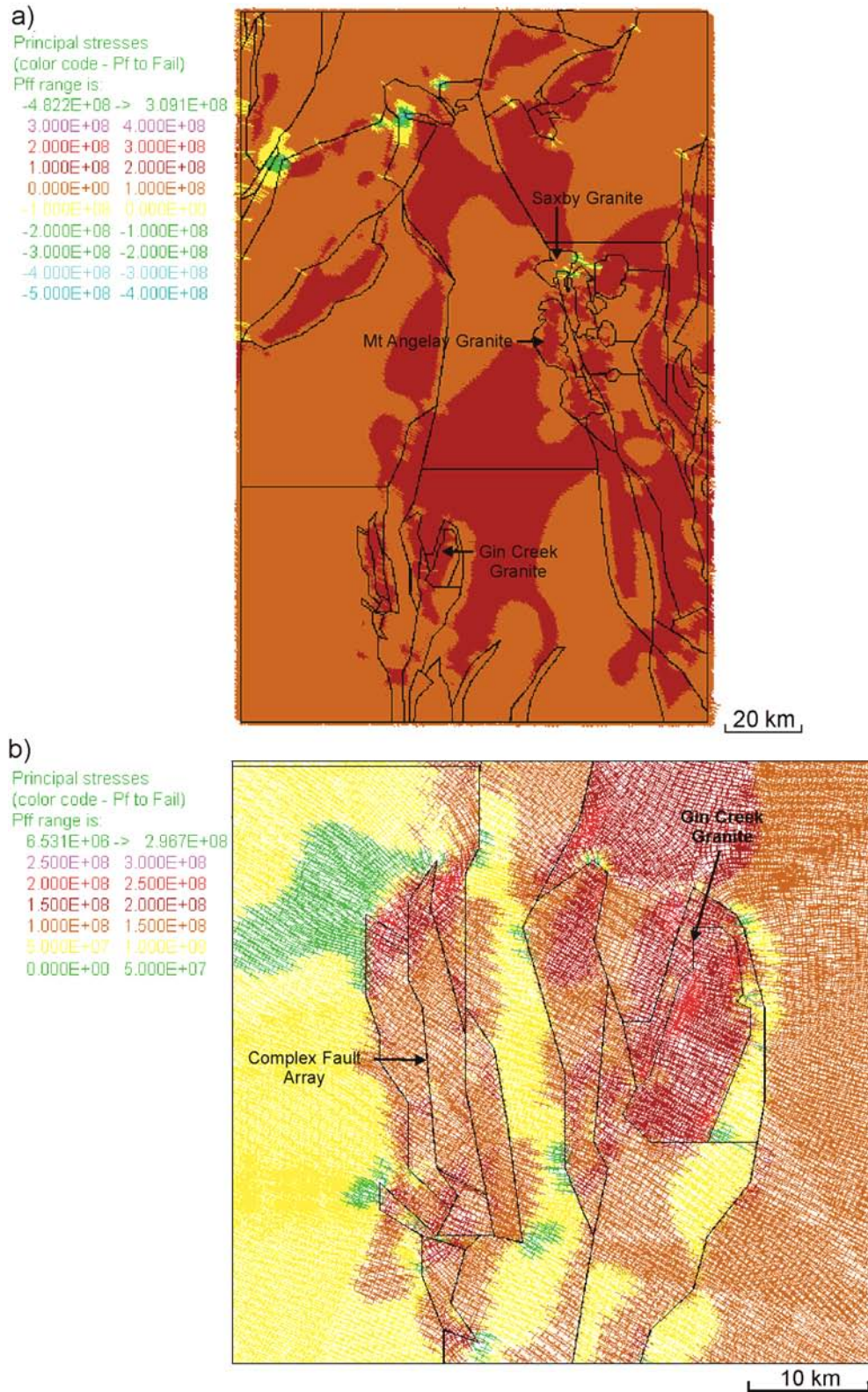


Figure 5.26. Plots of fluid pressure required for failure for Model 1d **a)** regional plot displaying areas of interest in the Saxby granite regions and west of the Cloncurry region **b)** magnified plot of the Selwyn area displaying areas of low PF_f which correspond with both low σ_3 and high $\Delta\sigma$.

In summary, the rotation of σ_1 and addition of fluid has had an influence on the distribution of the σ_m relative to the previous models. A distinct change in the distribution of σ_3 and $\Delta\sigma$ is also apparent, with an increase in the range of $\Delta\sigma$ and PF_f values.

5.6 Results Model 2

Four different variants of this model were run to examine the effects of rotation of σ_1 and the addition of fluid to the fractures. All conditions are the same as for Model 1; however, a more complex geometry and younger granite suites have been added, to simulate the effects of potential syn-mineralisation fluid flow and deformation after 1530 Ma.

5.6.1 Model 2a: no fluid pressure, E-W compression ($\sigma_1 = 90^\circ$)

The values of σ_m in the majority of the model correspond reasonably well with the values of Model 1a, and higher values of σ_m are preferentially located on fault intersections, bends and lithological contacts (Fig. 5.27a). Areas that show the largest variation in σ_m from Model 1a are primarily located on the model boundaries, which may suggest a boundary effect. The Selwyn region displays lowest values of σ_m at fault intersections, particularly with faults of S/E, E/W and E/NE orientations (Fig. 5.27b). The distribution of σ_3 shows both similarities to and variations from Model 1a, with similar patterns indicated by low values in the S/E and N/W corners of the model (Fig. 5.28a). However, a distinct low σ_3 area at the northern tip of the Squirrel Hills granite can be attributed to the additional fault geometry and competence contrasts of the granite and metasediments. Within the Selwyn region similarities to Model 1a are evident,

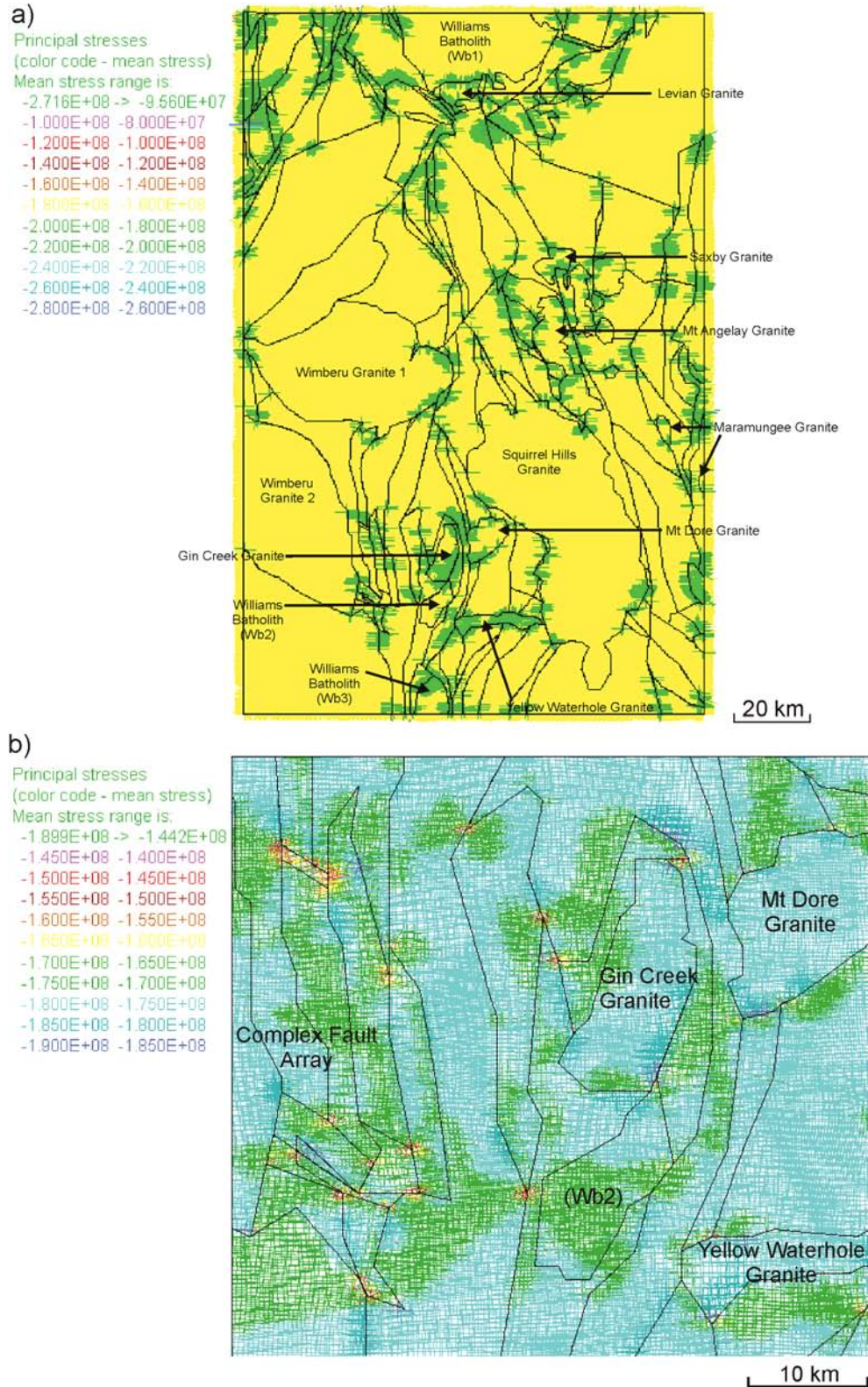


Figure 5.27. Plots of mean stress for Model 2a **a)** regional plot displaying higher mean stress values at many fault intersections and fault bends **b)** magnified plot of the Selwyn area showing partitioning of stress in and around fault contacts. Lowest mean stress values are associated with fault bends and around intersections.

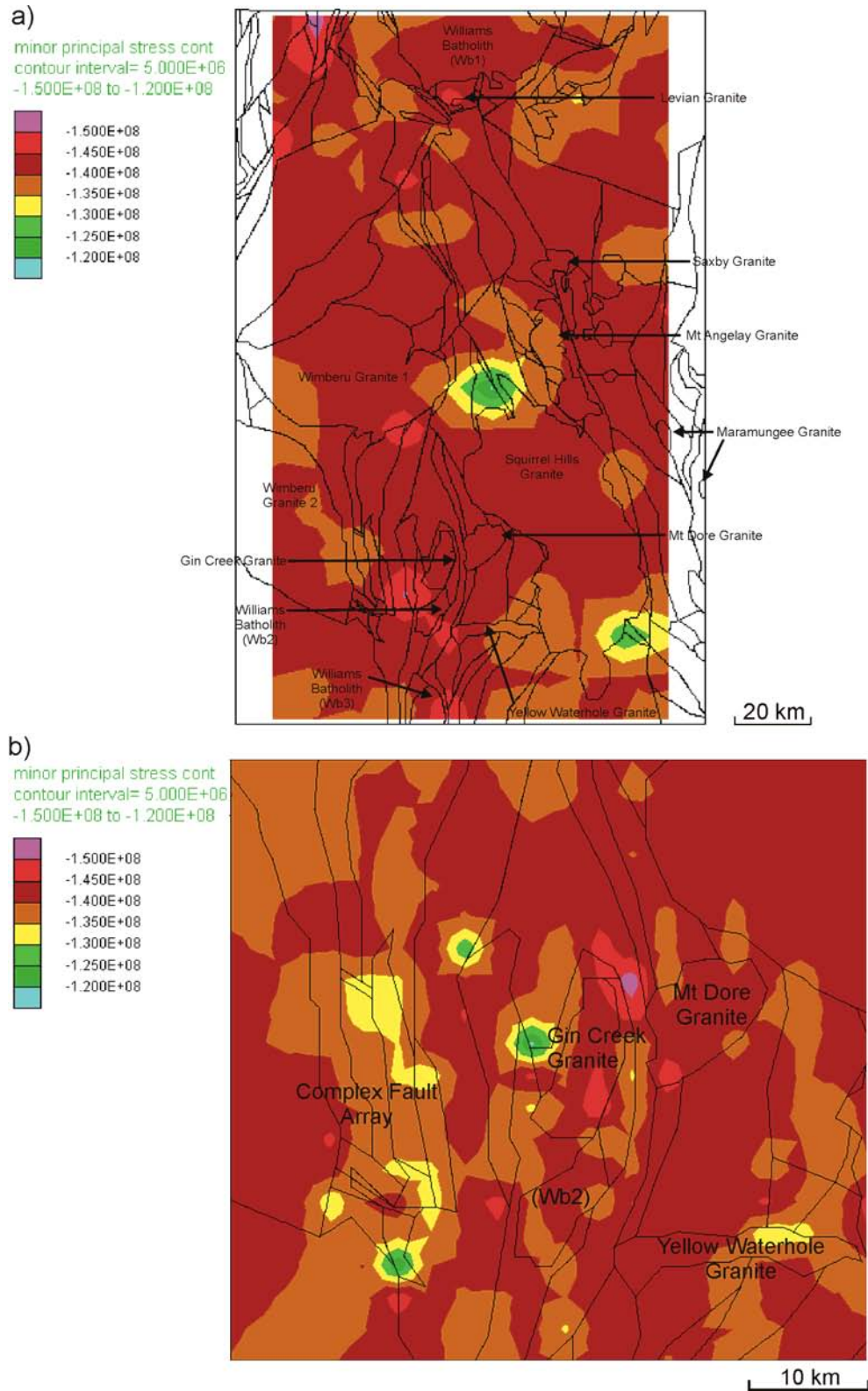


Figure 5.28. Plots of minor principal stress for Model 2a **a)** regional plot indicating lowest values at the north and south of the Squirrel Hills granite and highest values in the Selwyn region **b)** magnified plot of the Selwyn area showing low values at specific fault intersections and a notable high value between the Mt Dore Granite and the Gin Creek Granite.

indicated by low values of σ_3 associated with fault intersections in the complex fault array to the west of the Gin Creek granite (Fig. 5.28b). However, the fault array directly on the west side of the Gin Creek granite displays two areas of low σ_3 , which are situated at fault intersections. These two areas have values of around 30 to 40 MPa less than in Model 1a. The other obvious difference is the high σ_3 area at the NE corner of the Gin Creek granite and west of the Mt Dore granite. On the regional scale, values of $\Delta\sigma$ have a greater range (58 to 80 MPa) than in Model 1a, and areas of high $\Delta\sigma$ are evident at the north and south ends of the Squirrel Hills granite (Fig. 5.29a), and at the Selwyn scale high values of $\Delta\sigma$ are mostly related to fault intersections and bends (Fig. 5.29b). Lowest values of PF_f are found at fault intersections N to N/W of the Squirrel Hills granite and also near the Cloncurry region (Fig. 5.30a). The Selwyn region shows very similar distribution patterns to Model 1a; however values are around 20 to 30 MPa less (Fig. 5.30b).

In comparison to Model 1a (equivalent conditions), the addition of younger intrusions and a more complex fault pattern has a significant effect on many aspects of the model. The distribution and values of σ_m are relatively unchanged in comparison to Model 1a, and patterns at the smaller Selwyn scale are very similar. Variation is noted in the distribution and values of σ_3 however, which can be attributed to the more complex fault patterns and competence contrasts between the metasediments and intrusions. Both values and distribution of $\Delta\sigma$ are significantly different relative to Model 1a, and are more noticeable at the Selwyn scale. There are similarities in the distribution of

PF_f to Model 1a, but this model shows a significant variation in values, which are up to 30 MPa less.

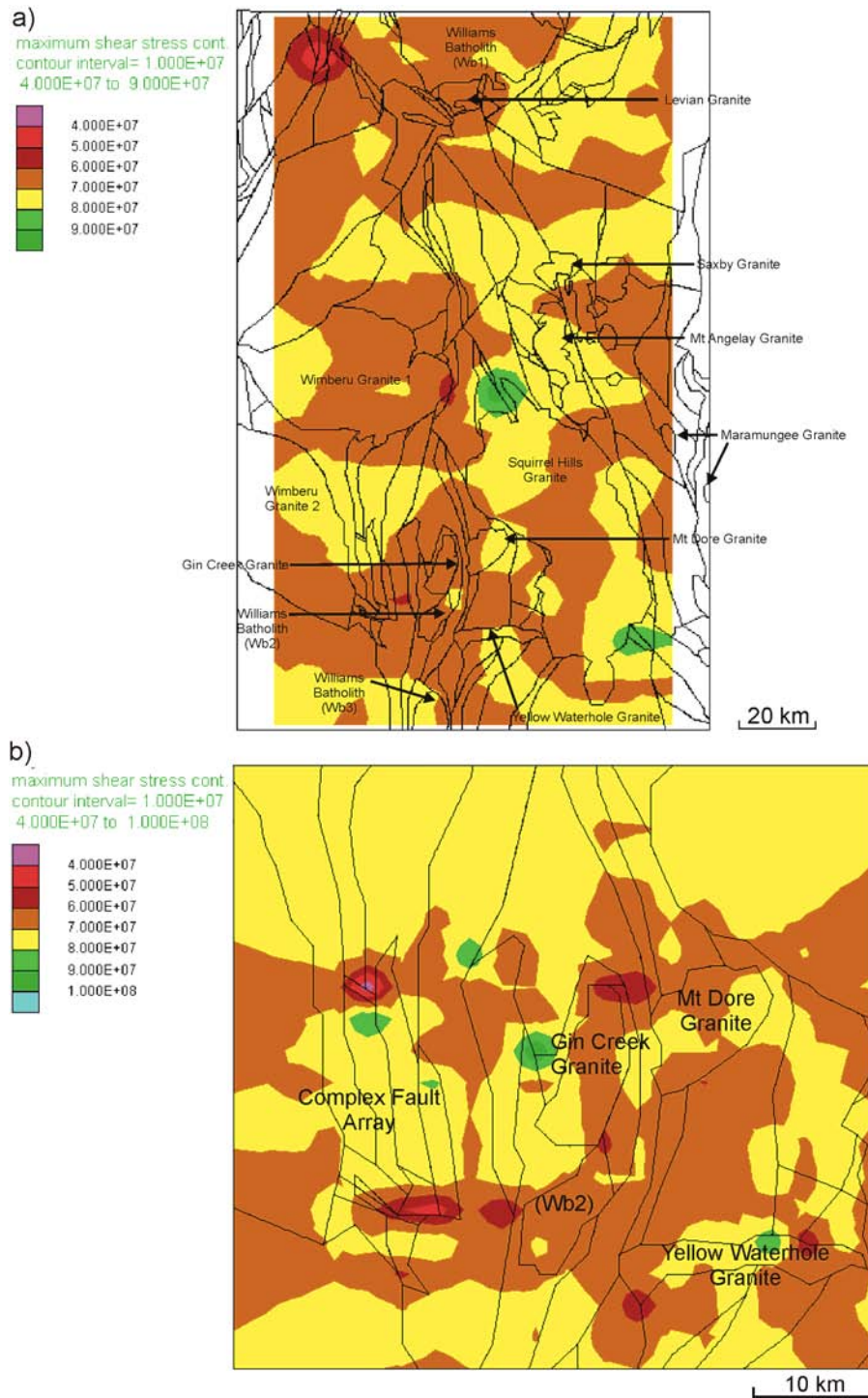


Figure 5.29. Plots of differential stress for Model 2a **a)** regional plot illustrating highest values located at the northern and southern ends of the Squirrel Hills granite **b)** magnified plot of the Selwyn region displaying several specific areas of both high and low values associated with fault intersections.

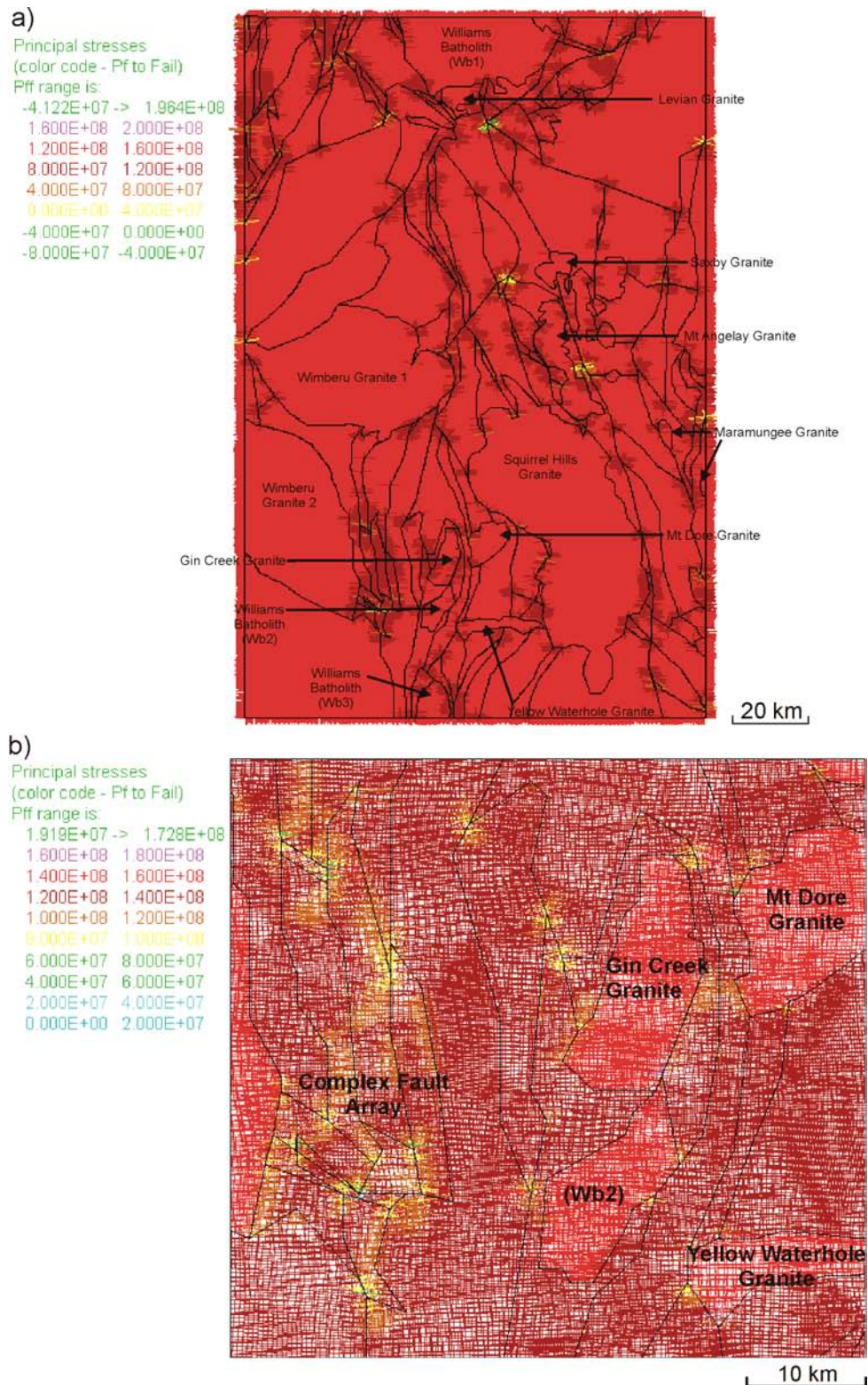


Figure 5.30. Plots of fluid pressure required for failure for Model 2a **a)** regional plot displaying higher potential for failure mostly on fault bends and intersections. Note areas with negative values at yield, which correspond to deposits at Greenmount, Great Australia and on the Cloncurry fault **b)** magnified plot of the Selwyn area displaying very low values for failure at fault intersections.

5.6.2 Model 2b: no fluid pressure, σ_1 orientated ESE-WNW (112.5°)

The rotation of σ_1 has little effect on the distribution or values of σ_m , in comparison to the previous model and to Model 1b (Fig. 5.31). On the regional scale, a variation is apparent in magnitude and distribution of σ_3 when compared to the previous model (Fig. 5.32a), and this is more noticeable (up to 50 MPa less) at the Selwyn scale (Fig. 5.32b). Higher values of $\Delta\sigma$ are noticeable in comparison to the previous model, as is the distribution of $\Delta\sigma$ at both the regional and Selwyn scales. At the regional scale, areas of high $\Delta\sigma$ are most apparent at the northern and southern ends of the Squirrel Hills granite (Fig. 5.33a), and in the south are more prevalent in the complex fault array to the west of the Gin Creek granite and the east side of the Williams batholith (WB2) to the south (Fig. 5.33b). No major change relative to the previous model is noted in the PF_f on a regional scale (Fig. 5.34a), however an apparent compartmentalised pattern of PF_f emerges at the smaller scale (Fig. 5.34b), as a result of stress partitioning between intrusive bodies and fault arrays.

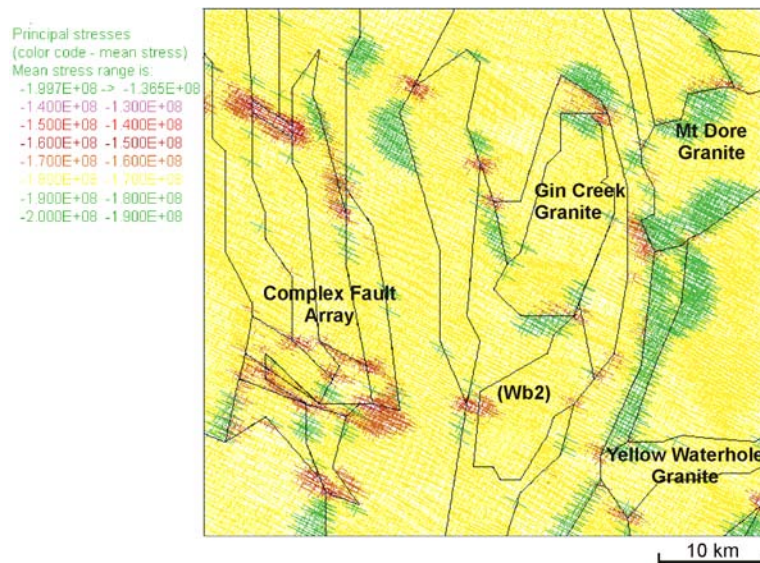


Figure 5.31. Plot of mean stress for Model 2b in the Selwyn region, illustrating a modified stress distribution from Model 1b, particularly around the northern and eastern ends of the Gin Creek Granite.

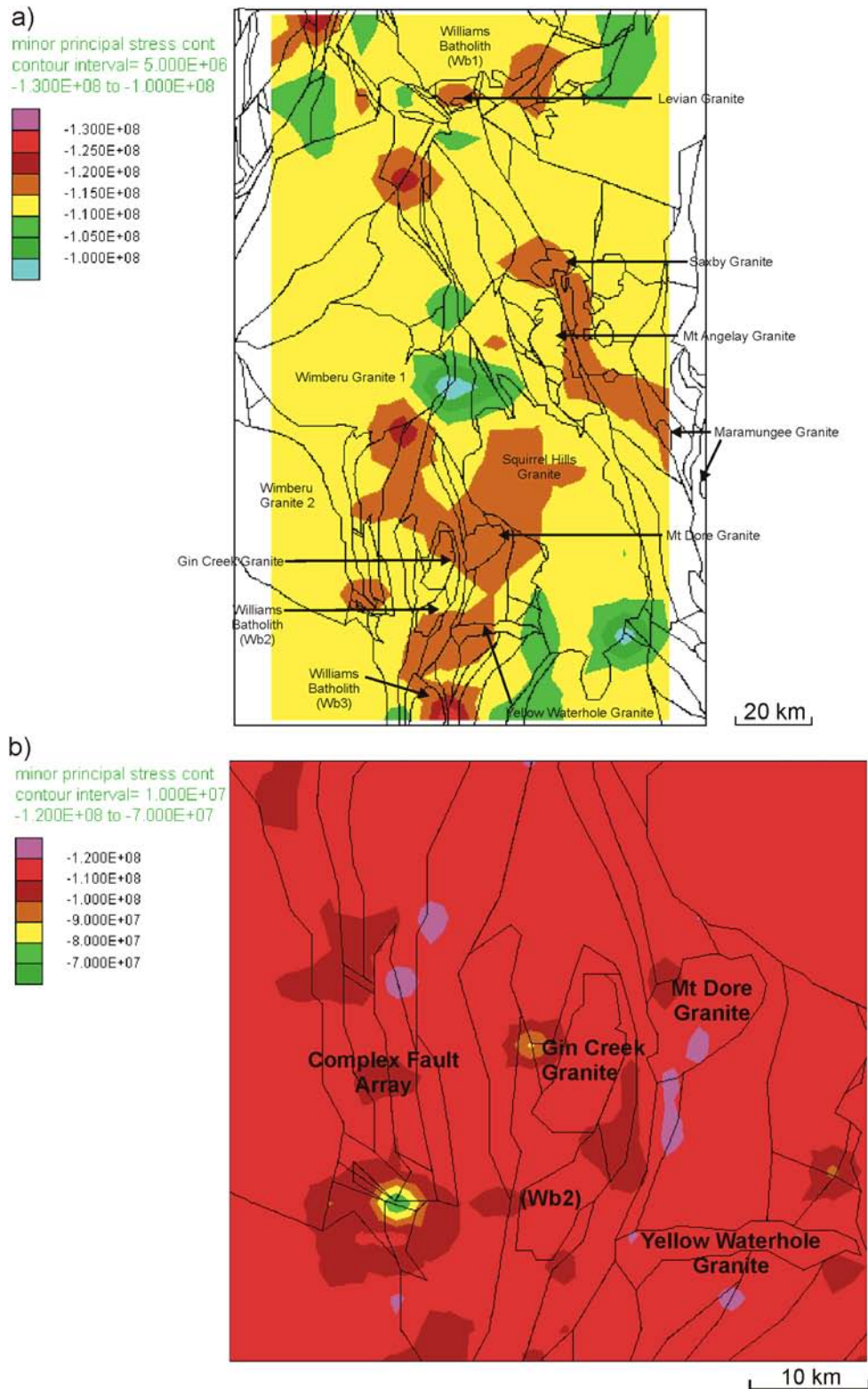


Figure 5.32. Plots of minor principal stress for Model 2b a) regional plot indicating lowest values at the northern and southern ends of the Squirrel Hills Granite and the eastern side of the Wimberu granite b) magnified plot of the Selwyn area showing isolated low values to the west and south-west of the Gin Creek Granite. Values are considerably lower than the previous model.

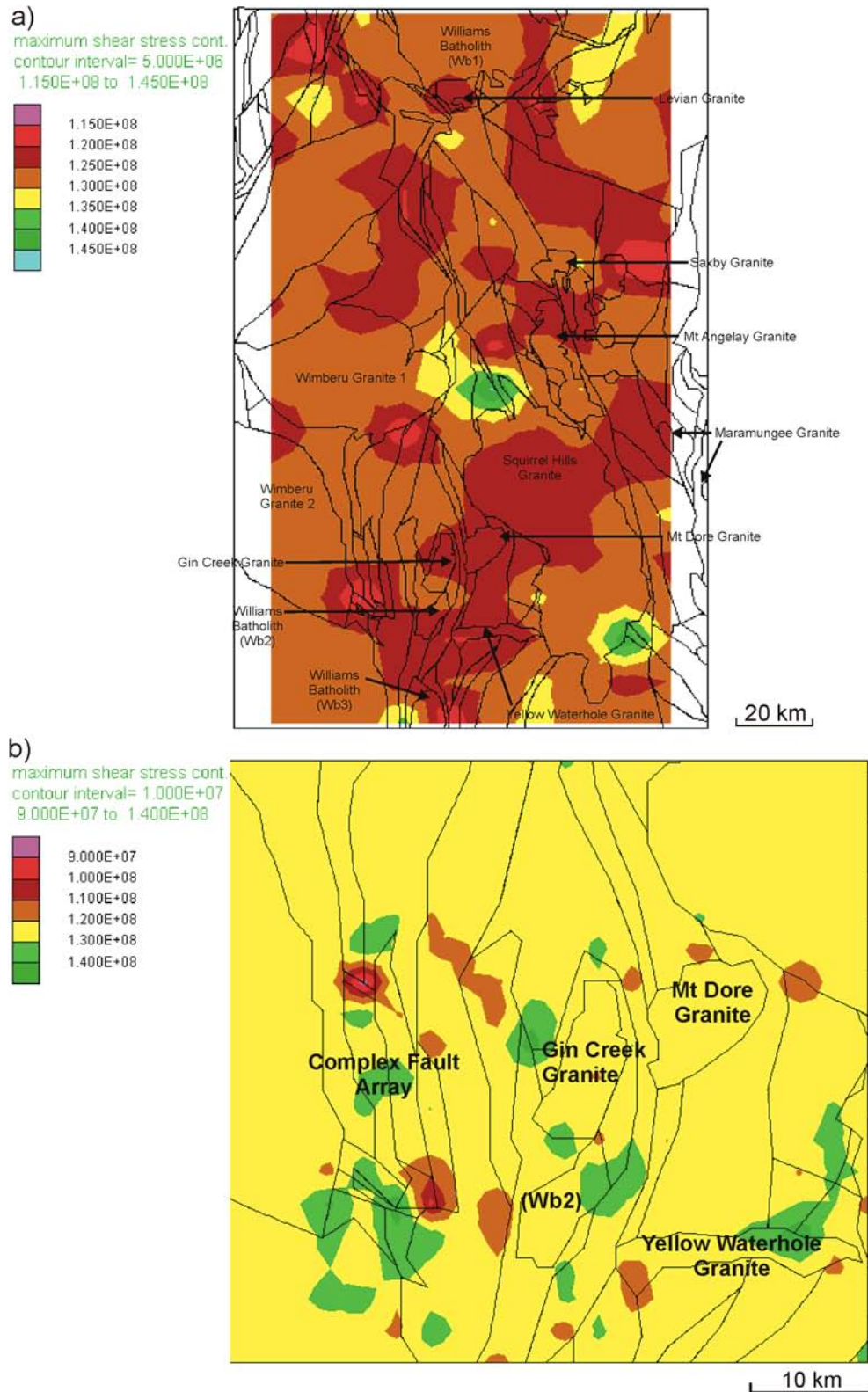


Figure 5.33. Plots of increased differential stress for Model 2b in comparison to the previous model **a)** regional plot illustrating high values particularly in the northern and southern ends of the Squirrel Hills Granite **b)** magnified plot of the Selwyn region with high values again associated with fault intersections.

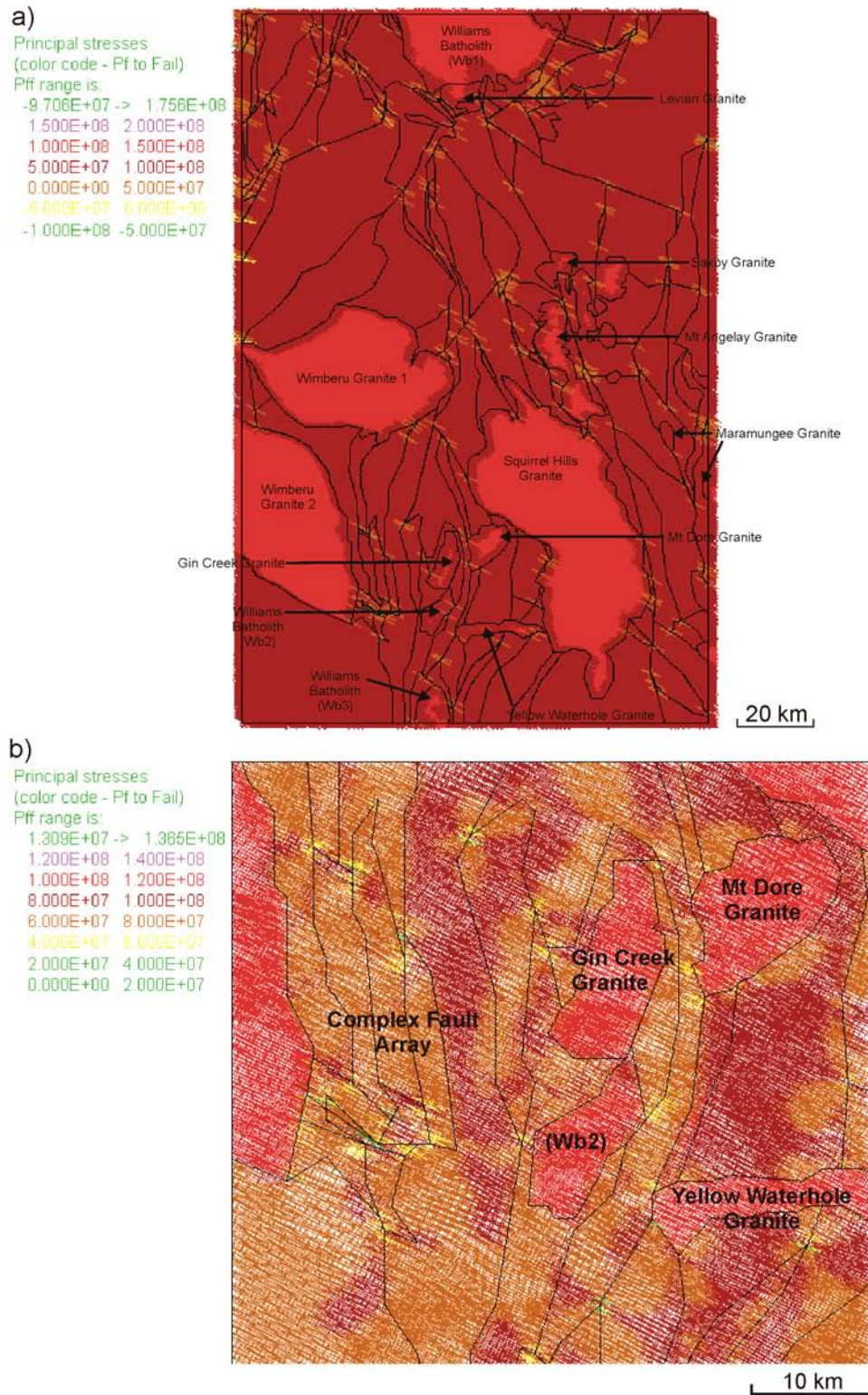


Figure 5.34. Plots of fluid pressure required for failure for Model 2b, showing an overall decrease in values from the previous model a) regional plot displaying a distinct variation between granites and metasediments b) magnified plot of the Selwyn area displaying very low values for failure at fault intersections and a compartmentalised pattern emerging. Note: negative values indicate areas at yield.

In summary, no significant variation on the magnitude of σ_m is noted relative to Model 1b, although there are minor effects on the distribution of σ_m surrounding some of the new granites and faults. There is a considerable variation in the magnitude and distribution of σ_3 relative to the previous model. The regional distribution of $\Delta\sigma$ remains broadly similar to the previous model, however values generally increase. Overall a decrease in values of PF_f and significant compartmentalisation of PF_f is seen in this model.

5.6.3 **Model 2c:** fluid pressure, E-W compression ($\sigma_1 = 90^\circ$)

The introduction of fluid into the model fractures results in a considerable variation in the distribution and magnitude of σ_m relative to Model 2a, with highest values concentrated around granite contacts in the Cloncurry and Selwyn regions, and around the northern parts of the Squirrel Hills granite (Fig. 5.35a). The Selwyn region also displays a significant change in distribution of the magnitude of σ_m , with a notable partitioning of stress between fault blocks (Fig. 5.35b). Two distinct areas of low σ_3 are evident in the regional model, west of the Gin Creek granite and at the southern tip of the Squirrel Hills granite (Fig. 5.36a) with values around 20 MPa less than in Model 2a. At the Selwyn scale a significantly different distribution of σ_3 is apparent with low values associated with fault bends and intersections (Fig. 5.36b) which do not correspond to similar areas in Model 2a. On the regional scale, $\Delta\sigma$ is distinctly different from the previous two models, showing highest values in the Selwyn region and the northern tip of the Mt Dore granite (Fig. 5.37a). The Selwyn region displays highest values of $\Delta\sigma$ in the corridor between the Gin creek and Mt Dore granite and on the Squirrel Hills granite contact north of the Mt Dore granite (Fig.

5.37b). Minimum PF_f on the regional scale is more apparent around the Cloncurry region, the Selwyn region and the southern tip of the Squirrel Hills granite (Fig. 5.38a) and two distinct corridors can be seen near the Gin Creek and Mt Dore granite. This is more obvious at the Selwyn scale, which displays two distinct corridors of low PF_f anastomosing between the more competent granite bodies and compartmentalised by fault arrays (Fig. 5.38b).

In summary, the influence of fluid pressure within the fractures of the model results in a distinct variation in the distribution of σ_m and σ_3 relative to Model 2a. Low values of σ_3 correspond well to dilation and these areas correspond to areas of increased values of $\Delta\sigma$. Within the Selwyn region two distinct corridors, separating the Mt Dore and Gin Creek granite and the more complex fault array to the west, show high values of $\Delta\sigma$ and low values of PF_f .

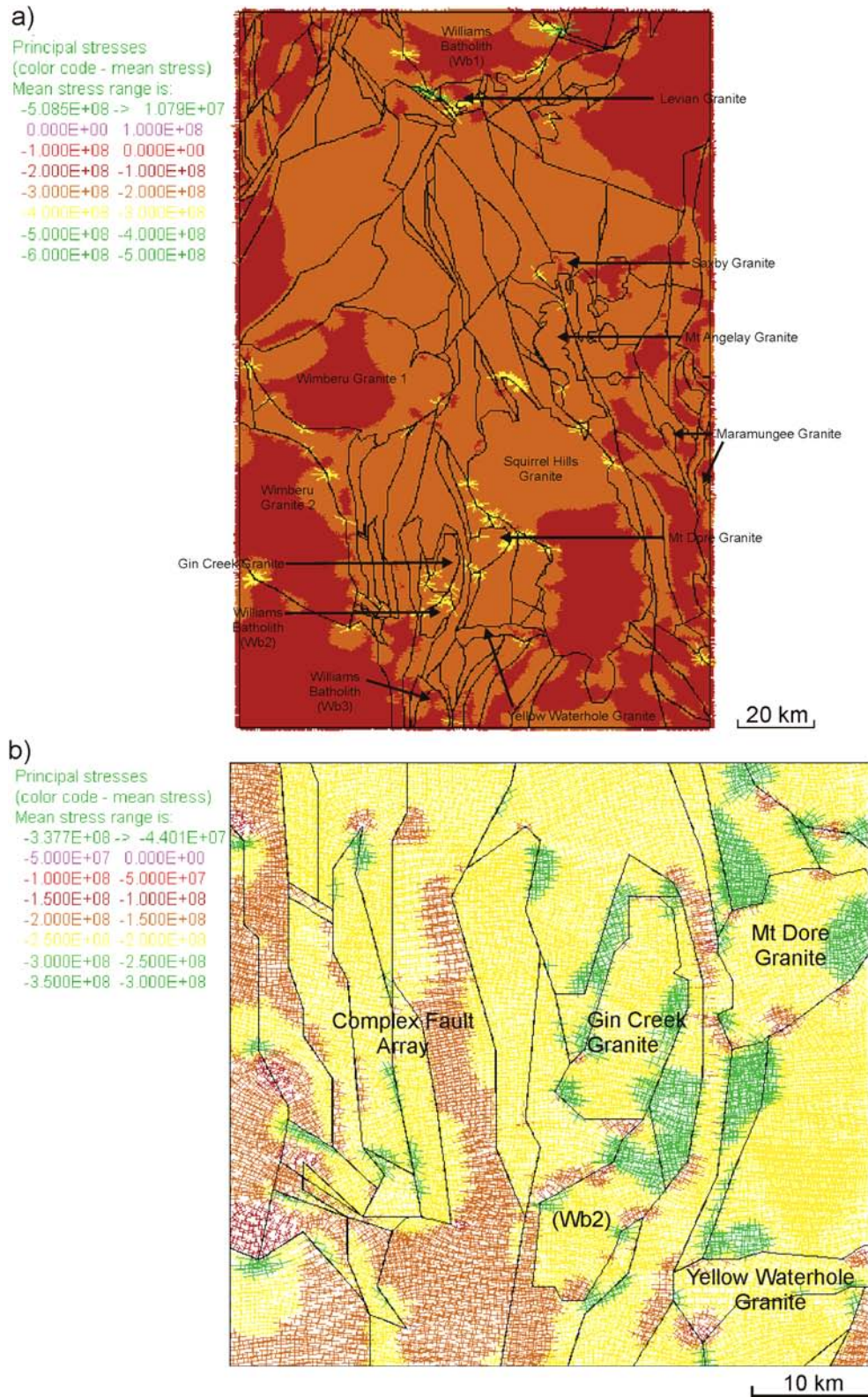


Figure 5.35. Plots of mean stress for Model 2c showing a marked increase from previous models a) regional plot displaying high mean stress values at metasediment-granite contacts, isolated fault intersections and bends b) magnified plot of the Selwyn area showing a large variation in values.

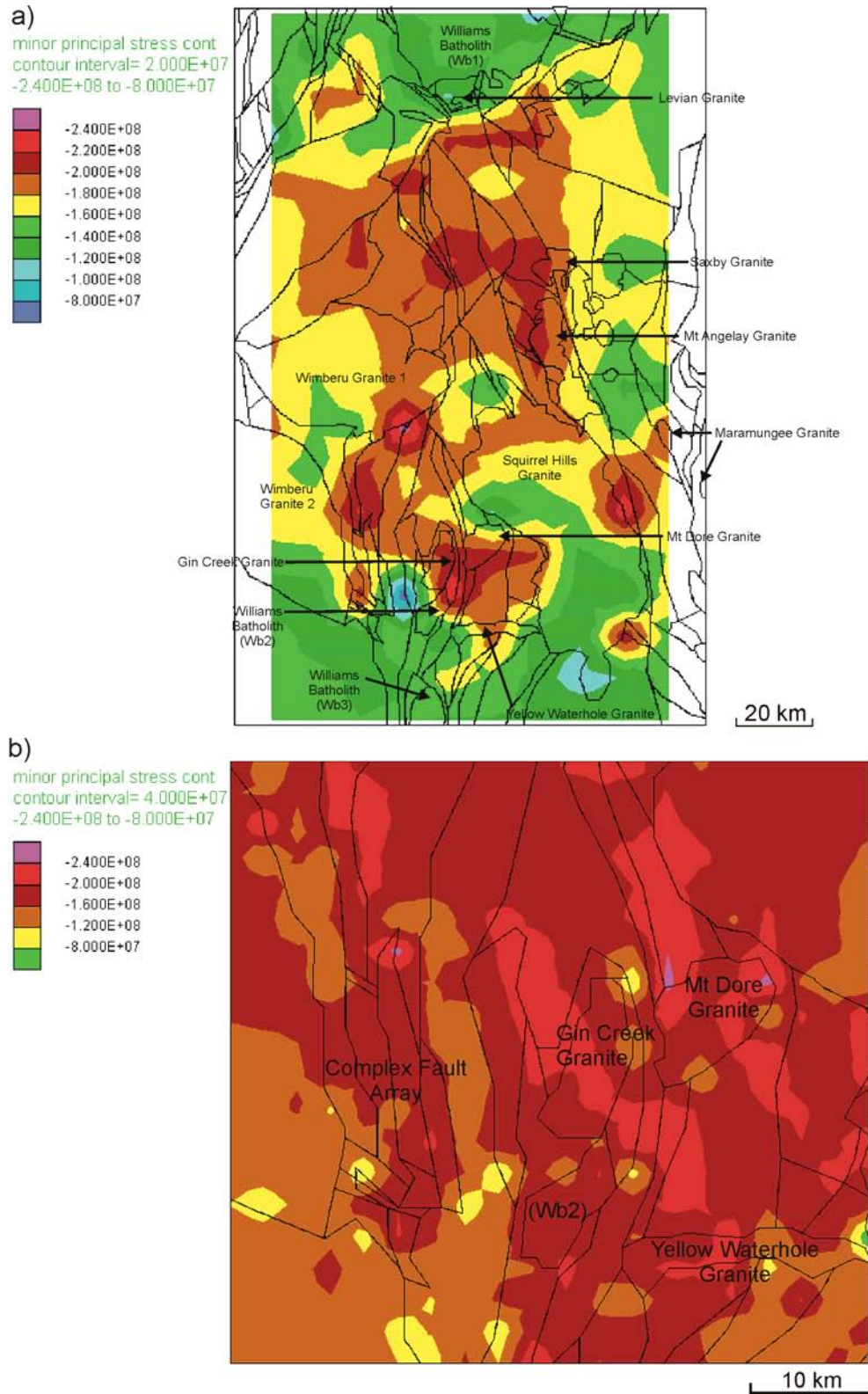


Figure 5.36. Plots of minor principal stress for Model 2c **a)** regional plot indicating lowest values in the Selwyn region and southern end of the Squirrel Hills Granite **b)** magnified plot of the Selwyn area showing distinct trends in low values particularly between the Mt. Dore and Gin Creek granites and fault bends and intersections.

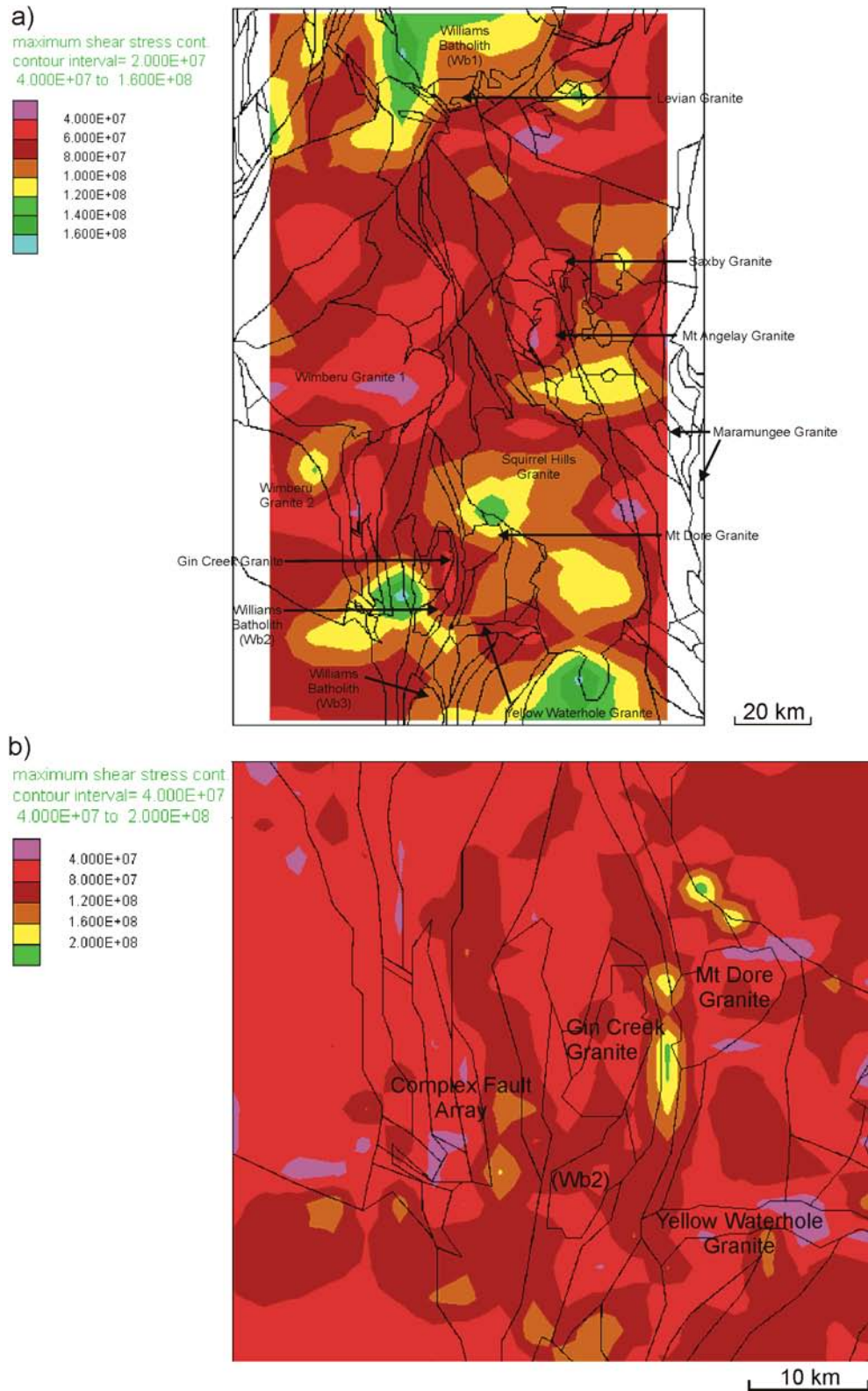


Figure 5.37. Plots of increased differential stress for Model 2c in comparison to the previous model a) regional plot illustrating high values particularly in the northern region, Selwyn region and the Squirrel Hills Granite b) magnified plot of the Selwyn region with high values apparent in the Selwyn high strain zone.

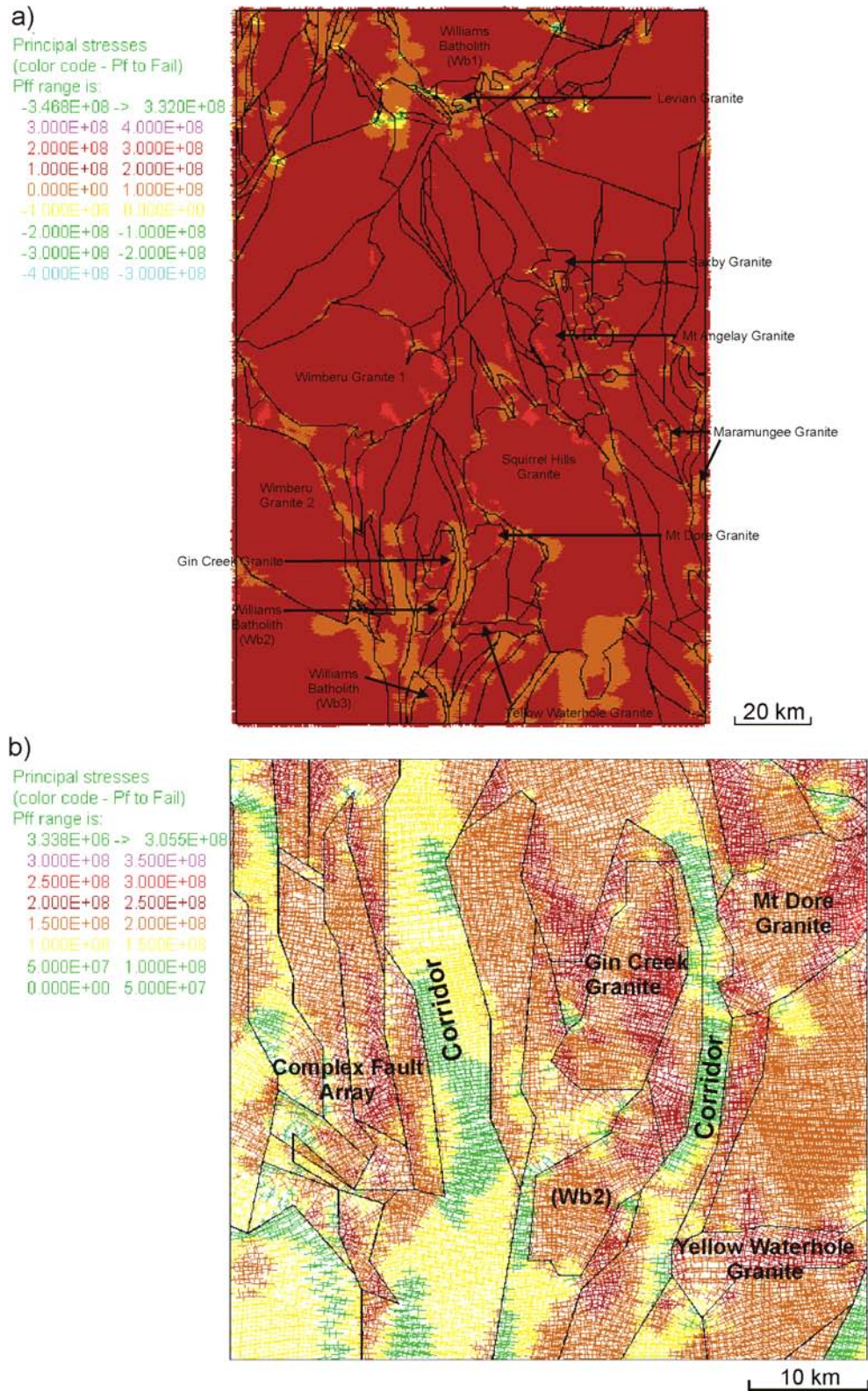


Figure 5.38. Plots of fluid pressure required for failure for Model 2c, a) regional plot displaying several areas in the northern region at yield, and strong trends in the Selwyn region anastomosing the granite bodies b) magnified plot of the Selwyn area displaying distinct north-south trends forming 'corridors'. Note: negative values indicate areas at yield.

5.6.4 **Model 2d:** fluid pressure, σ_1 orientated ESE-WNW (112.5°)

Rotation of σ_1 results in a similar but more intense distribution of high σ_m around lithological contacts and little variation at fault bends or intersections when compared to the Model 2c (Fig. 5.39). On a regional scale both the magnitude and distribution of σ_3 show similarities to Model 2c, however areas such as the east side of the Wimberu granite (1) and the southern tip of the Squirrel Hills granite display much lower σ_3 values (Fig. 5.40a). At the Selwyn scale, similarities to the Model 2c are also apparent, although areas of low σ_3 can be found around the Yellow Waterhole and Mt Dore granite (Fig. 5.40b). The distribution of $\Delta\sigma$ has some marked differences to the Model 2c, primarily a very high value at the southeast contact of the Squirrel Hills granite (Fig. 5.41a); however at the Selwyn scale these differences are less obvious (Fig. 5.41b). One striking difference is the three areas of high $\Delta\sigma$ to the northeast of the Gin Creek granite, which indicate values of up to 200 MPa greater than the same area of Model 2c. Both the distribution and magnitude of PF_f on the regional scale have little variation relative to Model 2c (Fig. 5.42a). At the smaller scale, patterns and values of PF_f are broadly similar to Model 2c, with distinct corridors of PF_f noted between granite bodies and fault arrays (Fig. 5.42b).

In summary, the rotation of σ_1 intensifies the distribution of high σ_m which is primarily noted on lithological contacts. Several differences in distribution of σ_3 are also apparent relative to Model 2c. The most marked effect in this model is the change in both distribution and magnitude of $\Delta\sigma$, which indicates the potential for more intense deformation in these regions. PF_f is overall relatively unchanged in comparison to the previous model.

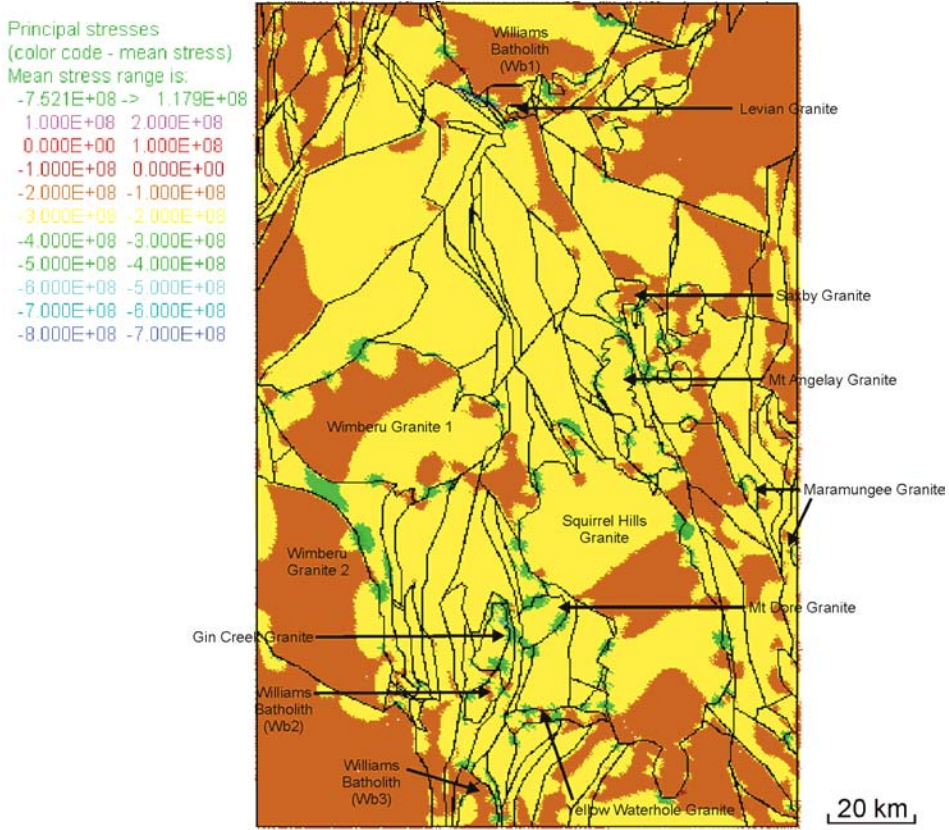


Figure 5.39. Regional plot of mean stress for Model 2d displaying high mean stress values at metasediment-granite contacts, isolated fault intersections and bends.

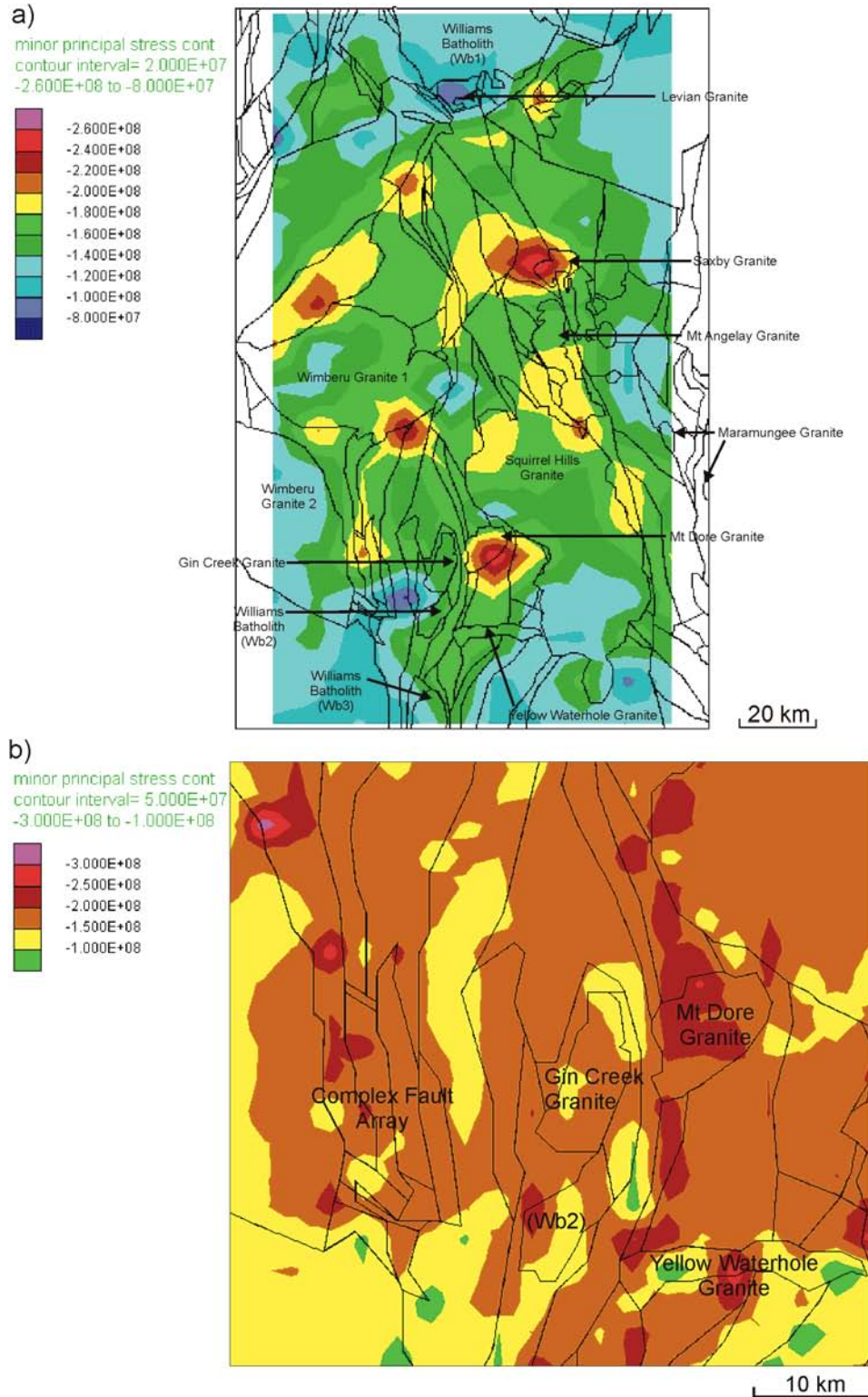


Figure 5.40. Plots of minor principal stress for Model 2d a) regional plot indicating isolated areas of increased values north of the Mt. Angelay Granite, northern and southern contacts of the Wimberu Granite and the southeast side of the Mt. Dore Granite. Lowest values correspond to the south end of the Squirrel Hills Granite, the Cloncurry region and around the Selwyn region b) magnified plot of the Selwyn area showing distinct trends in low values particularly between the Mt. Dore and Gin Creek granites.

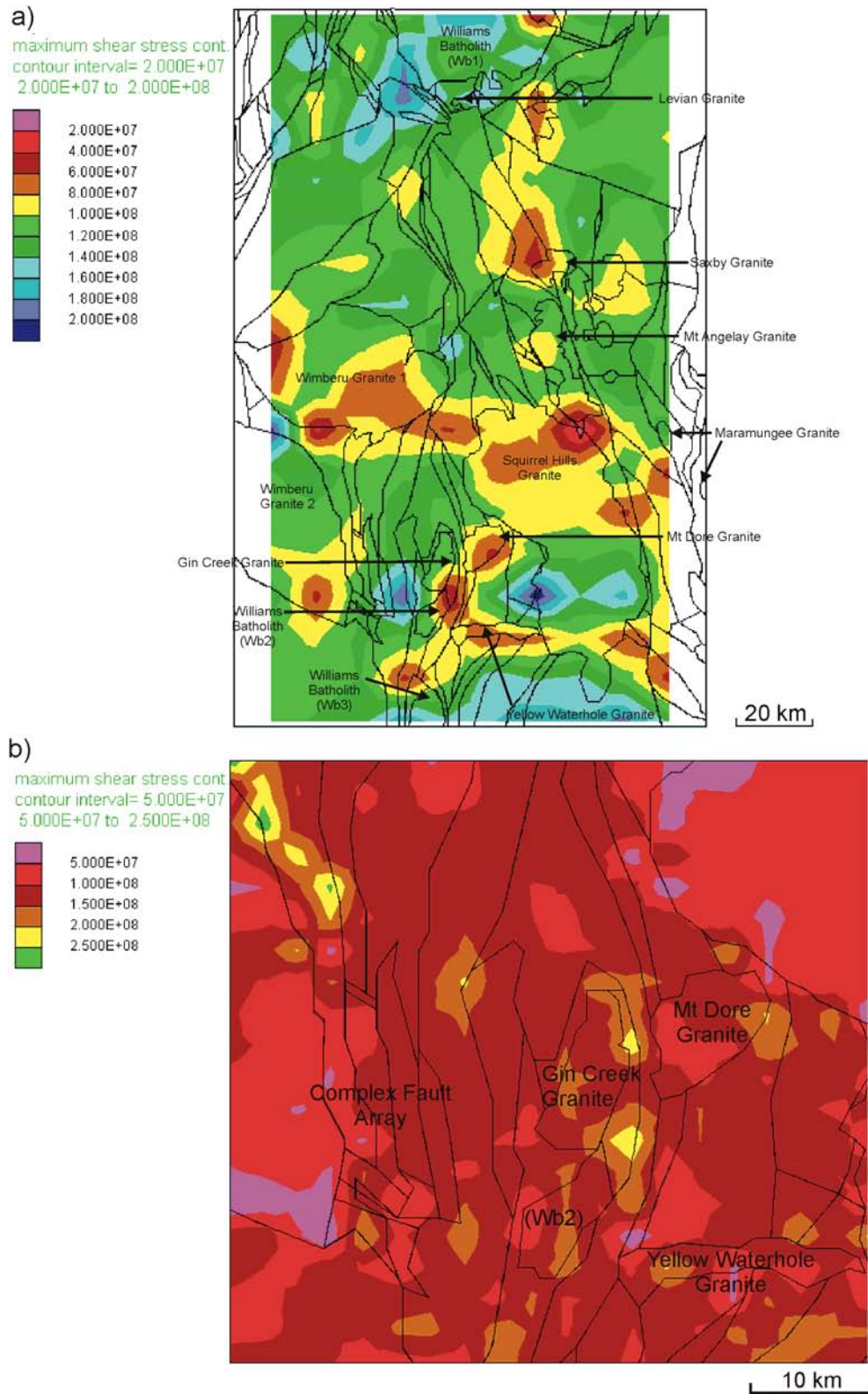


Figure 5.41. Plots of increased differential stress for Model 2d in comparison to the previous model **a)** regional plot illustrating high values particularly in the Selwyn region and on the west side of the Squirrel Hills Granite **b)** magnified plot of the Selwyn region with very high values apparent east of the Gin Creek Granite and close to the Wimberu Granite (2).

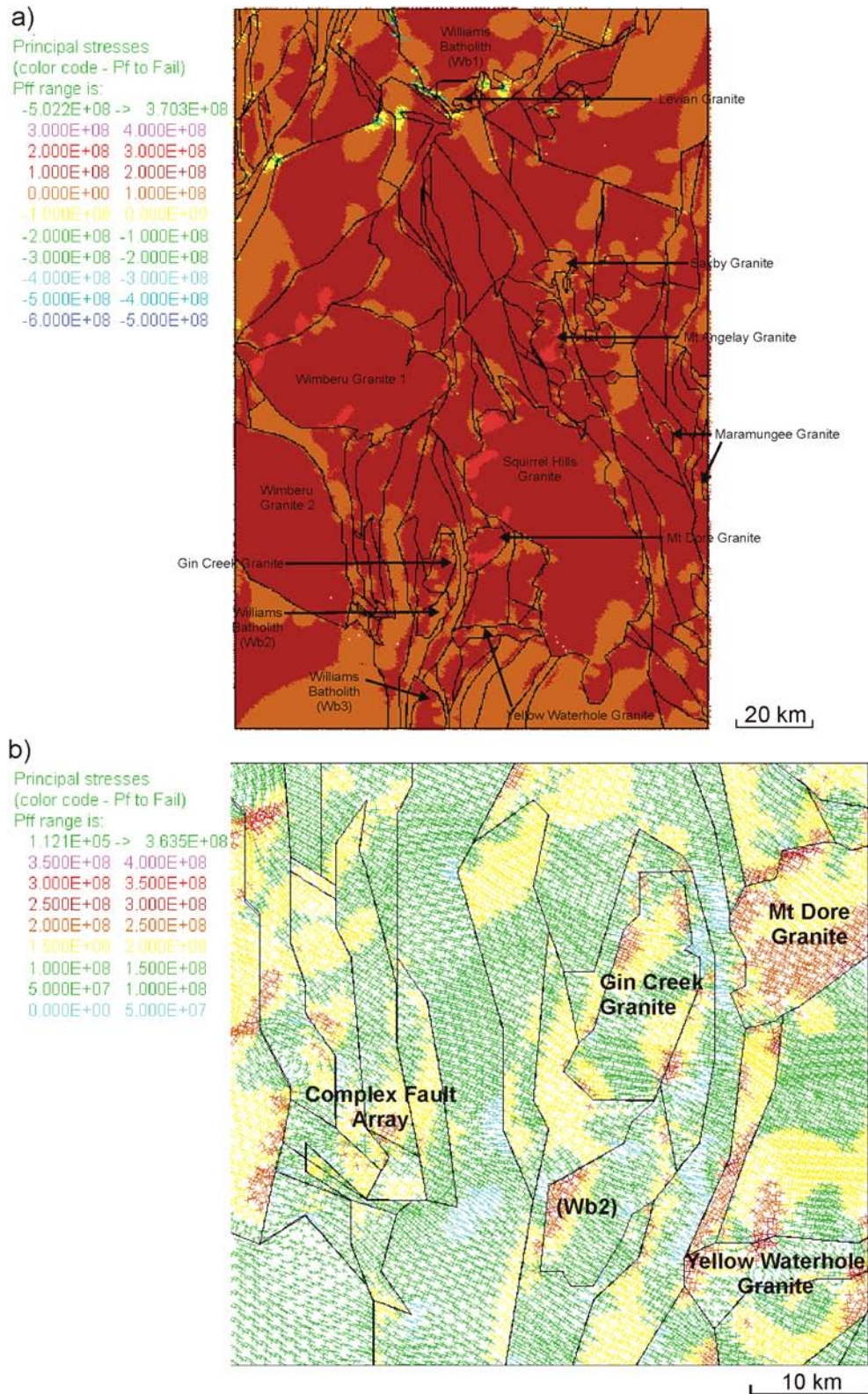


Figure 5.42. Plots of fluid pressure required for failure for Model 2d **a)** regional plot displaying a general decrease in area requiring high P_f ; **b)** magnified plot of the Selwyn area showing lowest values focussed between the Mt. Dore and Gin Creek granites. Note: negative values indicate areas at yield.

5.6.5 Aperture and fluid flow behaviour

The effect of stress on the opening and closing of fractures, and its relationship to fluid flow, was explored. Models were set up with the same geometry as Model 2, and given initial fracture properties such as permeability and aperture sizes. Flow was then initiated from source points around younger granite bodies e.g. < 1530 Ma (see Fig. 5.4) and direction, flow velocities and rates of flow were monitored. Due to limitations of two dimensional modelling, fluid flow directions only represent a component of three dimensional flow, and may have little actual significance. The potential for lateral fluid flow in this area is less likely than upward or vertical fluid migration, even during strike-slip deformation, as described by Sibson (1996); hence these results are used only to estimate potential maximum values of lateral flow within this system. These results have little bearing on the overall prospectivity analysis of the area in comparison to the results stated previously, as areas that show a higher potential for mineralisation are primarily related to the partitioning of stress during deformation. However, these results do provide insight into lateral flow rates from potential fluid point sources.

Faults or contacts at low angles to σ_1 generally display an increase in aperture, with maximum apertures recorded at 0.15m which correspond to maximum flow velocities in the Cloncurry region of up to $3.337e^{-5} \text{ ms}^{-1}$ and maximum volumetric flow of up to $9.767e^{-7} \text{ m}^3\text{s}^{-1}$ (Fig. 5.43ab). Volumetric flow rates (volume/time) were examined in the Selwyn and Cloncurry regions at history points pp1 and pp3 (see Fig. 5.4). Volumetric flow rates in the Cloncurry region display an initial sharp increase, which then becomes stable and attains a

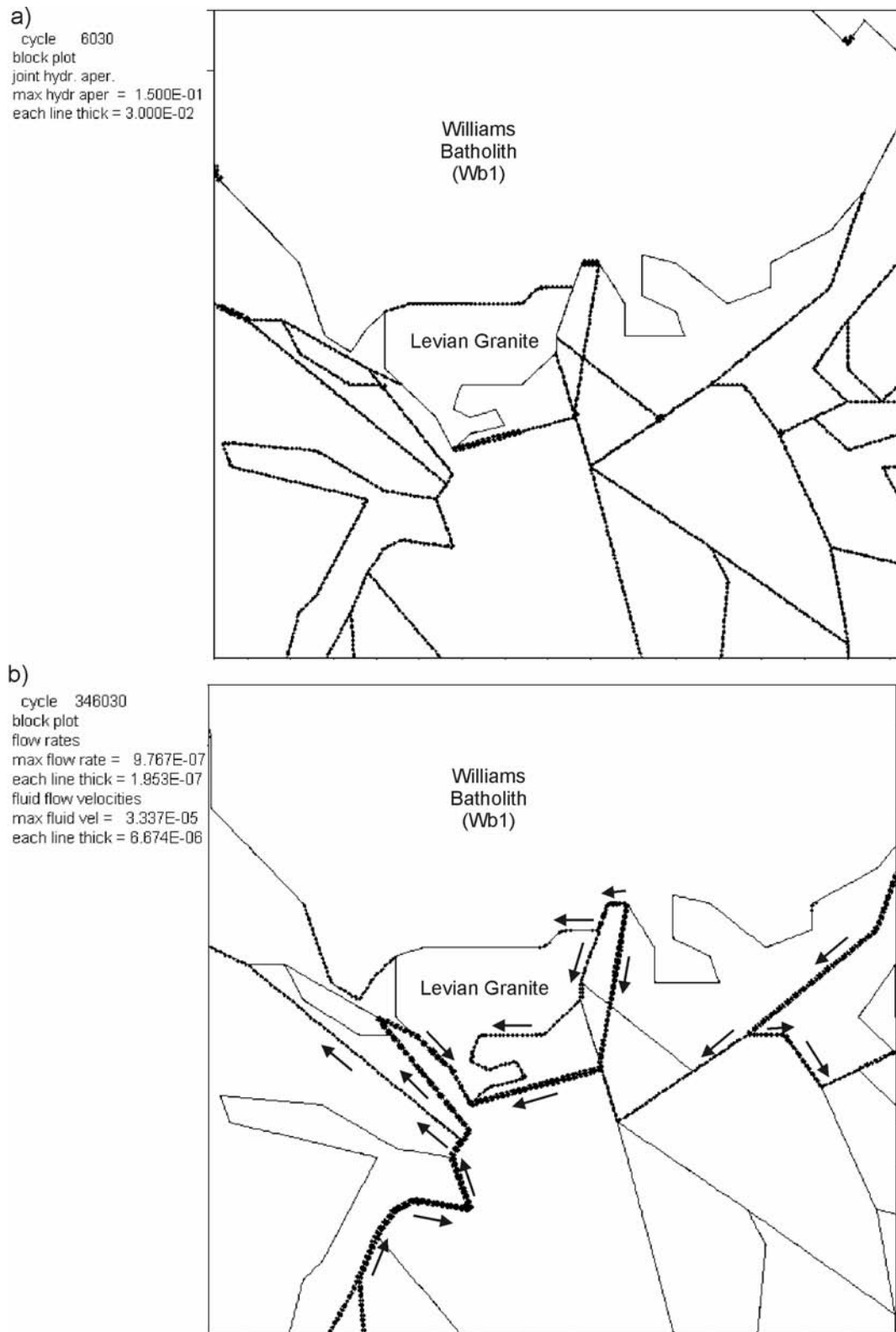


Figure 5.43. Plots of joint hydraulic aperture, flow rates and velocities for the Cloncurry region Model 2 a) aperture widths of the fractures, maximum aperture opening generally found on faults at low angles to maximum principal stress b) maximum flow rates of the Cloncurry region (arrows represent flow direction).

steady state flow condition (Fig. 5.44a), whereas flow rates in the Selwyn region display an initial sharp increase followed by a relatively constant increase throughout time (Fig. 5.44b). These differences may be linked to the spatial association of these areas with fluid point sources, as the Selwyn area has a greater number of proximal fluid sources relative to the Cloncurry region, therefore higher volumetric rates would be expected. On closer examination, dilatancy of fractures or increase in aperture, and hence volumetric flow, has a close association with decreased values of σ_3 and increased values of $\Delta\sigma$ and dependant on relative orientation to σ_1 (Fig. 5.45a). However, this statement is a generalisation, as aperture behaviour and ultimately fluid flow is strongly controlled by local stress fields. As complex patterns of deformation partitioning emerge, it is clear that local patterns and block geometry (i.e. orientation to σ_1) have a strong influence on fracture behaviour, as similarly orientated fractures throughout the model behave differently. Fractures that exhibit dilation and increased aperture width are primarily controlled by a decrease in normal stress adjacent to the fracture walls, and this is commonly related to the fracture orientation to σ_1 and local deformation patterns (Fig. 5.45b). Further useful work on this aspect of the model could only be achieved in 3D.

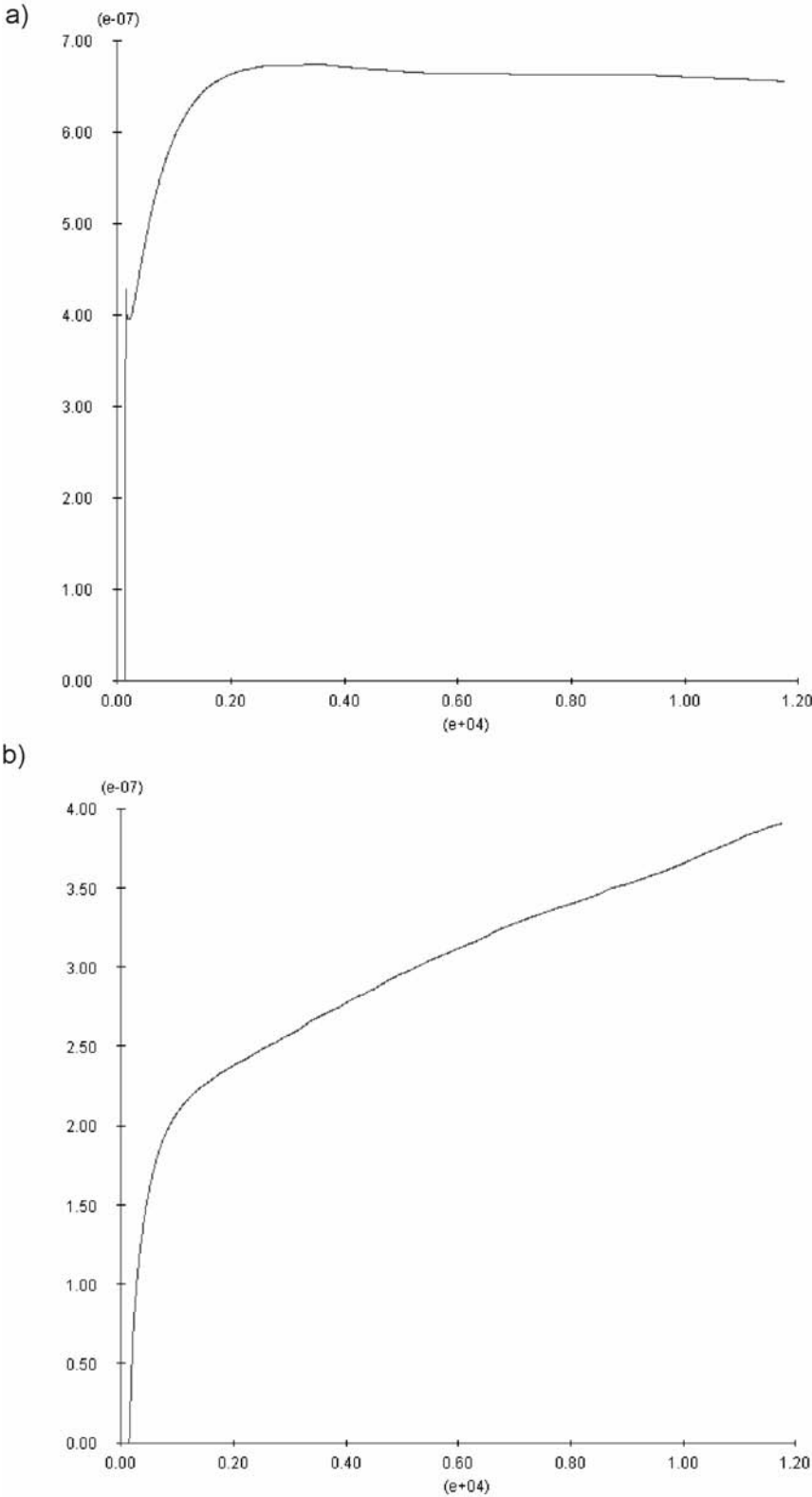


Figure 5.44. Volumetric flow rates at history points pp1 (Cloncurry region) and pp3 (Selwyn region) **a)** history point pp1 displays an initial rapid increase in flow rate which after reaching its peak produces a stable rate **b)** history point pp3 displays an initial rapid increase in flow rate and continues to increase throughout the model run.

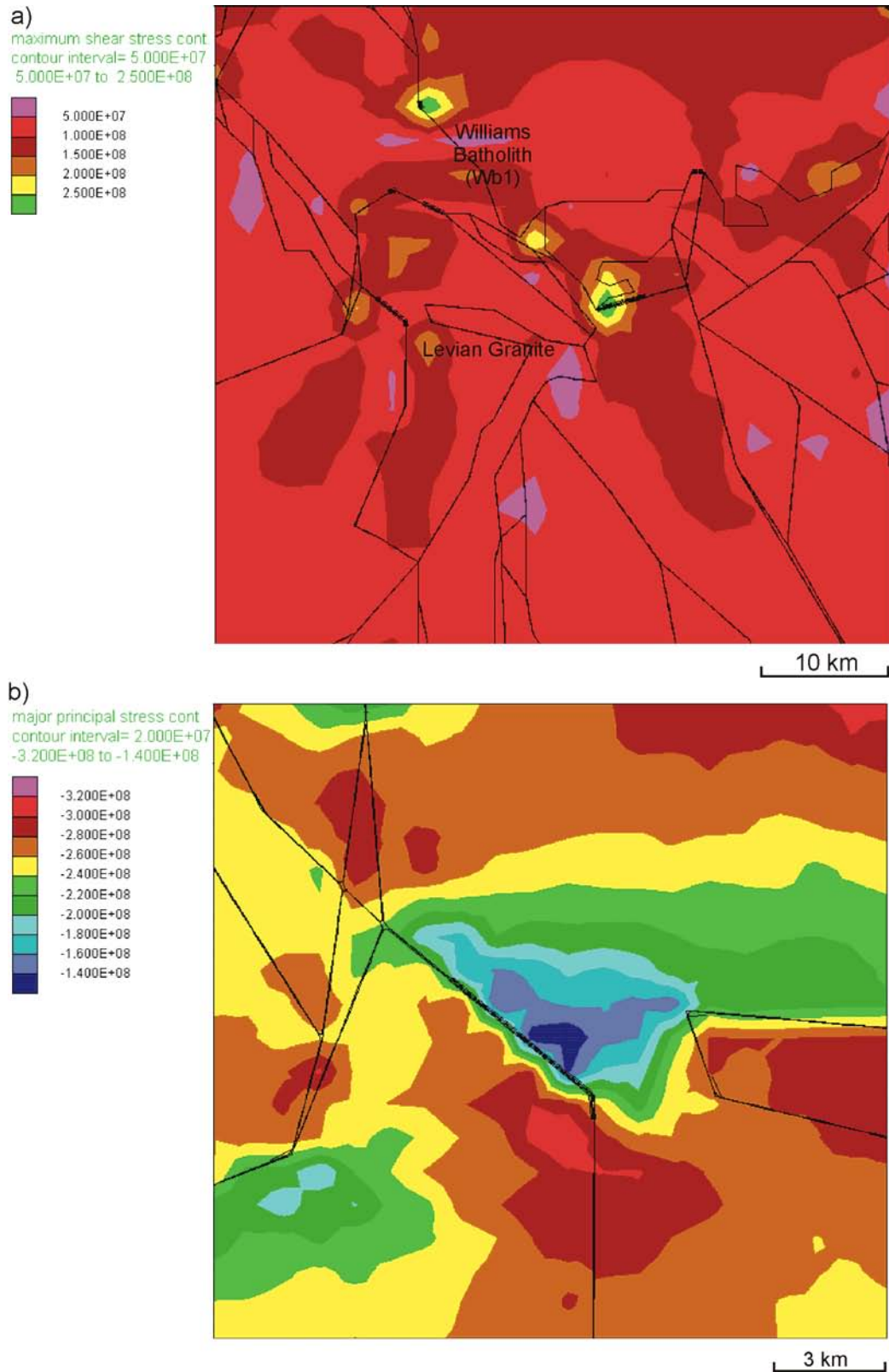


Figure 5.45. Plots of aperture widths and mean stress **a)** Cloncurry region illustrating the relationship between high values of differential stress and increased aperture width **b)** fracture indicating the relationship between low values of major principal stress and aperture width.

5.6.6 Prospectivity and comparison to mineralisation

Mustard *et al.* (2004) identified several ingredients in their prospectivity analysis that favoured deposit localisation. In order of importance, these were considered to be a) fault orientations, b) fault intersections, c) fault bends, d) magnetic anomalies and e) proximity to the boundary between Corella Formation and Soldiers Cap contacts. Butera (2004) also notes a strong correlation between deposit distribution and mafic intrusions in a more detailed area of the Eastern Succession, similar in size to the Selwyn region of this study. Unlike the work by Mustard *et al.* (2004), this work focuses on the complex interactions involved in both the mechanical and fluid plumbing systems within the Eastern Succession. No single specific factor has been highlighted as highly prospective, however, the main combinations of ingredients required to increase the potential for mineralisation have been explored.

Comparisons with known areas of mineralisation has been encouraging, in that several areas have been highlighted that contain medium to large deposits (e.g. Selwyn, Greenmount, Pegmont, and Great Australia) and many smaller deposits and prospects. Another interesting observation is the fact that 'barren' areas have also been highlighted (e.g. N/NE trending faults north of the Selwyn region, N/NW trending faults east of the Squirrel Hills granite, and N/E trending fault northwest of the Wimberu granite). Several areas have also been highlighted that at present have no current known deposits.

The ability to predict areas at yield or failure within the region allows a better understanding on the effects of fluid pressure and stress on the architecture of the system, and ultimately potential sites for fluid focussing and mineralisation. The plasticity indicator in UDEC allows the examination of these potential sites. The initialisation of fluid pressure within the fractures has a significant effect on failure within the model, as does changing the orientation of the stress field. The 'dry' models indicate only a few sites at yield (Fig. 5.46ab), and a significant effect can be seen when fluid pressure is added and then rotation of σ_1 both at the regional scale (Fig. 5.47ab) and the Selwyn scale (Fig. 5.48ab). The results from this study indicate that a 'wet' model with a rotation of σ_1 to 112.5° provides the best correlation with known deposits in the region, hence better for predicting mineralisation. The correspondence between the results of the prospectivity analysis by Mustard *et al.* (2004) and these results, show many correlations with many areas considered prospective within this study both regionally (Fig. 5.49ab) and at the Selwyn scale (Fig. 5.50ab). Of the many deposits and prospects indicated by Mustard *et al.* (2004), around 80% of them are predicted by this UDEC modelling. Further targets areas have been predicted by this UDEC modelling and these locations may make good exploration targets.

A major consideration relevant to highlighting areas with potential prospectivity appears to be linked to deformation and fluid flow relationships. As this modelling is mainly focussed on fracture systems, areas that provide a combination of low values of σ_m , σ_3 PF_f , increased $\Delta\sigma$ and high volumetric flow rates provide the best targeting solution for mineralisation.

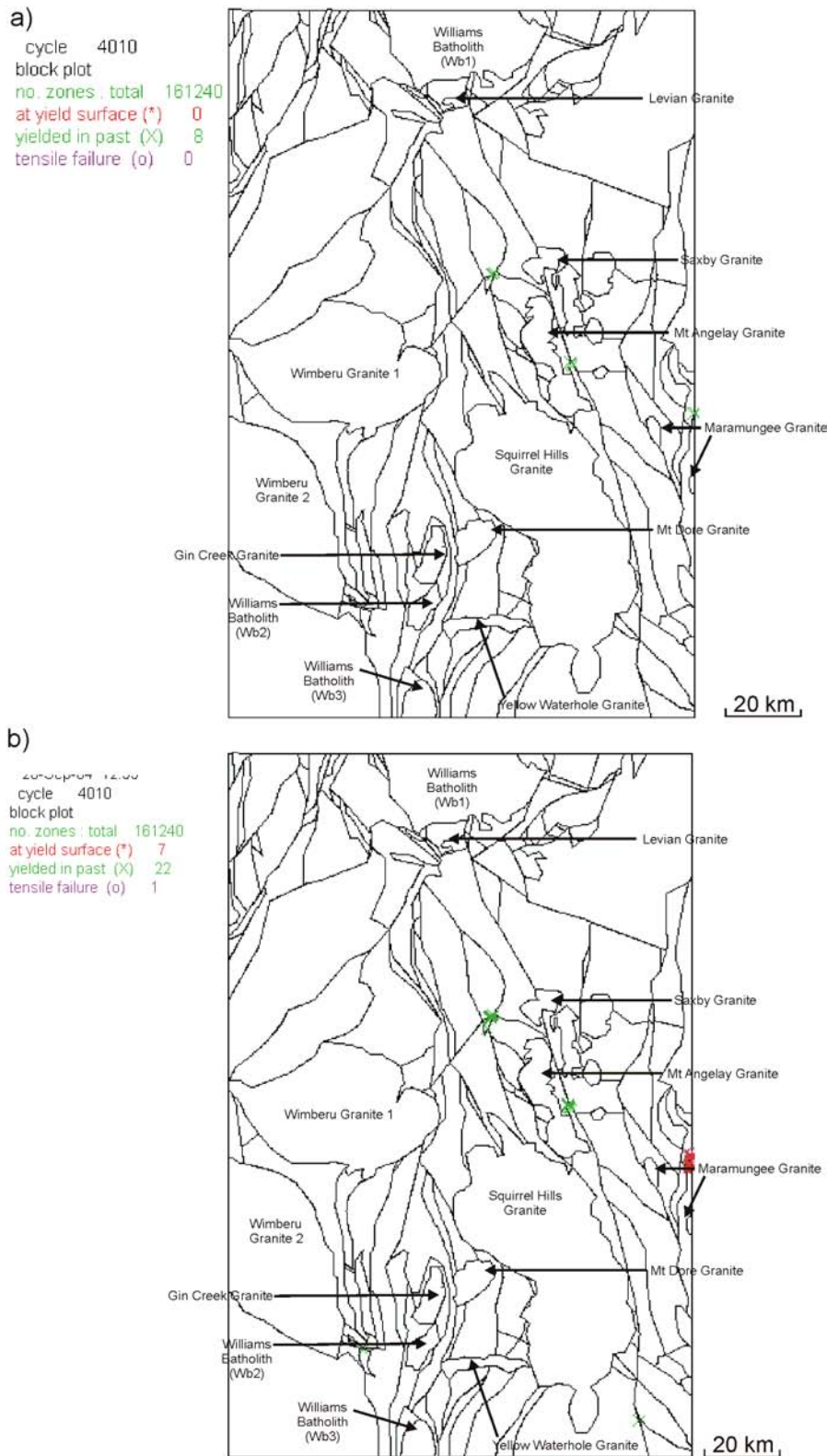


Figure 5.46. Plasticity state comparison of Models 2a and 2b a) 'dry' model $\sigma_1 = 90^\circ$ and b) 'dry' model $\sigma_1 = 112.5^\circ$. Rotation of σ_1 has caused greater failure although has limited effect on distribution. Note: red indicates areas at yield, green indicates previously at yield but now not in contact with the failure envelope, and purple indicates areas in yield in tension.

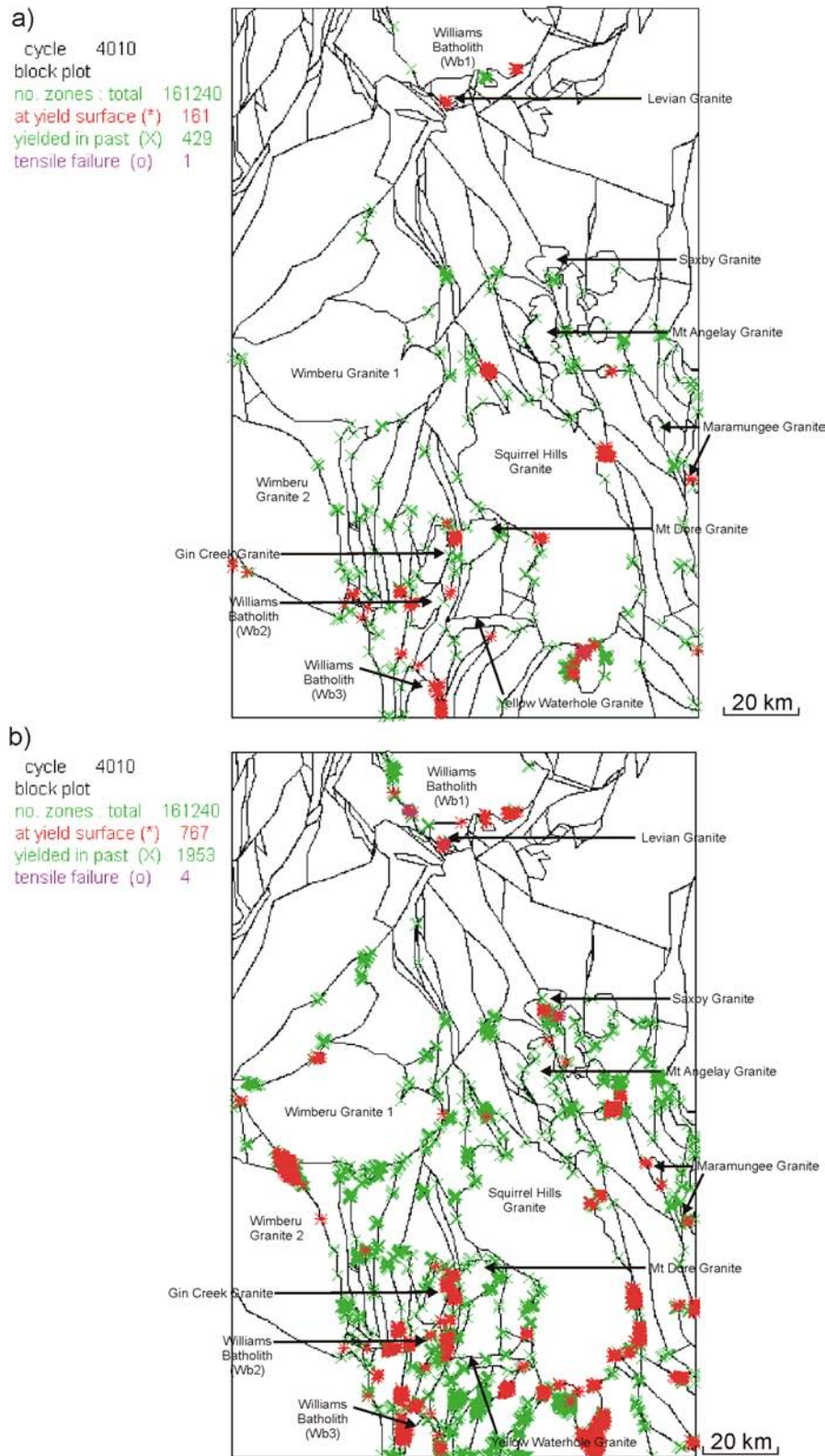


Figure 5.47. Plasticity state comparison of Models 2c and 2d a) 'wet' model $\sigma_1 = 90^\circ$ and b) 'wet' model $\sigma_1 = 112.5^\circ$. Rotation of σ_1 has a strong influence on failure and distribution. Note: red indicates areas at yield, green indicates previously at yield but now not in contact with the failure envelope, and purple indicates areas in yield in tension.

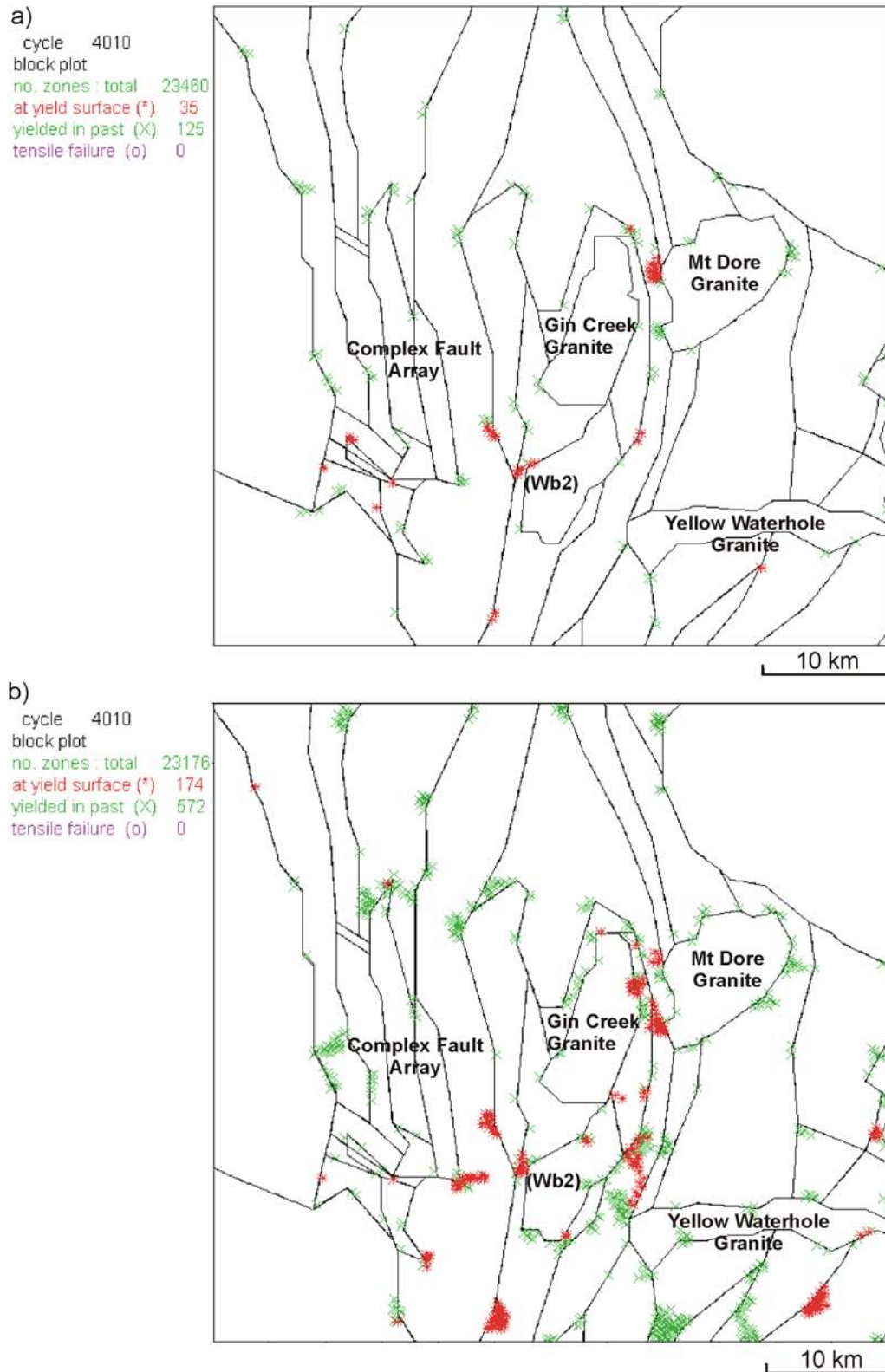


Figure 5.48. Plasticity state comparison of Models 2c and 2d a) ‘wet’ model $\sigma_1 = 90^\circ$ and b) ‘wet’ model $\sigma_1 = 112.5^\circ$ at the Selwyn scale. Rotation of σ_1 has a strong influence on failure and distribution. Note: red indicates areas at yield, green indicates previously at yield but now not in contact with the failure envelope, and purple indicates areas in yield in tension.

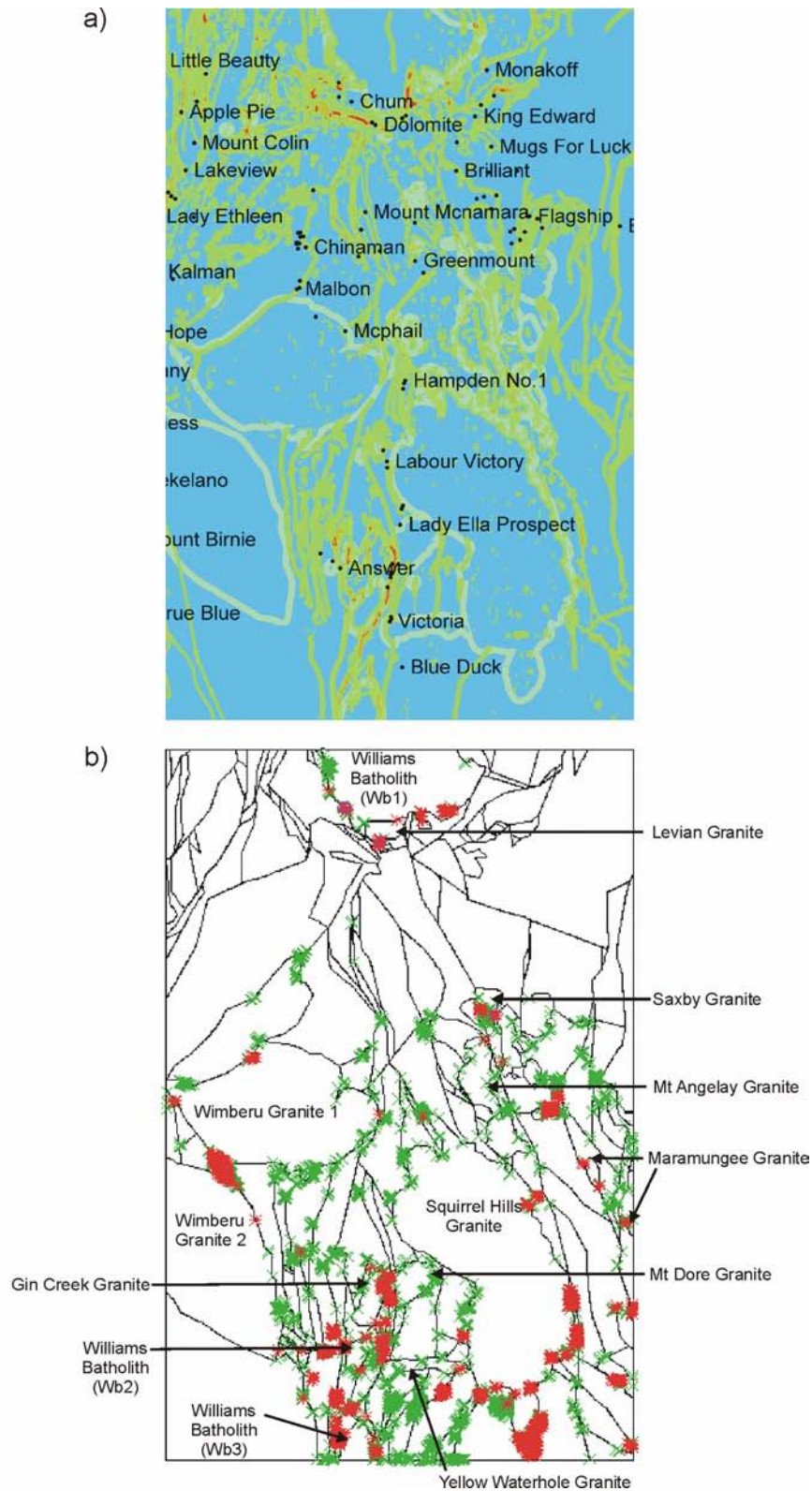


Figure 5.49. Comparison of prospectivity analysis by Mustard *et al.* (2004) and plasticity indicators for Model 2d. **a)** prospectivity analysis, blue colours indicating no prospectivity and yellow to red indicating lower to higher prospectivity, with deposits and prospects indicated **b)** plasticity indicator for Model 2d (see Fig. 5.48 for legend).

a)



b)

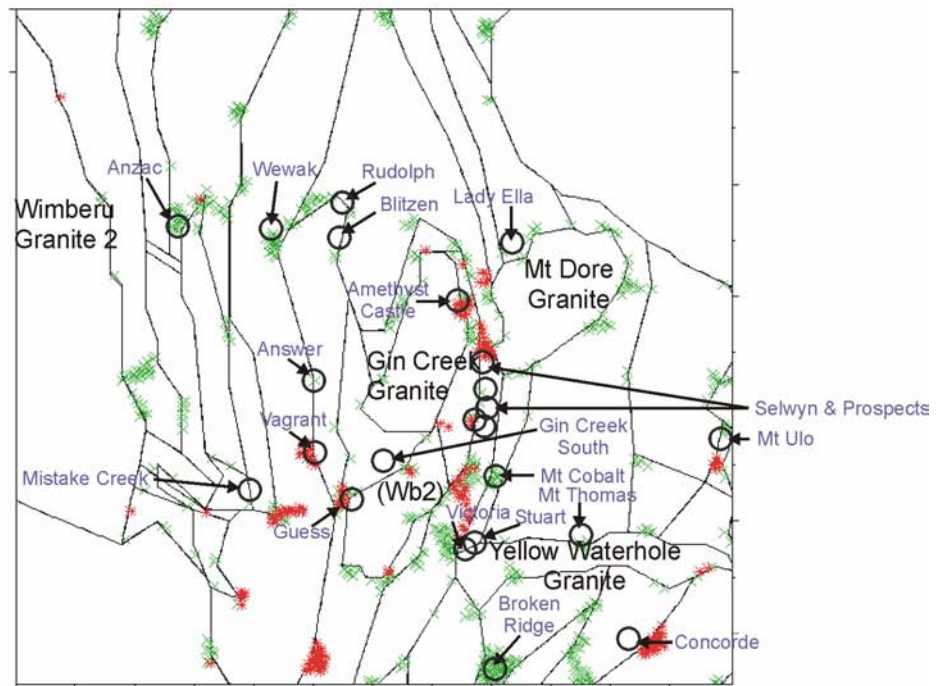


Figure 5.50. Comparison of prospectivity analysis **a)** by Mustard *et al.* (2004), blue colours indicating no prospectivity and yellow to red indicating lower to higher prospectivity respectively **b)** plasticity indicators for Model 2d of the Selwyn region, indicating areas at yield.(see Fig. 5.48 for legend). Known deposits and prospects of the Selwyn area are named and marked by circles.

5.7 Discussion and Conclusions

Several factors and locations have been highlighted in these models that appear to contain the essential ingredients for a potentially mineralised system. The modelling procedure and analysis have also highlighted the effects of increasing the complexity of the geometry, rotating the orientation of σ_1 and introducing fluid into specific parts of the system. This section will discuss the results of the main models and the relationship between mechanical and fluid processes, leading to a summary which focuses on prospectivity of the Eastern Succession.

Competency contrasts between the granitic intrusions and metasediments in association with a fault or fracture system, results in significant changes in the partitioning of stress around these structures. The initial model (Model 1) has few pre-tectonic intrusions and a basic fault array, which provides a baseline model for examining the response to tectonic processes that correspond to an E/W shortening episode. This model displays preferential failure conditions around many fault bends and intersections, and along faults orientated at a low angle to the maximum principal stress. Although this orientation of faults provides the best conditions for failure, not all faults of this orientation show the same results throughout the entire model. This is due to the more complex interactions of block geometry or fault blocks, which assists in partitioning stress as these blocks move and deform. Many areas of interest can be highlighted, which display lower magnitudes of mean stress, minimum principal stress and fluid pressure required for failure. These parameters indicate a higher potential for failure at specific locations within the model, and hence

provide an increased prospectivity interest. The rotation of the maximum principal stress to 112.5° significantly modifies the distribution and variation in magnitudes of both minimum principal stress and differential stress, with lower values of minimum principal stress and mean stress corresponding well with areas showing higher differential stress. These conditions provide a greater likelihood of shear failure and probable dilation, and have a strong potential for focussing fluid flow. Areas that show a decrease in the values of mean stress, minimum principal stress in combination with low differential stress provide conditions most suitable for tensile failure, which is a particularly good environment for mineralisation. Altering the orientation of the maximum principal stress has little consequence on the distribution of magnitude of the mean stress in the Model 1; however it does have a strong influence on redistribution of minimum principal stress values. This can be attributed to the orientation of faults in relation to the maximum principal stress and as stated before, this is variable throughout the models due to complex geometry and block interactions. The introduction of distributed fluid throughout the model fractures results in a considerable variation in the range of values of all parameters investigated, and leads to a significant modification in the pattern of distribution. Overall values of all parameters decrease for many areas, which provide more suitable conditions for failure. In a Mohr space this corresponds to reduced effective stress values and a shift of the Mohr circle towards the failure envelope, with enhanced potential for failure in these rocks. With both fluid introduction and a rotation of the maximum principal stress we see distinct changes in the distribution of many parameters, increases in the range of many

values, an increased incidence of failure within the models and a better correspondence with known deposits.

Increasing the complexity of the models by introducing younger intrusions and faults, allows a comparison of stress partitioning on a broad scale with the earlier models. Model 2 displays similar effects to Model 1 when fluid pressure is introduced into the fractures and a rotation of the minimum principal stress to 112.5° is initiated. As a result of the more complex geometry there is less confidence in a generalised fault orientation within the whole region being more prone to failure, due to the heterogeneous patterns of deformation and stress partitioning. Unlike the work of Mustard (2004) no clear or obvious fault orientations or intersections were highlighted overall, due to the complexity of stress partitioning. Interesting observations were made in smaller areas, such as the Selwyn region, where the localisation of deformation was compartmentalised. Areas of high differential stress correspond well to high strain zones e.g. Selwyn high strain zone, which is situated between the Mt Dore and Gin Creek granites. Due to shear displacement of blocks between the granite bodies and the fault systems, this area has accommodated higher strains.

In conclusion, this work has shown that the partitioning of stress during deformation is a complex process, and that no single attribute can be shown to be a high level indicator for mineralisation. However, these models show that a combination of low mean stress, minimum principal stress and high differential stress are good indicators for deformation and dilation as a result of shear

failure in the rocks, and in combination with low fluid pressure required for failure, may act as a prospectivity guide. The results of these models have a good correlation with present known deposits and prospects, and also highlight areas that currently have no known mineralisation. This UDEC analysis has proven to be an effective tool and compares well with at least several prospectivity layers from the work of Mustard *et al.* (2004).

Implications for exploration in the Eastern Succession may be enhanced by the findings of this study. To fully develop this process as an effective exploration tool, areas that show a strong potential for mineralisation should be re-examined and modelled at a local scale, incorporating a more detailed geometry including lithological contacts and small-scale structures. To fully constrain the stress distribution in the Eastern Succession, a three-dimensional model would be preferable, as low angled faults and vertical fluid flow on steep fault intersections would have an effect on the partitioning of stress. However, this would require detailed information on all structures involved and considerable computational time to process the model. In cases where low angle faults are present, cross sectional modelling could be utilised to provide an understanding in the third dimension. However, these two-dimensional models provide a basis for further modelling studies, and highlight the basic conditions required to ascertain why certain areas may be more prospective than others.